

Design and Synthesis of Novel pH-Sensitive Anticancer Drug and Efflux Pump Inhibitor Conjugates

by

Klis Keith Ramdeen-Lessey

Dr. Sharon Rossiter and Prof. Mire Zloh

Submitted to the University of Hertfordshire in partial fulfilment of the requirement of the degree of Master of Science by Research

Department of Clinical and Pharmaceutical Sciences, School of Life and Medical Sciences
University of Hertfordshire

2020

31st January 2020

Table of Contents

Acknowledgements	i
Abstract	ii
1.0. Introduction	1
1.1. Cancer chemotherapy	2
1.1.1. How cancer cells differ from normal cells	2
1.1.2. Major drug targets.....	4
1.1.3. Standard chemotherapy agents	5
1.1.3.1. Doxorubicin	5
1.1.3.2. Epirubicin	6
1.1.3.3. Paclitaxel	6
1.1.3.4. Methotrexate	7
1.1.3.5. Fluorouracil	8
1.1.3.6. Microtubule-target agents.....	9
1.2. Resistance.....	10
1.2.1. The issue of resistance	10
1.2.2. Drug efflux: Mechanisms and types of pumps	11
1.2.2.1. P-glycoprotein (P-gp)	12
1.2.2.2. Monocarboxylate transporters (MCTs)	13
1.2.2.3. Multidrug resistance proteins (MRPs).....	14
1.2.2.4. Breast cancer receptor protein (BCRP).....	14
1.2.3. Efflux pump inhibitors	15
1.2.3.1. Inhibitors of P-gp	15
1.2.3.2. Inhibitors of MCTs.....	16
1.2.3.3. Inhibitors of MRPs.....	16
1.2.3.4. Inhibitors of BCRP	16
1.3. Drug delivery	17
1.3.1. Ways of improving the delivery of drugs to tumours	17
1.3.2. How a low pH in cancer cells can be a drug target	18
1.3.3. Type of linkers	19
1.3.3.1. The cis-aconityl linker	19
1.3.3.2. The hydrazone linker	23
1.3.3.3. The orthoester linker	24

1.4. The use of computational chemistry in drug design.....	26
1.4.1. Electronic structure methods	27
1.4.2. Force field methods.....	29
1.5. Precedence for this research	30
1.6. Aim and objectives of this project.....	32
2.0. Design of novel drug-EPI conjugates	33
2.1. Methods for selection of conjugates	33
2.2. Computational methods	37
2.2.1. Prediction of HOMO/LUMO	38
2.3. Results and discussion.....	39
3.0. Synthesis.....	55
3.1. General.....	55
3.2. Methods	56
3.3. Discussion.....	76
3.3.1. Analysis of compounds.....	79
4.0. Future work	83
4.1. Drug-EPI linker conjugate synthesis, pH release studies and <i>in vivo</i> testing.....	83
4.2. Pharmacological studies.....	84
4.3. Alternate studies and treatments	85
4.4. Conclusion	85
5.0. References	86

Acknowledgements

To my supervisors: Dr. Sharon Rossiter and Professor Mire Zloh for their constant encouragement and guidance. To Dr. Ilaria Passarini, Dr. Lisa Gerstmann, Dr. Mehrnoosh Ostovar and all laboratory technical staff for support with my research. Finally, a major thanks to all postgraduate research students, my friends and parents for their continual encouragement and advice.

Abstract

Resistance to anti-cancer therapies has proven a challenge for effective treatments. Efflux pumps when overexpressed in cancer cells, eject drugs from the cell, rendering them ineffective. The pH of cancer cells is generally lower than that of normal cells, due to their raised metabolic rate. This disparity can be exploited using a prodrug that is activated at an acidic pH, resulting in improved efficacy for treatments. Co-administration of an efflux pump inhibitor (EPI) with an anticancer drug can prevent drug efflux, reduce normal cell cytotoxicity, and improve the efficacy.

Using the cytotoxic drug, doxorubicin, the EPIs, MC70 and norverapamil with the *cis*-aconityl linker, possible conjugates were modelled. We chose the *cis*-aconityl linker because it is acid-labile at pH values <7 and, is suitable for targeted release of doxorubicin in tumours. Linker conjugates for glucosamine and 4-aminotetrahydropyran, model compounds for doxorubicin, 4-phenylphenol, the model compound for MC70, and dibutylamine, phenethylamine and N-methyl-phenethylamine, model compounds for norverapamil, were synthesized and analysed.

This study has laid the groundwork for a novel way of increasing the efficacy of doxorubicin, and possibly other medicine, which will hopefully lead to more studies and eventual treatments and therapies.

1.0. Introduction

Cancer is classified as a collection of diseases, arising from the uncontrolled proliferation of cells (Chiarugi & Cirri, 2016). It is the by-product of a set of genetic mutations in altered gene expression and DNA (Hanahan, 2014) which results in a cell's structures and DNA becoming damaged. This can be the outcome of mutations, cancer-causing chemicals, termed; carcinogens, radioactive compounds, pathogens, diet, exercise, heredity, physical agents, hormones or autoimmune diseases (Blackadar, 2016).

When a group of these cancer cells form a mass, this is referred to as a neoplasm or a tumour (Chiarugi & Cirri, 2016). A tumour is termed benign when an uncontrolled proliferation of cells is confined to the point of cells of origin, resulting in dysplasia. Metastasis could occur where cancer cells and growth factors invade neighbouring tissues, and so, the tumour is now termed malignant (Hanahan, 2014). Oncology is the subject area that specialises with the study and treatment of tumours (Chial, 2008).

Globally, 9.6 million people are expected to have died from cancer in 2018, with 1 in 6 deaths being because of cancer (WHO, 2020). In the UK, 1 in 2 people will develop a form of cancer over their lifetime, with over 200 different types having been documented (NHS, 2019). On average, in the UK, between 2015-2017, there were 367,167 new cases of cancer, with 164,901 deaths from 2015-2017. There was a 50% chance of survival for patients diagnosed in 2010-2011 in England and Wales, and 38% of cases in 2015, were preventable (Cancer Research UK, 2020a). Pancreatic cancer had the lowest percentage survival out of all cancer with 5% in 2013-2017 in England and Wales. There were 10,257 new cases of cancer, on average between 2015-2017. There were 9170 deaths from 2015-2017, and 37% of cases were preventable (Cancer Research UK, 2020b).

There were 47,838 new cases of lung cancer, on average, between 2015-2017. There were 35,349 deaths from 2015-2017. There was a 10% survival rate in 2013-2017 in England, and in 2015, 79% of cases were preventable (Cancer Research UK, 2020c). With bowel cancer having 42,317 new cases between 2015-2017, 16,272 deaths from 2015-2017, 53% of survival in 2013-2017 in England, and 54% of cases were preventable (Cancer Research UK, 2020d).

1.1. Cancer chemotherapy

1.1.1. How cancer cells differ from normal cells

Tumour cells contain most of the structures present in an ordinary human cell. Tumours differ from normal tissue by possessing dissimilar subpopulations of cancer cells in the tumour stroma. This, in turn, is made up of immune, endothelial, and mesenchymal stromal cells (MSCs) and fibroblasts. Secretion of vesicles, cytokines and soluble factors by cancer cells can modify the surrounding environment. Cancer-associated fibroblasts (CAFs) are the active form of fibroblasts and are present in the tumour stroma at different states of activation and tissue specialization (Chiarugi & Cirri, 2016).

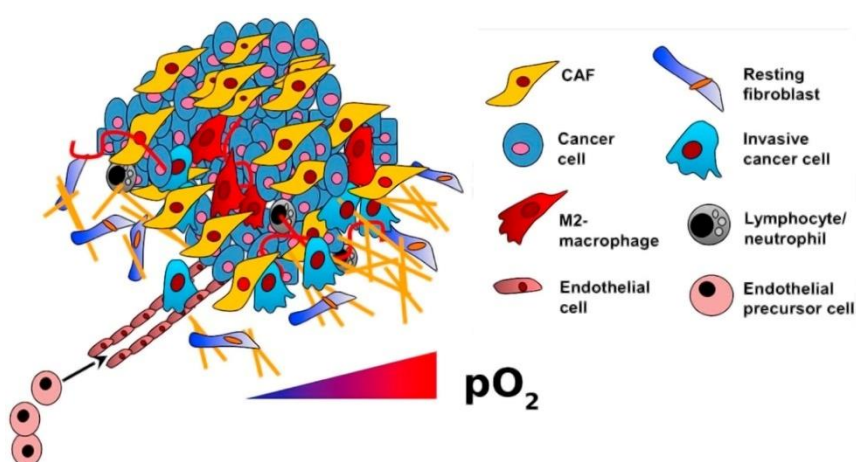


Figure 1: The structure of a typical tumour cell mass with all cell and structure types present in the above legend (Chiarugi & Cirri, 2016).

There are several other aspects which differentiate cancer cells from normal cells. Some of these differences can be exploited to target tumours when designing new therapies. These include the continuous proliferation of cells, the increase in angiogenesis via regional stimulation of blood vessels, invasion of cancer cells into neighbouring healthy cells, vascular and lymphatic metastasis, evasion of cytotoxicity by cells, and inflammatory reactions mediated by tumour cells (Kim *et al.*, 2016). The new blood vessels formed, however, do not resemble the normal, webbed structure, but are more disorganised (Chiarugi & Cirri, 2016).

The environment of a cancer cell is another aspect. The extracellular environment of primary and metastasized tumours has a lower pH than that of normal tissues and blood (Manchun, Dass, & Sriamornsak, 2012). While the intracellular environment is the opposite. The reason for this disparity is due to glucose metabolism in cancer cells. However, because the mitochondria of cancer cells are poorly functioning, they use an alternate mechanism (Chiche *et al.*, 2009).

Glycolysis which takes place in the cell cytoplasm results in the formation of lactic and carbonic acid. These acids are sources of H⁺ ions which concentrations increase to higher than normal levels due to the need for nutrients and oxygen by proliferating tumour cells. The reduced pH also causes hypoxia. All these factors result in an upregulation of glycolysis under both aerobic and anaerobic conditions (Manchun, Dass, & Sriamornsak, 2012). This metabolic reprogramming of each cancer cell from oxidative phosphorylation to aerobic glycolysis is termed the Warburg effect (Shirmanova *et al.*, 2015).

However, this effect produces a lot of acidity via H⁺. Since cancer cells have a low pH in their cytosol, cancer cells have evolved to have many more cell transporters than normal cells. Some of these are the sodium/hydrogen ion transporter (Chiche *et al.*, 2009) which transports protons extracellularly and sodium ions intracellularly. Transporting these protons into the extracellular matrix leads to the low pH. Monocarboxylate 4 (MCT4) transporter, exports lactate, a by-product of glycolysis (Choi *et al.*, 2016).

Another reason for this is due to the abnormal blood circulation in the tumour. Vascular permeability is also higher than in normal cells, leading to lower blood flow rates in tumour vessels, and a longer transit time due to the disorganised blood vessels.

While normal cells have intracellular and extracellular pH values of 7.00-7.20 and 7.30-7.40 respectively, tumour cells have intracellular and extracellular pH values of 7.12-7.65 and 6.20-6.90 respectively (Shirmanova *et al.*, 2015). This necessitates increased rates of angiogenesis to maintain a blood supply to the tumour. Blood arriving can provide more glucose and nutrients for the cancer cells and can take away the lactate removed by MCT4. The reduced pH in the tumour also triggers the activation of matrix metalloproteinases (MMPs) which aid in impairing the immune response (Chiarugi & Cirri, 2016).

Each type of cancer can have varying values of pH in their cells. For breast cancer, between all tumour types, the extracellular pH was on average pH range of 6.78-6.85 in tumour cells. With lung cancer, the average was 6.78-6.88 (Manchun, Dass, & Sriamornsak, 2012). In colon cancer cells, the pH of the lumen in the human colon ranges from 5.50-7.50 (Lan, Lagadic-Gossmann, Lemaire, Brenner, & Jan, 2007).

Another difference in the tumour environment is the amount of oxygen (PO₂). The concentration decreases as you travel further into a tumour mass. This low concentration of oxygen or hypoxic tissue, facilitated by hypoxia-induced factors (HIFs), promotes the activation of the epithelial-mesenchymal transition (EMT) process, which promotes local invasiveness, cancer cell migration and secondary organ establishment (Chiarugi & Cirri, 2016).

Reactive oxygen species (ROS) are chemical species which are associated with carcinogenic potential and with tumour promotion (Irani *et al.*, 1997). Some examples of ROS include superoxide ion (O_2^-), hydroxyl radical ($\cdot OH$), and single oxygen ($O=O$) (Hayyan, Hashim, & Alnashef, 2016). In cancer cells, the regulatory mechanism of ROS is under a greater workload due to the increased respiratory rate (Irani *et al.*, 1997), Warburg effect (Shirmanova *et al.*, 2015) and the malfunctioning of cell mitochondria result in low concentrations of ROS which can facilitate cancer cell survival via tumour growth factors and protein kinases (Irani *et al.*, 1997). Higher concentrations of ROS may suppress tumour growth and induce cell death (Takahashi *et al.*, 2006).

1.1.2. Major drug targets

Ideally, cancer treatments need to be selective in targeting cancer cells. However, chemotherapy treatments use a systemic approach, targeting a cell's division mechanisms. This results in the targeting of cancer cells, but also actively dividing healthy cells as well. Targeted therapies are more localised in their treatment. They are used on driver mutations which could have caused/could cause cancer (Hanahan, 2014). However, care must be taken as cancer cells can become resistant, often re-emerging on a larger scale and in more aggressive growths (Hanahan, 2014). To target specific processes which are specific to some cancers, rather than general cell divisions, for example, tyrosine kinase inhibitors (Glivec) which target a mutated Abl kinase, overexpressed enzymes or receptors. The method enables a selective effect on the tumour and not on normal dividing cells (Wu, Chang, & Huang, 2006).

Treatments in development can target one part of the cancer cell, for example, anti-cancer drugs focus on proliferation by using molecular targets in the cancer cell. Some of these targets are phosphatase and tensin homolog PTEN, mammalian target of rapamycin mTOR kinase (Kim *et al.*, 2016) or oncogene proteins which regulate proliferation (Chial, 2008). Both pRb and p53 suppress proliferation and apoptosis (Kim *et al.*, 2016). These differences have aided research in developing novel treatments which target said cells, without risking harm to healthy tissue.

Model compounds which have the same functional groups as their full-scale counterparts will be tested. This will be done before moving on to the full-scale counterparts. Several major anticancer drug targets are the first line of treatment for several types of cancers and they are discussed below.

1.1.3. Standard chemotherapy agents

Chemotherapy uses drugs (i.e. chemicals, hence “chemo” therapy) and many standard chemotherapy drugs are given either intravenously in treatment cycles, intrathecally, subcutaneously or orally. These cytotoxic drugs constitute a systemic therapy and aim to disrupt the mechanisms of rapidly dividing cells during cell division or protein synthesis. This aims to prevent new cancer cells from forming and metastasis from occurring (Nagai & Konishi, 2013). The role of these drugs has varied since their discovery, from the use as one form of anti-cancer treatment, to their use in conjunction with surgery and adjuvant treatments (DeVita & Chu, 2008). Some of the examples listed below are traditional drugs.

1.1.3.1. Doxorubicin

Doxorubicin, an anthracycline derivative, is part of a group of medicines which target the topoisomerase II enzyme (Nagai & Konishi, 2013). Doxorubicin enters cells via endocytosis or carrier-mediated transport via ABCB1 (Nagai & Konishi, 2013), also known as p-glycoprotein (P-gp) (Gottesman, Fojo, & Bates, 2002) and either is metabolised or enters the nucleus. Once inside the nucleus, molecules of doxorubicin intercalate with strands of DNA, causing disruption to topoisomerase-II-mediated DNA repair (Thorn *et al.*, 2011). This, in turn, causes DNA strands to be tightly wound, and unable to take part in cell proliferation, resulting in cell death (Nagai & Konishi, 2013). Intercalation would also cause DNA replication, RNA and protein synthesis to not occur (Gupta, Sung, Prasad, Webb, & Aggarwal, 1976). Metabolism of doxorubicin leads to the formation of ROS that in turn causes lipid peroxidation, cellular membrane, protein and DNA damage, oxidative stress and the initiation of apoptotic pathways (Thorn *et al.*, 2011).

It is commonly used to treat acute leukaemia lymphomas, stomach, breast and ovarian cancers, Kaposi’s sarcomas and bone tumours (Nagai & Konishi, 2013). Doxorubicin is given intravenously and can be in combination with other chemotherapy drugs. The maximum recommended cumulative dose is 450 mg m⁻², over a treatment period. Precautions need to be taken in case side effects occur. These include an increased risk of myocardial infarction, alopecia, nausea or myelosuppression (NICE, 2019a).

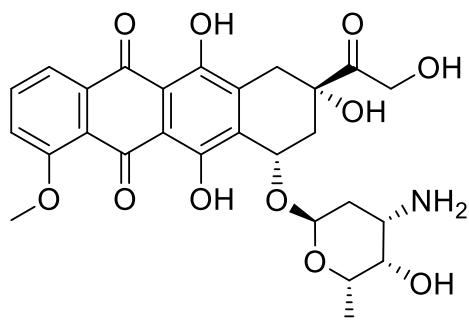


Figure 2: The structure of doxorubicin.

1.1.3.2. Epirubicin

Epirubicin, a chiral isomer of doxorubicin, is also an anthracycline derivative with the same mechanism of action (Bonfante, Bonadonna, Villani & Martini, 1980). The maximum cumulative dose is 900 mg m^{-2} , and it has the same side effects of doxorubicin (NICE, 2019b).

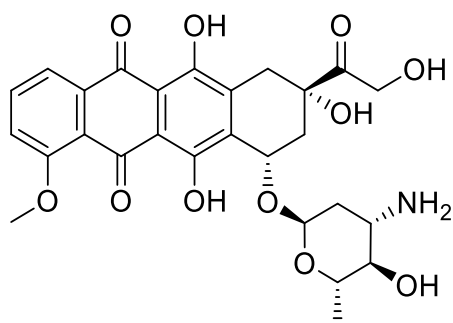


Figure 3: The structure of epirubicin.

1.1.3.3. Paclitaxel

Taxanes are natural occurring microtubule-stabilizing anticancer agents with paclitaxel being the most common. Paclitaxel binds to tubulin and inhibits the disassembly of microtubules (Rangel, 2013 & NICE, 2019c) by preventing the formation of spindle fibres during mitosis. By the inhibition of the normal promotion of β -tubulin polymerisation, these microtubules are frozen in place, preventing mitosis from continuing and leading to cell apoptosis. This, in turn, results in no cell division. Paclitaxel also blocks the function of the apoptosis inhibitor protein, Bcl-2, found in B-cell leukaemia 2 (Rangel, (Ed.), 2013). Paclitaxel is used to treat ovarian and breast cancers, metastatic ovarian and breast cancers, adenocarcinomas of the pancreas and non-small cell lung cancer, all by intravenous infusion. Usually, paclitaxel is co-administered with carboplatin or cisplatin when treating ovarian cancer. Common side effects range from myelosuppression, alopecia, muscle pain, nausea and vomiting (NICE, 2019c).

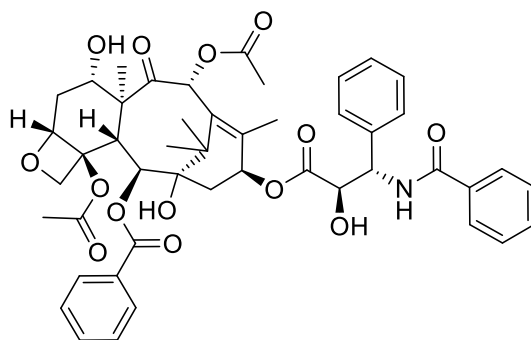


Figure 4: The structure of paclitaxel.

1.1.3.4. Methotrexate

Methotrexate is an antimetabolite which acts as a high-affinity substrate for the enzyme, dihydrofolate reductase (NICE, 2019d). This excludes the natural substrate, folic acid and prevents the formation of tetrahydrofolate, a substrate for the synthesis of thymidylate. This, in turn, is used in the synthesis of purines and pyrimidines (Rangel, 2013). It is used to treat choriocarcinoma, non-Hodgkin's lymphoma and other solid cancer tumours. It has the same main side effects as other chemotherapy drugs, including leukopenia, abdominal distress and oral disorders, among others (NICE, 2019d).

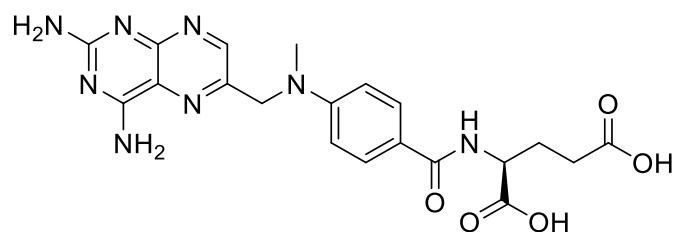


Figure 5: The structure of methotrexate.

1.1.3.5. Fluorouracil

Fluoropyrimidine 5-fluorouracil (5-FU) is an analogue of uracil with a fluorine atom on carbon 5. Entering the cell via facilitated transport, it is converted intracellularly to active metabolites: fluorodeoxyuridine monophosphate (FdUMP), fluorodeoxyuridine triphosphate (FdUTP) and fluorouridine triphosphate (FUTP) (Longley, Harkin, & Johnston, 2003).

FdUMP, FdUTP and FUTP disrupt RNA synthesis and the action of thymidylate synthase (TS). The enzyme dihydropyrimidine dehydrogenase (DPD) which converts 5-FU to dihydrofluorouracil, DHFU. TS catalyses the reductive methylation of deoxyuridine monophosphate (dUMP) to deoxythymidine monophosphate (dTMP) with reduced folate 5,10-methylenetetrahydrofolate (CH_2THF). The 5-FU metabolite FdUMP binds to the nucleotide binding site on TS. Forms a complex with TS and CH_2THF . This blocks the binding of the normal substrate dUMP and inhibiting dTMP synthesis. FdUMP becomes incorporated into strands of RNA, thereby inhibiting protein translation. This results in the inhibition of cell proliferation (Longley, Harkin, & Johnston, 2003).

It is used to treat a variety of solid cancer tumours, including colorectal, gastrointestinal and breast cancers. Side effects are also like other chemotherapy drugs, but also include, arrhythmia, agranulocytosis and malaise, among others (NICE, 2019e).

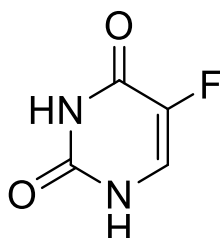


Figure 6: The structure of fluorouracil.

1.1.3.6. Microtubule-target agents

Microtubule-target agents (MTAs) are a group of drugs which target the α - β -tubulin heterodimers and associated proteins which make up a cell's cytoskeleton. MTAs take part in the maintenance of the cell structure, formation of spindle fibres during mitosis and protein transportation, there are essential. MTAs are used to target solid tumours and haematological cancers. For example, vincristine and other vinca alkaloids cause depolymerisation, suppress the dynamic stability of these polymers and block mitotic progression which leads to cell apoptosis (Rangel, (Ed.), 2013).

Vincristine was derived from the Madagascan periwinkle that binds to tubulin, prevent metaphase from occurring in actively dividing cells. Based on this, vincristine cytotoxicity was observed in a broad spectrum of cancer cells including leukaemias, small cell and non-small cell lung cancers, colon, central nervous system, melanoma, ovarian, renal, prostate and breast carcinomas (Waterhouse et al., 2005).

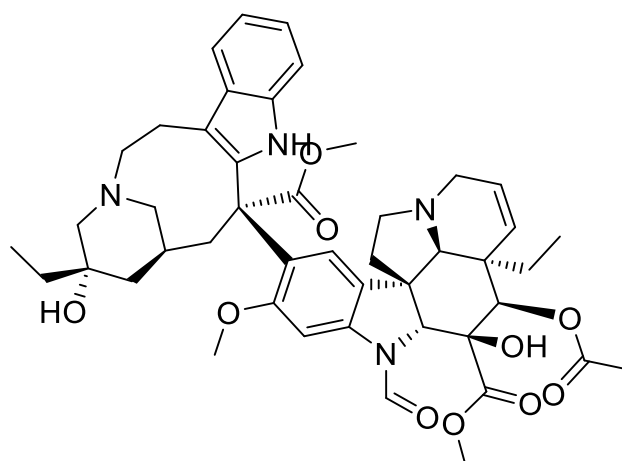


Figure 7: The structure of vincristine.

1.2. Resistance

1.2.1. The issue of resistance

Tumours are widely known to develop multi-drug resistance (MDR) to treatments. This can make treatments longer, difficult and more expensive (Roast, 2015). It lowers the overall efficacy of treatment and causes severe systemic toxicity (Gottesman et al., 2002). There are several ways in which a cancer cell can develop resistance to treatment. Firstly, as mentioned before, the pH of cancer cells is lower and more varied. A lower level of intracellular pH allows for cell proliferation to take place, as well as the evasion of apoptosis and the Warburg effect. The Warburg effect, as mentioned before, is the metabolic switch from oxidative phosphorylation to aerobic glycolysis. Possible effects of lower levels of pH are promoting genetic instability in addition to MDR (Shirmanova *et al.*, 2015).

A final type of multi-drug resistance was observed with methotrexate-resistance cells. Gene amplification was observed with the dihydrofolate reductase gene (Matsui, Ihara, Suda, Mikami, & Semba, 2013). As mentioned before, methotrexate acts as a high-affinity substrate for the enzyme dihydrofolate reductase, but with resistant cells, increased transcription of this gene results in cells which are not affected by methotrexate.

Enhanced DNA repair is another example which was shown in cisplatin-resistant cells. Increased amounts of the nuclear protein XPE-BF increased the rate of DNA repair from overexpression of the gene for XPE-BF (Luqmani, 2005). This directly affects the development of resistance to anti-cancer drugs. CAFs could enhance cancer mechanisms to increase the rate of oxidative phosphorylation to supply nutrients and maintain levels of proliferation. A reason which may benefit researchers to develop a drug compound for this target is that targeting non-neoplastic cells using a pharmacological agent may be able to bypass the common route in classic therapy resistance (Chiarugi & Cirri, 2016).

1.2.2. Drug efflux: Mechanisms and types of pumps

The environment is filled with substances which are detrimental to us. Whilst our immune systems are the primary defence at the holistic level; our cells have defensive mechanisms in place to eliminate undesired substances. One such way is the use of specialized cell membrane pumps which can efflux toxins outside of a cell for safe disposal (Aller et al., 2009). Normally, the desired drug would enter the tumour mass via the bloodstream, to inhibit cell proliferation. With the onset of drug resistance however, drugs can be pumped out of the cells by efflux pumps, thereby preventing treatment (Mu *et al.*, 2017 & Kim *et al.*, 2016). This occurs due to overexpression of gene which codes for certain cell pumps, for example, ABCB1, or P-gp, to increase the rate of drug efflux out of the cell. This will be discussed later. One adaptation a cancer cell makes is by overexpressing genes corresponding to cell transporters. This can add to existing levels of cytotoxicity of chemotherapy drugs in normal cells (Nagai & Konishi, 2013).

Drug receptors play an important role in the pharmacokinetics of several drugs and the resulting regulatory aspects. From the early developmental stages in an embryo to controlling the flow of substances in and out of cells. With the roles of some transporters having been elucidated, this helps to understand the effects of agonists, inhibitors, and substrates on them. Pharmacological and clinical data have shown that drug transporters handle a diverse set of drugs and toxins (Nigam, 2014).

Drugs can interact with a variety of transporters, for example, methotrexate acts on ABCC1, ABCC2, ABCC3, ABCC4, ABCC5 and ABCG2 for the ATP-binding cassette (ABC) the family of transporters. Also, it acts on SLC22A6, SLC22A8, SLC22A11, SLCO1A2, SLCO1B3 for the solute carrier (SLC) the superfamily of transporters. They are also located all over the body, for example, SLC22A6 is in the kidney and choroid plexus, SLC22A8 is in the kidneys, choroid plexus and testes, and SLC22A11 is found in placenta and kidneys. With SLC22A6 and SLC22A8 controlling the flow of metabolites, drugs and toxins (simple gene-knockout showed mice had altered renal urate clearing) (Nigam, 2014).

1.2.2.1. P-glycoprotein (P-gp)

P-gp or multidrug resistance protein (MDR1/ABCB1) (Gottesman *et al.*, 2002) is a cell membrane protein which is part of the ABC transporter family (Lin & Yamazaki, 2003). It is also the human multidrug resistance protein with the most research carried out (Cholkar, Dasari, Pal, & Mitra, 2013).

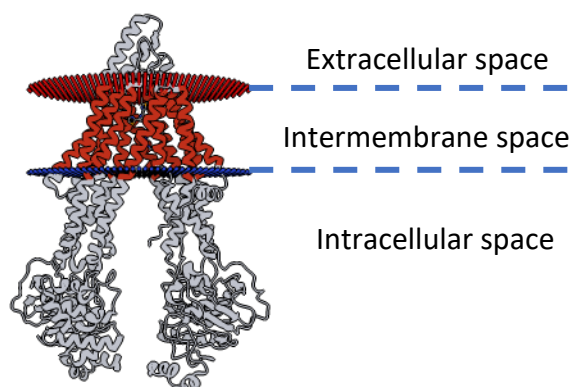


Figure 8: A transmembrane view of P-glycoprotein (P-gp) (Aller *et al.*, 2009).

P-gp is responsible for forcing toxins and xenobiotics out of a cell via exocytosis. It acts as a defence mechanism which controls the flow of endogenous and exogenous substances in a cell. When a substrate enters this pump, either via an opening in the inner leaflet of the membrane or the cytoplasmic side. ATP binds to the cytoplasmic side, ATP hydrolysis shifts the substrate into a position for exocytosis. Following this, a phosphate molecule is released. ADP is then released, following the binding of ATP to a secondary binding site, this rests the protein for the process to start again (Gottesman *et al.*, 2002).

It is highly expressed in the hepatocytes, and the epithelial cells of the intestine, placenta, capillaries of the brain and proximal tubules of the kidney. The structure of P-gp consists of two homologous and symmetrical halves (cassettes), each containing six transmembrane domains. An intracellular polypeptide linker loop with an ATP-binding motif separates these domains (Lin & Yamazaki, 2003).

Consequently, P-gp needs to be very efficient in its role, with the need to identify many different types of molecules and efflux ones which are harmful (Aller *et al.*, 2009). Substrates which bind to this transporter are typically hydrophobic; it contains one substrate binding site and two ATP-binding domains. Compounds with a molecular weight ranging from 250 to 1202 can bind. The larger the lipophilicity and number of hydrogen bonds on the substrate, the more likely it can bind to the transporter (Lin & Yamazaki, 2003). This means that the efflux effect can be beneficial or harmful depending on the effectiveness of medicine taken (Aller *et al.*, 2009).

When a drug is present, stimuli, in turn, may cause overexpression of ABC transporters, mediating an efflux of the desired drug. Stimuli due to a drug may also, after DNA repair, lead to a further increase in cytochrome P450 function and reduction in cell apoptosis (L. M. Mu *et al.*, 2017).

1.2.2.2. Monocarboxylate transporters (MCTs)

MCTs are a family of proton linked cell membrane transporters, present in a wide range of tissues in the body, which contain 12 transmembrane domains. They transport molecules across membranes that possess one carboxylate group, examples include lactate, pyruvate and ketone bodies. Transport of lactic acid across the cell membrane via MCTs helps to regulate cell metabolism and pH by its' removal. MCTs are very important with regards to cancer cells. The Warburg effect necessitates efflux of the resulting lactic acid to prevent a toxic environment for the tumour. The mechanism is as follows, a proton binds, followed by L-lactate, which in turn induces a conformational change, leading to the translocation of this substrate across the cell membrane. This is followed by the release of lactate and a return to its' rest state (the substrate-binding site returning to its' extracellular position) (Halestrap & Meredith, 2004).



Figure 9: Structure of the human MCT-1 complex (EBI, 2020a & Lomakin, Dmitriev, & Steitz, 2019).

1.2.2.3. Multidrug resistance proteins (MRPs)

MRPs are a subclass of the ATP binding cassette family of proteins. MRPs consist of MRP1 (ABCC1), MRP2 (ABCC2), MRP3 (ABCC3), MRP4 (ABCC4), MRP5 (ABCC5) and MRP6 (ABCC6). MRPs are present all tissues with some subtypes being present in more tissues than other, example MRP2 in the liver, kidneys and intestines or MRP6 in the liver and kidneys (Gottesman et al., 2002). MRP1 transports methotrexate relatively well but not paclitaxel. It has the propensity to substrates which are organic anions, e.g. drug conjugated to glutathione or sulphate compounds. MRP2 transports a wide range of anticancer agents such as vincristine, doxorubicin and cisplatin. In overexpressed cancer cells with MRP2, the transport became resistant to these agents (Borst, Evers, Kool, & Wijnholds, 2000).



Figure 10: Structure of human MRP1 complex (EBI, 2020b & Ramaen et al., 2006).

1.2.2.4. Breast cancer receptor protein (BCRP)

BCRP is encoded by the ABCG2, and it is also part of the ATP binding cassette family of proteins responsible for transmembrane transport. This means its function is dependent on ATP binding. It is located in the placenta, intestine, breast and liver (Gottesman et al., 2002).

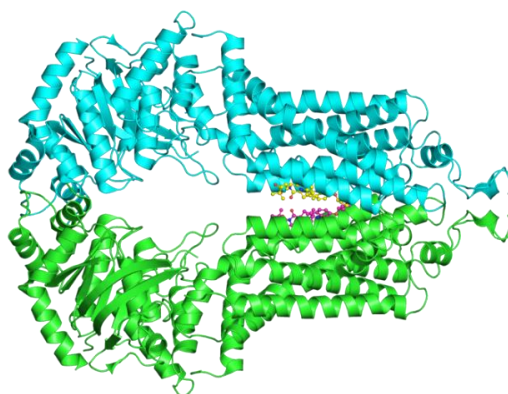


Figure 11: Structure of human BCRP with bound inhibitor (EBI, 2020c & Jackson et al., 2018).

1.2.3. Efflux pump inhibitors

1.2.3.1. Inhibitors of P-gp

The number of P-gp transporters, and the rate of drug efflux both increase as a response to drug resistance. There are several known inhibitors of this transporter which can limit or even halt this undesirable effect. Several drugs which were developed for a specific use, have been found to inhibit P-gp. Three examples of these are verapamil, cyclosporine A and nifedipine. Verapamil, a first-generation inhibitor of P-gp, was found to increase the intracellular concentrations of anti-cancer drugs. *In-vitro* studies were found to be pharmacologically active in the range of 1-50 μ M. Serum concentrations of similar values could cause immunosuppressive and cardiovascular effects (Abdallah, Al-Abd, El-Dine, & El-Halawany, 2015).

Over time more modifications were made to chemical structures to lessen cytotoxicity and improve efficacy. Dexverapamil, the *R*-enantiomer of verapamil, was found to be more potent, and have less cardiovascular toxicity than first-generation P-gp inhibitor analogues (Abdallah *et al.*, 2015).

Norverapamil is a phase 1 metabolite of verapamil (Pauli-Magnus *et al.*, 2000), the calcium channel blocker (Pubchem, 2019) and first-generation P-gp inhibitor (Zhang & Ma, 2010). Verapamil, by blocking calcium channels, treats hypertension, angina pectoris and supraventricular tachyarrhythmias (Pubchem, 2019). However, due to cardiovascular cytotoxic effects, it would not be suitable for medical use as an EPI. So, using a structural analogue with less toxicity would be beneficial. Norverapamil had an inhibitory potency of $IC_{50} = 0.3 \mu$ M and this exceeded that of verapamil, $IC_{50} = 1.1 \mu$ M in P-gp-mediated digoxin transport in Caco-2 cells (Pauli-Magnus *et al.*, 2000).

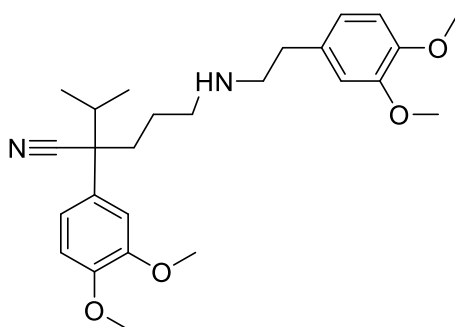


Figure 12: The structure of norverapamil.

A drug which is found to have marked success in limiting anti-cancer drug resistance is Tariquidar. This drug non-competitively binds to P-gp, causing the inhibition of transmembrane transport of anti-cancer drugs. However, this inhibition can increase intracellular concentrations of the cytotoxic drugs in normal cells due to these drugs targeting every P-gp channel in the body, adding to existing cytotoxicity (Patil, Sadhukha, Ma, & Panyam, 2009). Tariquidar and docetaxel have been in clinical trials in the US. These have given promising results and should lead to more efficacious treatments (NIH: NLM, 2012). As mentioned before, MDR can lead to overexpression of P-gp among other transports (Nagai & Konishi, 2013). This leads to free cytotoxic agents near healthy tissues which adds to existing cytotoxicity (Kuruville, Tiruchinapally, ElAzzouny, & ElSayed, 2017). This is in addition to the cytotoxic agents' cytotoxicity (NICE, 2019a & NICE, 2019b).

1.2.3.2. Inhibitors of MCTs

AZD3965 is an inhibitor of MCT1 which aims to modulate lactate transport to kill cancer cells reliant on glycolysis (Polanski et al., 2014). Inhibitors of MCT1 include aromatic monocarboxylates like phenyl-pyruvate or α -cyano-4-hydroxycinnamate (CHC) with K_i values of 50-500 μ M. Bioflavonoids such as quercetin and phloretin have $K_{0.5}$ of 1-10 μ M. 4,40-dibenzamidostilbene-2,20-disulphonate (DBDS) and 4,40-diisothiocyanostilbene-2,20-disulphonate (DIDS) also inhibit MCT1. CHC, DBDS and DIDS are also inhibitors of MCT2 (Halestrap & Meredith, 2004).

1.2.3.3. Inhibitors of MRPs

Inhibitors of MDR1 P-gp have a low affinity for MRP1 and MRP2. Inhibitors of MRPs include an analogue of cyclosporin A, PSC833, a carboxamide derivative GG918, leukotriene C4 and S-decylglutathione. However, inhibitors of MRP1 are not good inhibitors of MRP2, Sulfipyrazone does not inhibit the transport of dinitrophenyl S-glutathione (Borst, Evers, Kool, & Wijnholds, 2000).

1.2.3.4. Inhibitors of BCRP

Inhibitors of BCRP include fumitremorgin C (FTC) which was found to be neurotoxic in animals and patients, Ko143 (an analogue of FTC) which safe in mice, pantoprazole (is the most promising), elacridar (also a good inhibitor of P-gp), CI1033, gefitinib and quercetin. These may be beneficial to be co-administered with anti-cancer drugs, to improve oral bioavailability or to improve CNS penetration of these drugs (Breedveld, Beijnen, & Schellens, 2006).

1.3. Drug delivery

1.3.1. Ways of improving the delivery of drugs to tumours

The most used strategy for overcoming multi-drug resistance is the use of combination therapies. The rationale behind this approach is using a combination of different drugs which a tumour is susceptible to, which target several molecular pathways, and can lead to a more efficacious outcome (Luqmani, 2005).

A well-known fact of chemotherapy is the problem of MDR and cytotoxicity. One-way cytotoxicity can be reduced, is using liposomes. Liposomes, which are present in every cell, are comprised of a phospholipid vesicle, with single or multiple lipid bilayers. For nanoscale drug carriers, liposomes are biodegradable, and they have low toxicity. The purpose of drug carrier liposomes is to extend the effect of the drug, as well as provide necessary efficacy. These liposomes can contain an anticancer drug with an MDR inhibitor and can limit drug efflux of all ABC transporters. Liposomes could also be beneficial in novel treatments by eradicating cancer stem cells, stimulating apoptosis and regulating autophagy (L. M. Mu *et al.*, 2016).

Another method by which MDR and cytotoxicity can be minimized is by using nanotechnology. Nanotechnology is readily used in drug treatments as it can target more areas than traditional methods and make it easier to control drug release by avoiding biological barriers to reach intracellular drug targets. Nanoparticles are very beneficial to anti-cancer treatment; they can improve permeability and retention of drugs in solid tumours. They can be made to respond to a certain type of stimulus for drug release. For cancer treatment, pH, levels of oxygen, glucose or even inflammation can be made, they are then termed 'smart' nanomaterials. Designing a drug delivery system using a pH-sensitive nanomaterial could aid in the reduction of cytotoxicity. Using a trigger for release, for instance, the introduction of ionizable chemical groups like amines, carboxylic acids (Liu *et al.*, 2014).

This can lead to acceptance or loss of protons depending on the pH, and lead to swelling ratio or solubility, triggering drug release. There also reactions using polymers, for instance, using polymethacrylic acid (PMAA), with an attached polyethylene oxide (PEO) molecule, with a cross-linked polyanion core can be pH-sensitive and has been used to administer doxorubicin. PMAA and other pH-sensitive polymers, like some nanomaterials, are also termed 'smart' (Liu *et al.*, 2014).

An alternate way to overcome anti-cancer drug resistance is by modifying the delivery of the drug to the tumour. This can be done by using molecular linkers to combine a ligand or peptide with the desired drug, thus forming a conjugate or pro-drug (Chen *et al.*, 2017).

1.3.2. How a low pH in cancer cells can be a drug target

Several mechanisms differ from normal cells which cause different conditions. With cancer cells due to the Warburg effect, having a low pH environment due to glycolysis, this provides a differentiating factor between these cells and normal cells. Molecules called linkers, can 'link' an existing anticancer agent and another molecule which improve the efficacy of this agent. If a linker could release its' contents when entering the low pH environment, this could provide selective release. This was shown by multiple studies but initially with Shen and Ryser in 1981. Daunorubicin was released from the ADM-poly(D-lys) conjugate in the unaltered form inside the lysosomes. The pH-mediated release was observed from pH 4.00 to 6.00 with both daunorubicin and N-methyl daunorubicin (Shen & Ryser, 1981).

The following example shows how exploiting a low pH, with a delivery system, and a drug can provide more alternative treatments for cancer. A paper by Zhao *et al.* in 2016, highlighted the importance of H₇K(R₂)₂, a tumour-specific pH-responsive peptide, as a valid drug target. Liposomes sensitive to pH have been indicated as a possible vehicle for drug compounds which would then trigger a release of the encapsulated drug, in this low pH environment. In this case, they used doxorubicin (DOX) release, with the ligand complex of DOX-PSL- H₇K(R₂)₂ in C6 tumour (glioma or nervous system tumour) and U87-MG orthotopic tumour bearing mice. Both groups showed signs of reduced anti-tumour and antiangiogenic activity.

1.3.3. Type of linkers

1.3.3.1. The *cis*-aconityl linker

The *cis*-aconityl linker, a derivative of the naturally occurring, *cis*-aconitic acid, has a carboxylic acid in the *cis* or Z position (i.e. the *cis* or Z isomer), on carbon 4. When this molecule is in a low pH environment, this linker undergoes acid-catalyzed hydrolysis of the carboxylic acid moieties of the carbons 1 and 6. Depending on the moiety conjugated, either hydrolysis of an amide or ester bond can occur (Liu *et al.*, 2014).

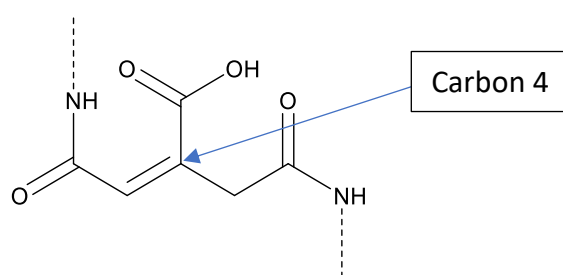


Figure 13: The structural formula of the *cis*-aconityl linker. This was drawn using ChemDraw Professional 16.

The *cis*-aconityl linker is acid-labile at a pH of 6 or less, meaning the drug complex should be stable in the pH of the bloodstream. As a result, rapid drug release under acidic conditions favours targeted delivery of anti-cancer drugs (Du *et al.*, 2013). The drug conjugate would enter the cancer cell by P-gp (Gottesman *et al.*, 2002) or via exocytosis (Thorn *et al.*, 2011). The endosome would reach the endosomal compartment of (Kakinoki, Kaneo, Ikeda, Tanaka, & Fujita, 2008) the cancer cell (Du *et al.*, 2013), and the *cis*-aconityl spacer would release the drug and EPI in this compartment (Kakinoki *et al.*, 2008). Following intramolecular amide or ester bond hydrolysis inside the cell, the desired compounds should then be released (Du *et al.*, 2013). This was shown in a paper by Shen and Ryser in 1981 where daunomycin polymer *cis*-aconityl linker conjugates caused 90% inhibition of cell growth in WEHI-5 cells. The linker had a half-life hydrolysis of 3 hours at pH 4.00 and 96 hours at pH 6.00 or higher.

Kuruvilla, Tiruchinapally, ElAzzouny and ElSayed in 2017 used targeted delivery of doxorubicin polymer poly(amidoamine), PAMAM, conjugates to observe the effects on unmodified or free doxorubicin cytotoxicity and metabolomics on hepatic carcinomas. Using the NAcGal β targeting ligand conjugated to the acid-labile *cis*-aconityl linkage with polyethylene glycol (PEG), receptor-mediated endocytosis occurred. The *cis*-aconityl linkages present were hydrolysed in the cancer cell's endosomes. Shedding of the PEG brush then occurred with the release of the conjugate into the cytoplasm as shown in figure 14. Flow cytometry studies showed 100% uptake of doxorubicin dendrimer conjugates. Metabolomics identified doxorubicin metabolites rather than free doxorubicin. Free doxorubicin reduced glycolysis and increased fatty acid oxidization. Conjugates also increased the rate of glycolysis.

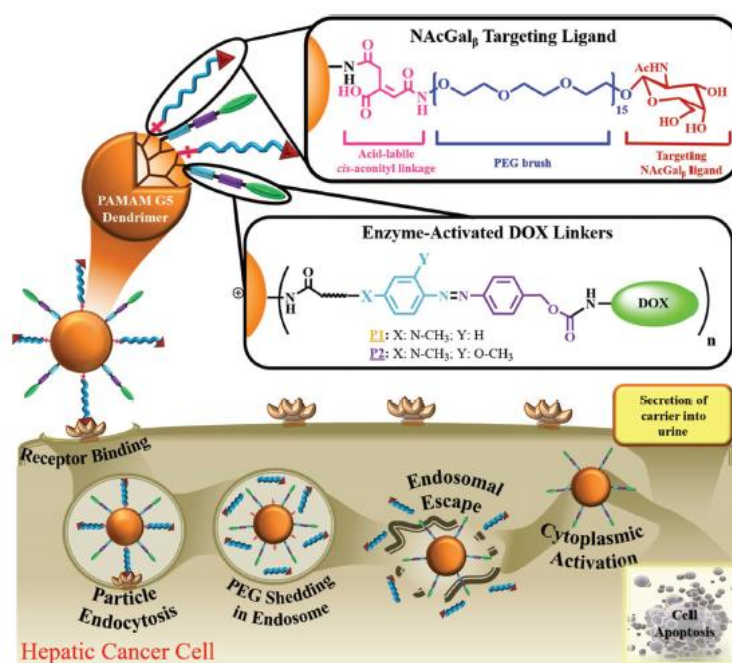


Figure 14: The usage of a *cis*-aconityl linkage, as part of the N-acetylgalactosamine targeting ligand with enzyme activated DOX linkers entering the hepatic cancer cell via endocytosis (Kuruvilla et al., 2017).

In a preliminary study by Srinophakun and Boonmee in 2011, a molecular model of a drug release mechanism using doxorubicin-conjugated glycol chitosan via a *cis*-aconityl linkage was made. It aimed to investigate a possible drug release mechanism using a *cis*-aconityl linkage to improve the interaction between the anti-cancer drug and a polymer. Using the present pH differences between a healthy cell and a cancer cell, the complex would release doxorubicin (or the prodrug as in this case), into the target area. In acidic cancer cells, doxorubicin will be cleaved off, forming a glycol chitosan-aconityl cation and water. However, in normal cells, a higher pH would result in doxorubicin and glycol chitosan-aconityl complex. Under acidic conditions, glycol chitosan would then form 2-glucosamine and ultimately, forming 1-glucosamine, 1-glucosamine cation and water. In a normal pH, 2-glucosamine would form 2 molecules of 1-glucosamine. All reactions above, have a transition state, as the pH reaches the desired level, it will form the products. Then the glycol chitosan carrier was degraded, and doxorubicin released.

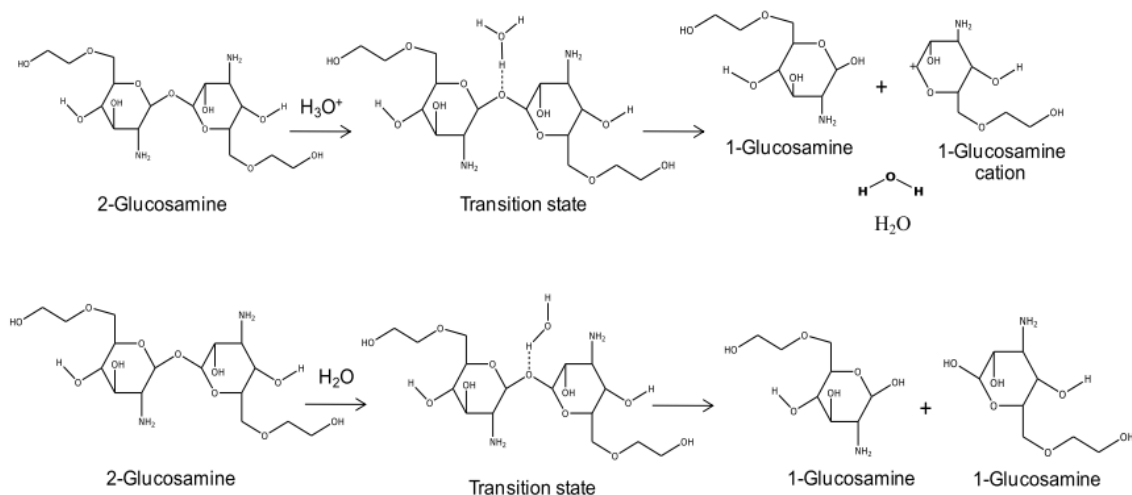


Figure 15: The proposed glycol chitosan degradation mechanism in acid and normal conditions (Srinophakun & Boonmee, 2011).

In this example, in a patent by Hawaii Biotech, inc, in 2004, the reaction of astaxanthin and *cis*-aconitic anhydride with DIPEA was carried out. This resulted in the formation of mono and di ester linker conjugates.

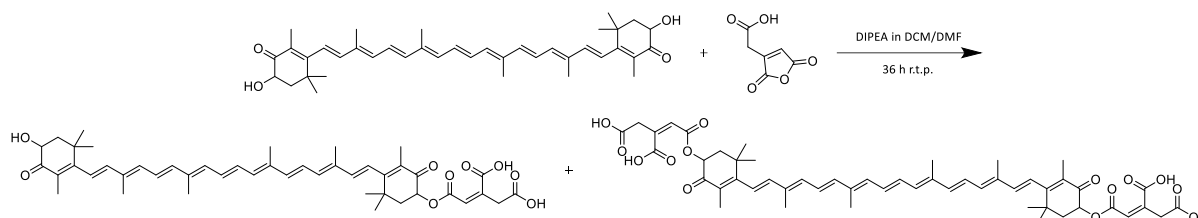


Figure 16: Reaction of *cis*-aconitic anhydride with astaxanthin. This was drawn using ChemDraw Professional 16.

It might be beneficial to look at aromatic amine conjugation as there is more literary precedence. In a study by Dinand, Zloh and Brocchini in 2002, was with *cis*-aconitic anhydride and an aromatic amine.

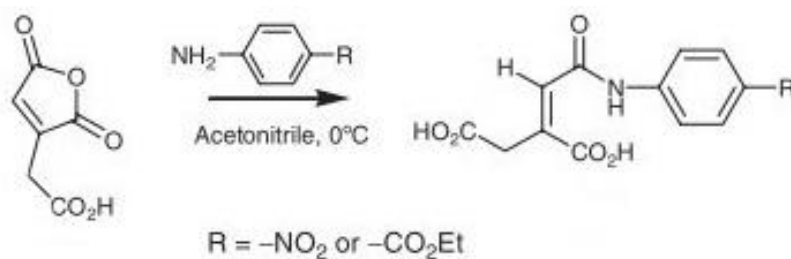


Figure 17: Reaction of *cis*-aconitic anhydride with an aromatic amine forming the resulting amide conjugate (Dinand, Zloh, & Brocchini, 2002).

1.3.3.2. The hydrazone linker

The hydrazone linker is a pH-dependant linker, like the *cis*-aconityl linker which can be conjugated to a possible aldehyde or ketone group on several anticancer drugs. While they are usually not acid-labile at physiological pHs, they are cleaved at lower pH ranges of less than 5.00. However, at more than 6, the drug of conjugate hydrolysis is reduced (Hassanzadeh, Atyabi, & Dinarvand, 2018).

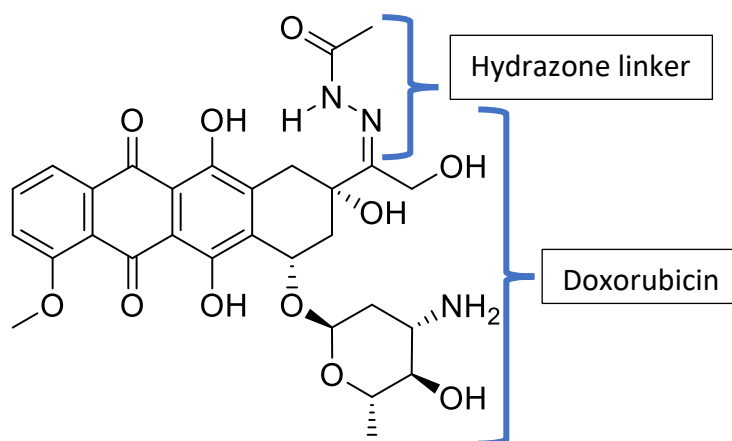


Figure 18: The hydrazone linker conjugated to doxorubicin (Prabaharan, Grailer, Pilla, Steeber, & Gong, 2009). This was drawn using ChemDraw Professional 16.

In a study by Ulbrich, Etrych, Chytil, Jelínková, & Říhová in 2003, pH-release studies showed that the aconityl conjugates released doxorubicin at a slower rate than the hydrazone conjugates. But hydrazone conjugates are more toxic. With hydrazone conjugates usually being cleaved at pH value of 5 in either endosomes or lysosomes but being stable in the bloodstream (pH 7.40). *Cis*-aconityl conjugates as stated before are also stable in the bloodstream but undergo bond hydrolysis about the *cis* positioned hydroxyl group at pHs of 6.50 and less.

Another example of using a linker involved the use of a peptide and a linker to treat osteoarthritis. Hyaluronic acid is used to provide viscoelasticity in synovial fluid via injections into a knee joint. Oral methotrexate has an anti-inflammatory effect but also has cytotoxic effects. Using a linker system for release, the aim was control inflammation and reduce the cytotoxic effect of oral methotrexate. The conjugate formed was methotrexate conjugated to a peptide chain with 4,7,10-trioxa-1,13-tridec-anediamine (PEG13) and hyaluronic acid. The peptide chains used were Gly-Phe-Leu-Gly or Asn-Phe-Phe (glycine (Gly), phenylalanine (Phe), leucine (Leu), and asparagine (Asn)). The peptide chains were cleaved by lysosomal enzymes cathepsins B, D and L (Homma et al., 2009).

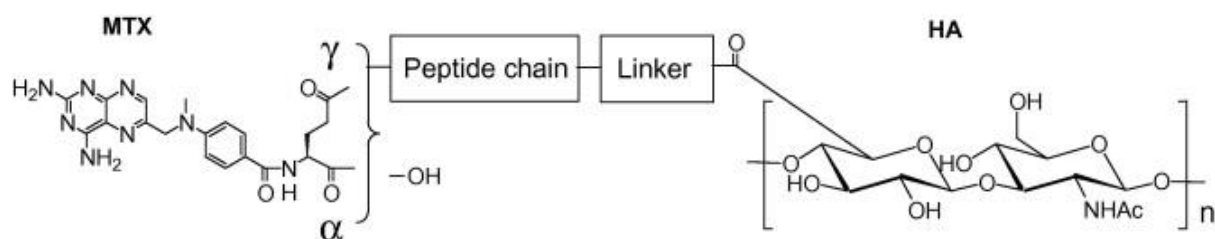


Figure 19: The structure of the methotrexate (MTX), hyaluronic acid (HA) conjugate (Homma et al., 2009).

1.3.3.3. The orthoester linker

An orthoester is a functional group that has three alkoxy groups attached to one carbon atom the degrades to form a ketone and hydroxide ion. It has the longest history with the first study being carried out in 1970 (Liu et al., 2014).

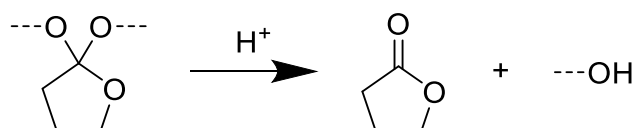


Figure 20: The orthoester linker showing the linker and then its' degradation products. This was drawn using ChemDraw Professional 16.

A study used hydrophilic PEG and hydrophobic poly(γ -benzyl L-glutamate) (PBLG) conjugates which became an amphiphilic block copolymer containing the orthoester linker. This the aim of selectivity releasing hydrophobic drugs in mildly acidic conditions. *In vitro* cytotoxicity studies found Dox-loaded pH-sensitive micelles showed higher toxicity of SCC7 cancer cells that Dox-loaded micelles without the linker, shown in figure 21 (Thambi, Deepagan, Yoo, & Park, 2011).

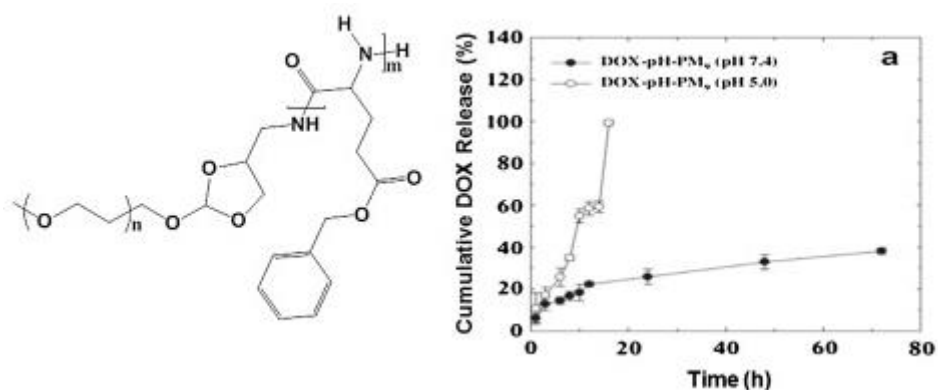


Figure 21: Showing a greater cumulative percentage of Dox loaded micelles at pH 5.0 than pH 7.4 (Thambi, Deepagan, Yoo, & Park, 2011).

Another study used paclitaxel orthoester PEG-acid labile micelles copolymer conjugates. These cross-linked micelles showed paclitaxel release at mild pH conditions, as compared to normal physiological conditions, shown in figure 22. With the rate of hydrolysis being dependent on the mild conditions and occurring at a faster rate. No cytotoxicity was found for the cross-linked micelles at a concentration as high as 800 mg L⁻¹ (Yuan et al., 2011).

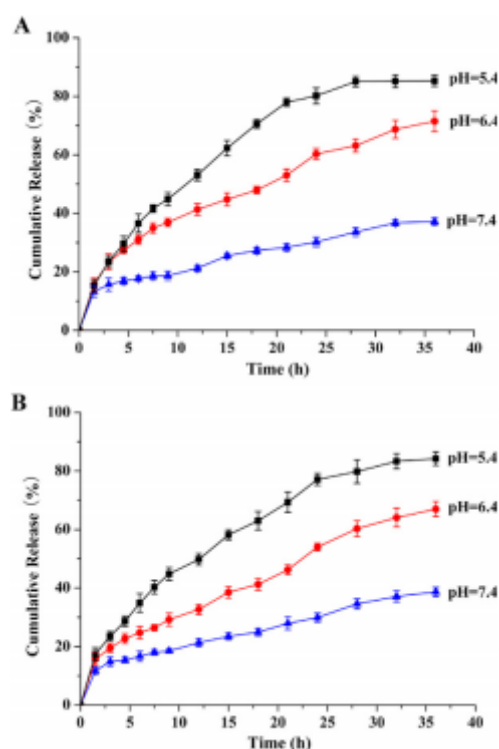


Figure 22: Graphs showing the pH-dependent release of paclitaxel at 37°C from cross-linked micelles of A (P₁) and B (P₃). P₁ and P₃ are different polymer systems (Yuan et al., 2011).

1.4. The use of computational chemistry in drug design

While chemistry is the science encompassing the creation, transformation and properties of atoms and molecules; theoretical chemistry is a subdiscipline which uses mathematical methods in conjunction with the fundamental laws of physics to analyse processes related to chemistry. This field of chemistry seeks to calculate, for example, what are the relative energies of a molecule, its dipole moment, how molecules interact and the rate of transformation with one stable molecule (Jensen, 2017).

Computational chemistry arose with the advent of computers in mainstream research. It allowed for complex or large-scale calculations to be carried out, at a faster rate (Dykstra, Frenking, Kim & Scuseria, 2011). It often involves troubleshooting, and some techniques can allow for, either quantitative or qualitative understanding of chemical processes. It provides several advantages, firstly, it enables scientists to test a method *in silico* before synthesis. Secondly, it can minimize the cost of raw materials, and minimize the risk of encountering hazards, this is due disproving or improving methods before they are carried out in a lab (Jensen, 2017).

Molecular modelling (MM), a subdiscipline of computational chemistry, aims to predict the three-dimensional structure and electronic properties of a molecule in a system. This has led to the development of a range of methods that can be used for different applications (Jensen, 2017).

1.4.1. Electronic structure methods

An electronic structure is defined as the electrostatic field created by the state of motion of electrons, by stationary nuclei. Electronic structure methods consist of several theories and methods which are used in computational chemistry. The molecular orbital theory is used to determine electrons in a molecular structure, which are not assigned to individual bonds but are assumed to be under the influence of nuclei. This is made up of the Hartree-Fock method (HF), semi-empirical quantum methods (SQM) and others (Jensen, 2017).

Quantum mechanics (QM) aimed to overcome the limitations of MM, but QM required more computational power. QM is generally used for the study of small molecules (Hostaš *et al.*, 2013). *Ab initio* methods do not use any empirical or semi-empirical parameters but are derived from theoretical principles with no experimental data (Ohno, Esfarjani & Kawazoe, 2018). Density functional theory, DFT, uses the *ab initio* methods (Stephens, Devlin, Chabalowski, & Frisch, 1994). DFT is an alternative to the Hartree-Fock approximation, with the main principle being that electron to electron interactions replace some potential action on electrons. By using functionals, it can determine the properties of a multiple electron system, using spatially dependent electron density (Jensen, 2017). These methods allow the accurate study of the electronic structure of compounds, with moderate computational effort (Ohno, Esfarjani & Kawazoe, 2018).

Semiempirical QM methods (SQM) were developed to increase the size of systems that can be analysed while reducing computational costs (Hostaš *et al.*, 2013). Semiempirical calculations differ from *ab initio* methods, as the number of integrals is reduced. One variation, NDDO, neglect of diatomic differential overlap, was the most popular. AM1 (Austin model 1), and its' by-product, PM3 (parametric model 3) are some examples of SQM methods. They, in turn, have been refined with the former having RM1 (Recife model 1), and the latter, PM6 and PM7 (Lewars, 2016). SQM can reproduce heats of formation, electrical energies, and geometries and measure spatial conformation of molecules of all sizes with good accuracy (Stewart, 2009). The software package of MOPAC uses SQM methods (Stewart, 1990).

Electronic structure methods aim to find molecular orbitals (MO), a molecular function that can be used to – calculate a probability of finding an electron in any specific position. Energy can be calculated for each molecular orbital, and orbitals occupied with electrons have lower energies than those which are unoccupied. The highest occupied molecular orbital (HOMO) and the lowest unoccupied orbital (LUMO) are believed to be involved in most chemical reactions. HOMO-LUMO gap in a single molecule can serve as a measure of a molecule's excitability. Frontier molecular orbital theory is the application of MO theory used to evaluate chemical reactivity by considering the possibility of HOMO-LUMO interactions of two chemical entities. This was developed by Kenichi Fukui in the 1950s. With each causing inference with energy levels, they can become indistinguishable and form an energy band. Electrons in the HOMO of a nucleophile are mostly free to participate in a reaction. LUMO being localized indicates this area would act as an electrophile (Dykstra *et al.*, 2011).

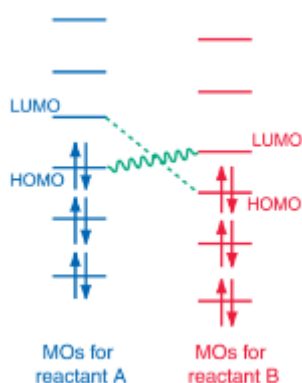


Figure 23: The HOMO-LUMO interactions between reactants A and B. The green wavy line indicates the smallest energy gap between the HOMO of A and the LUMO of B. The green dashed line indicates the largest energy gap between the LUMO of A and HOMO of B.

1.4.2. Force field methods

Molecular mechanic (MM) methods were developed to expand further the use of computational chemistry on large molecules and use force field methods (FF) approaches by eliminating electronic energy as a parametric function and including experimental parameters. Force field energies encompass the energy for the distortion of a molecule in a specific way, and this is shown in the force field equation (as shown in figure 24).

$$E_{FF} = E_{str} + E_{bend} + E_{tors} + E_{vdw} + E_{el} + E_{cross}$$

Figure 24: The force field equation (Jensen, 2017).

Each term in this equation relates to a form of energy. E_{str} is the *stretching* energy in a bond between two atoms, E_{bend} is the *bending* angle energy, E_{tors} is the *torsional* energy for rotation around a bond, E_{vdw} and E_{el} explain *non-bonded* atom to atom interactions in a system, and E_{cross} illustrates the coupling between E_{str} , E_{bend} and E_{tors} . Using optimisation and geometries, relative energies can be calculated from this equation (Jensen, 2017).

Modelling involving the calculation of thermodynamic or energetic factors could use several methods for calculation. MM, which is the same as FF (Jensen, 2017), can outline the structure conformation and energetics by running a conformation search and minimization algorithms such as steepest descent. A molecular conformation which has the lowest potential energy can be identified (Hostaš, Řezáč, & Hobza, 2013). There are several types of force fields which in turn, have their parameters. MMFFs (Merck Molecular Force Field), with one example being, MMFF94, is good in the reproduction of bond lengths in organic molecules and proteins. Parameters also reproduce intermolecular interactions in systems, such as hydrogen bonds, van der Waals interactions, like the good renown OPLS force field (Halgren, 1996).

UFF (Universal Force Field), contains the parameters for the potential energy of atoms; these are based on the element, the atomic hybridization and atoms connectivity. Despite MM not covering effects of formation and dissociation of covalent bonds, or of electron, proton transfer with a compound, it is widely used in calculating optimized structures of small molecules, polymers and biopolymers (Jensen, 2017).

1.5. Precedence for this research

This project aimed to model and synthesize a prodrug to release an EPI and anti-cancer drug with the *cis*-aconityl linker; so that release takes place selectively in cancer tissues below pH 6.90. The basis for this research was due to a precedent in literature for the co-administration of an EPI and an anti-cancer drug or with using linkers with anticancer drugs in general, but also with the *cis*-aconityl linker, to form a prodrug to treat drug resistance in tumours. In a study by Shen and Ryser in 1981, they looked at the use of this pH-sensitive linker when conjugated to daunorubicin, which has the same mechanism of action as doxorubicin (Nagai & Konishi, 2013 & Shen & Ryser, 1981) and poly-D-lysine polymers.

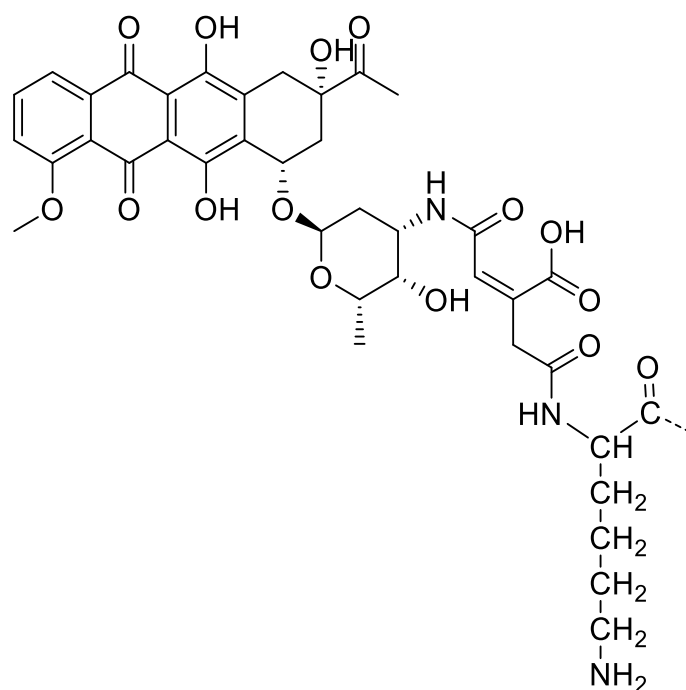


Figure 25: The formation of the N-cis-aconityl daunorubicin-poly(D-lysine) conjugate (Shen & Ryser, 1981). This was drawn using ChemDraw Professional 16.

This study by Shen and Ryser in 1981, involved the anthracycline derivative, **daunorubicin**. **Doxorubicin** was chosen as the anti-cancer drug for conjugation. As referred to earlier, Doxorubicin treats a wide range of cancers. It also contains an NH₂ (amino) group on its' amino sugar; this group would be conjugated to the OH group of a terminal carboxyl group, on the *cis*-aconityl linker, to form an amide bond. This is illustrated by multiple studies, including a preliminary study by Srinophakun and Boonmee in 2011. Since the amino group is more reactive than the other hydroxyl groups on the amino sugar, it is a target for conjugation. This is due to nitrogen having a lower electronegativity than oxygen; as a result, the amine's nitrogen is a better nucleophile than the hydroxyl's oxygen. For the EPI, this was chosen based on several criteria, as discussed in section 2.1.

The inclusion of the linker has two purposes, firstly, without it, upon administration of doxorubicin and the EPI to a patient, both compounds could be present in most tissues. The linker ensures that the EPI is isolated to the acidic environments of cancerous tissues. This 'free' doxorubicin would simply cause normal doxorubicin cytotoxic effects. Secondly, with the formation of stable bonds and the linker being pH-sensitive, it will only release both doxorubicin and the EPI when the pH values of surrounding tissues are between pH values of 6.00-6.90.

The *cis*-aconityl linker would degrade in the extracellular space of the cancer cell. Catalysed hydrolysis by the acidic conditions of cancer cells will speed up this degradation. With acidic conditions, the carbonyl bond will have an increased difference in charges, increasing the positivity of the carbonyl carbon, meaning amide/ester bond hydrolysis occurs quicker than normal.

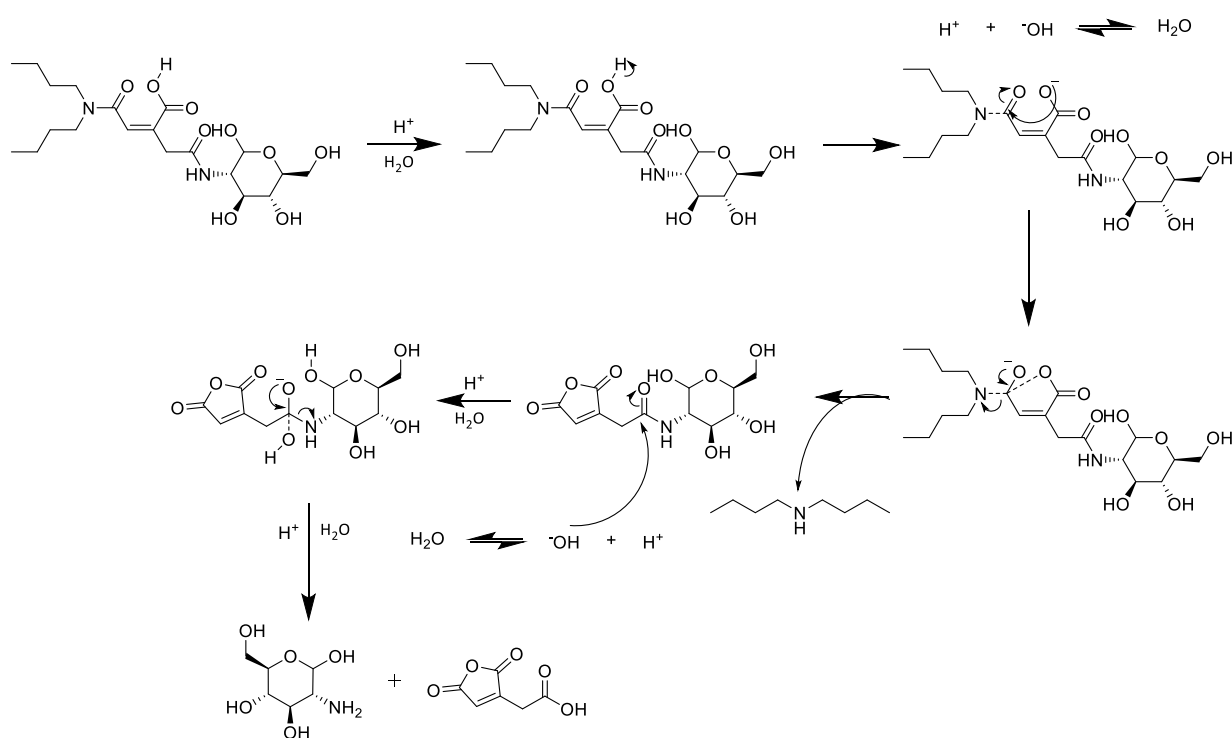


Figure 26: The mechanism for acid-catalysed amide hydrolysis with the glucosamine-*cis*-aconityl-dibutylamide conjugate.

Model compounds will be used before we scale to their full-scale counterparts. These model compounds are glucosamine and 4-aminotetrahydropyran (for doxorubicin), 4-phenylphenol (for MC70) and dibutylamine, phenethylamine and N-methyl-phenethylamine (for norverapamil). The degradation products by amide or ester bond hydrolysis would be the *cis*-aconitic acid, doxorubicin (Liu et al., 2014) and depending on the EPI used, either MC70 or norverapamil. The presence of the free *cis* hydroxyl group is known to catalyze the intramolecular hydrolysis of the amide bond (Kakinoki et al., 2008).

During a reaction, *cis*-aconityl anhydride can form *cis* and *trans* products. In an intracellular environment, the *cis* product released doxorubicin resulting in higher intracellular concentrations of this product than the *trans* product. The *cis* product also shows more antitumor activity than the *trans* product (Kakinoki et al., 2008).

1.6. Aim and objectives of this project

The aim of this project is to design and synthesize *a drug and efflux pump inhibitor conjugate linked by the pH-sensitive cis-aconityl moiety to facilitate the targeted release of the cytotoxic drug and an EPI only at pH below 6.6, and to enable simultaneous delivery of these agents selectively into cancer cells and not in normal tissues.*

The objectives of this project are to:

1. Identify suitable cytotoxic drugs and EPIs that are commercially available and have the correct functionality to join to the *cis*-aconityl linker system.
2. To computationally model these drug conjugates to investigate the viability of synthesis.
3. To synthesize conjugates comprising simpler molecular systems to represent both the EPI and cytotoxic drug, with the aconityl linker.
4. To test the pH-dependent release of representative conjugates.

2.0. Design of novel drug-EPI conjugates

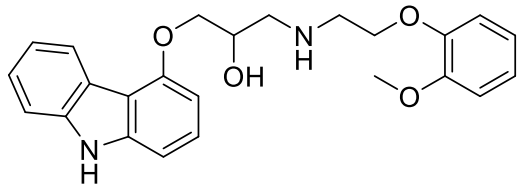
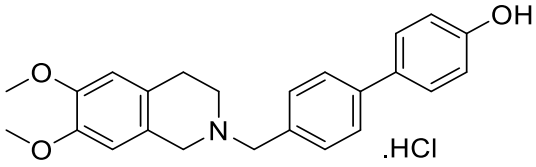
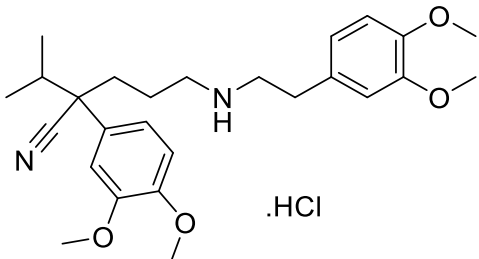
2.1. Methods for selection of conjugates

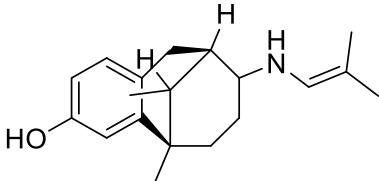
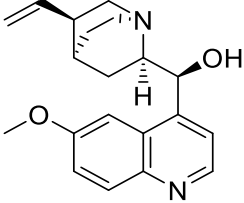
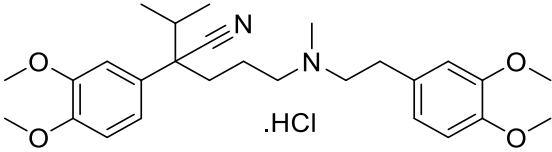
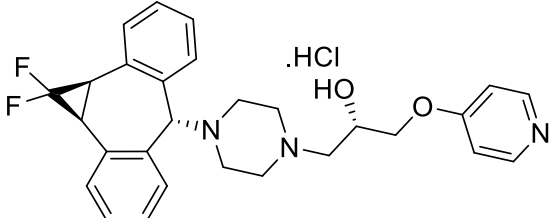
A review was carried out to identify a suitable drug and EPI that could be conjugated to the *cis*-aconityl linker. The chemotherapy drug, doxorubicin, was chosen due to the wide range of cancers it treats, from acute leukaemia lymphomas, stomach, breast and ovarian cancers, to Kaposi's sarcomas and bone tumours (Nagai & Konishi, 2013). Existing research already used doxorubicin in conjugation with the *cis*-aconityl linker for intracellular release. The structure of this drug also is easy to conjugate to as it contains an amino group on an amino sugar ring.

A problem with doxorubicin, despite being one of the most effective anti-cancer drugs, is its' cytotoxicity. As a result, therapeutic efficacy is greatly reduced. With the use of a prodrug however, these problems can be lessened, and efficacy improved. Using a pH-sensitive linker enables the release of a chosen anti-cancer drug via hydrolysis, in the acidic tumour environment (Du *et al.*, 2013). The use of a target for reducing cytotoxicity is necessary to improve therapeutic efficacy. Table 1 shows the P-gp inhibitors which are part of our compound library. Each compound has an IC₅₀ value and a summary on studies used to obtain those values.

Table 1: A selection of P-gp inhibitors with their structural formulae and prices from i and iii-vii (Sigma-Aldrich, 2018). Price for ii was obtained from Axon Medchem. All structures were drawn in ChemDraw Professional 16. References for IC₅₀ values:

- i – Used kinetic modelling for P-gp channels in microvilli and was compared to data for several P-gp inhibitors. This data showed digoxin transport inhibited by carvedilol when administered to expressed P-gp in human Caco-2 cells (Ellens, Meng, Le Marchand, & Bentz, 2018).
- ii – Determined inhibition of cell growth using MC70 and doxorubicin, with doxorubicin given at a 10% concentration, and MC70 given at 2 and 20 μM. In human Caco-2 cells, 2 days after MC70 exposure, 20 μM reached a 50% inhibition level (Azzariti *et al.*, 2011).
- iii – Characterisation of major metabolites of verapamil found norverapamil inhibited P-gp mediated digoxin transport in human Caco-2 cells (Pauli-Magnus *et al.*, 2000).
- iv – Sensitivity of multidrug-resistant cells on narcotic analgesics using inhibition of cell growth found human resistant MCF7/ADR cells were hypersensitive to pentazocine (Callaghan & Riordan, 1995).
- v – Study showed that vincristine binding to multidrug-resistant Ehrlich ascites plasma membrane vesicles, in MDR EHR2/DNR+ cells, was inhibited by 50% by quinidine (Sehested *et al.*, 1989).
- vi – Characterisation of major metabolites of verapamil found verapamil inhibited P-gp mediated digoxin transport in human Caco-2 cells (Pauli-Magnus *et al.*, 2000).
- vii – Study looked at the effect of zosuquidar P-gp modulation of human K562/R7 cells zosuquidar was found to inhibit P-gp channels using a DiOC₂ P-gp accumulation assay (Marcelletti, Multani, Lancet, Baer, & Sikic, 2009).

Structure	Structural formula	Price per mg	IC ₅₀
Carvedilol (i)		£124.00 for 100 mg	0.8 μM
MC70 hydrochloride (ii)		£793.26 for 100 mg	20 μM
Norverapamil hydrochloride (iii)		£192.00 for 5 mg	0.3 μM

Pentazocine (iv)		£758.00 for 100 mg	80 μ M
Quinidine (v)		£27.10 for 5 g	0.5 μ M
Verapamil hydrochloride (vi)		£273.00 for 200 mg	1.1 μ M
Zosuquidar hydrochloride (LY335979) (vii)		£1916.00 for 100 mg	0.17 μ M

Consequently, a P-gp inhibitor (EPI) needed to be selected from those published in the literature, as shown in Table 1. A library of EPIs was then created based on the following criteria. Firstly, we wanted to have a di-amide linker system with EPI and doxorubicin. When no example of such a conjugate could be found, we then expanded our search to compounds with hydroxyl groups to make an amide/ester-linked conjugate as there is literary precedence for this. Secondly, we wanted to preferably have only one reactive functional group for ease of conjugation. Thirdly, the price of the EPI had to be reasonable with the cost per 100 mg not being too high. Finally, we preferred simpler structures which had little to no steric hindrance near the reactive group to be linked. The inclusion of IC₅₀ values was to provide a measure of these compounds' level of inhibition. Following the creation of our EPI library, we did not think most of the compounds in table 1 were suitable due to some were very expensive to obtain, e.g. zosuquidar hydrochloride.

Subsequently, although MC70 hydrochloride was expensive to obtain, there were published synthesizes, so it was planned to use this as a model and then synthesize it later. We looked at norverapamil, a primary demethylated metabolite of verapamil, which has a secondary amine group and is a bacterial P-gp inhibitor, so it was selected as a model. Although verapamil would seem a more obvious choice as there is more literature present, it does not contain a functional group for linker conjugation (Pauli-Magnus et al., 2000).

Norverapamil appears to have a similar effect on P-gp substrates but, Verapamil has been shown to alter the pharmacokinetics of P-gp substrates *in vivo* and it is an accepted model (Kuhlmann, Carlile, Noe, & Bentley, 2014). Quinidine was a possibility that we did not consider as there was more literary precedence for MC70.

Research also gave further justification for our choice, with MC70 possessing a phenol moiety which can be conjugated to the linker. MC70 is a derivative of the compound PB28 which is a sigma-2 agonist with increased efficacy in ABCB1 inhibition (Azzariti *et al.*, 2011) and it has selectivity towards the BCRP transporter, with an EC₅₀ of 0.69µM (Guglielmo *et al.*, 2016). In a study by Azzariti *et al.* in 2011, MC70 has been co-administered with doxorubicin. MC70 slightly inhibited cell proliferation in breast cancer cells, whilst strongly enhancing doxorubicin effectiveness. In colon cancer cells, MC70 with topoisomerase I inhibitors did inhibit cell proliferation through cytostatic and cytotoxic behaviours. DNA laddering formation occurred as a response to drug-induced cell apoptosis. MC70 induced apoptosis by itself but favoured necrosis when given in combination with high concentrations of doxorubicin. MC70 and low concentrations of doxorubicin can only slightly trigger necrosis but not apoptosis. Cell death via the necrosis pathway involved the increased release of LDHs by cell swelling. This suggests that MC70 is a novel anticancer agent which could potentiate the efficacy of doxorubicin.

2.2. Computational methods

Following the creation of a compound library for EPIs, we needed to model these compounds to investigate the viability of synthesis for the selected compounds. This was necessary due to, firstly, the need to evaluate the availability of functional groups for conjugation due to potential steric hindrance in components and intermediates. Secondly, we evaluated if the location of HOMO and LUMO orbitals coinciding with functional groups where desired bonds were expected to form. Additionally, analysis of the HOMO and LUMO orbitals would provide information about selectivity for the second carboxyl group activation/coupling step. 2D structures for all compounds were drawn using chemistry drawing software and then imported into the 3D modelling software. The resulting 3D model compounds were then exported as input for semiempirical quantum chemistry software to evaluate the HOMO-LUMO gap.

Specifically, the 3D molecular modelling software, Avogadro 1.2.0., was used to create molecular models for all molecules including drug conjugates by conformational searching to find the lowest energy conformations. The feasibility of drug-conjugate formation was evaluated by analysis of the potential for steric crowding of functional groups. The SMILES strings generated by ChemDraw Professional 16 were imported into Avogadro. Hydrogens were added to all atoms to reflect their ionization states at pH 6.90. Molecular geometries of all compounds were optimized using the steepest descent algorithm and MMFF94 force field until either 5000 minimisation steps were reached or energy converged to the gradient at $10e^{-7}$. A conformer search was then carried out on all models and explore if the functional groups were not sterically hindered in moieties to be conjugated.

Using the MOPAC extension in Avogadro, a 'MOPAC Input Deck' (.mop) file was created with the appropriate charge was selected based on the molecule's ionization state at pH 6.90. The .mop file was then edited by Notepad++ by adding the phrase: 'AUX LARGE CHARGE=-2 SINGLET PM7 GRAPHF' on the title line. GRAPHF was also added to include a molecule's molecular orbitals with both HOMO and LUMO values to a formatted file. Then the file was saved and run in MOPAC (Stewart, 1990). The file was then opened, and the output file was read using Notepad++ (Don Ho) to obtain the heat of formation of every molecule. The heat of formation for each complex are listed below, in table 2. HOMO and LUMO orbitals of components and intermediates were visualized in Jmol (Jmol, 2020). All, calculations were performed using a workstation with Microsoft Windows 10 operating system, 3.0 GHz Intel i5 CPU and 8 GB of RAM.

2.2.1. Prediction of HOMO/LUMO

Frontier molecular orbital theory (FMO) relates to the electron orbitals of a molecule. It is an application of MO theory. Molecules form bonds when electrons can be shared. Occupied orbitals of different molecules can repel each other. Positive charges in one molecule can attract the negative charges of another molecule (Bredas, 2014).

As mentioned earlier, HOMO is an atom's highest occupied molecular orbital and its' LUMO, is its lowest unoccupied molecular orbital. This is of importance due to predicting orbital overlap. Another way of describing it, it is an atom's HOMO is the last energy level containing electrons. The LUMO does not contain electrons and is higher in energy than HOMO, this makes it the easiest orbital for electrons to occupy. The Pauli exclusion principle states that two electrons, in an electron pair, which occupy an orbital must be in opposite spin states (Dykstra *et al.*, 2011).

FMO is beneficial by investigating electrons in the furthest orbits, the attraction between them can be a predictor of a chemical reaction (Dykstra *et al.*, 2011). It is also important due to it predicting the likelihood in which the HOMO-LUMO orbitals overlap. HOMO-LUMO energy gaps are very important for organic reactivity, the closer in energy the HOMO of the nucleophile and LUMO of the electrophile are, the stronger the interaction (Dykstra *et al.*, 2011). We used these studies to observe the HOMO-LUMO of the reacting groups, i.e. the HOMO of the nucleophile (amine/phenol moiety) and LUMO of the electrophile (anhydride/acid moiety). Since anhydrides are always reactive this is more useful to predict the second step reactivity of the carboxyl groups.

Results below illustrate the position of HOMO/LUMO orbitals on reagents regarding their possible involvement in the conjugation with the *cis*-aconityl linker at pH 6.90.

2.3. Results and discussion

3D structures and molecular orbitals of reagents:

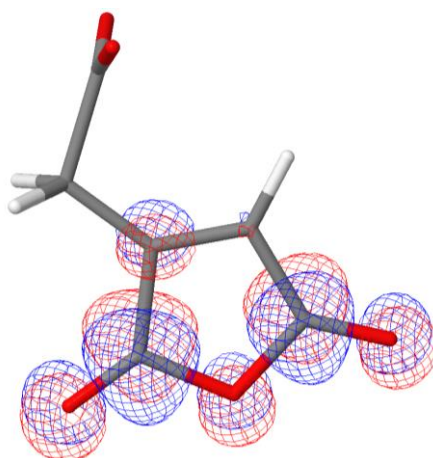


Figure 27: LUMO+1 of cis-aconitic anhydride (3.872 eV).

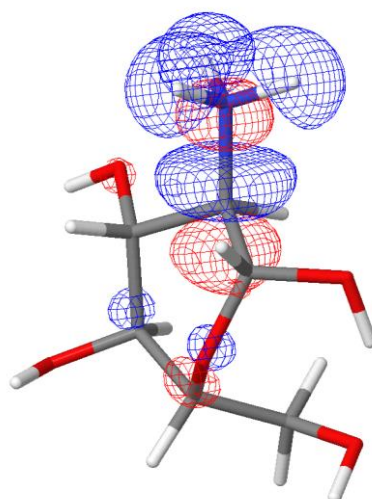


Figure 28: LUMO of glucosamine (-3.906 eV).

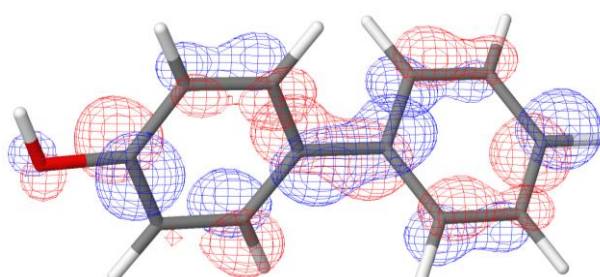


Figure 29: LUMO of 4-phenylphenol (-0.171 eV). Whilst a LUMO orbital is present on amino group, there are LUMO orbitals on the aromatic rings.

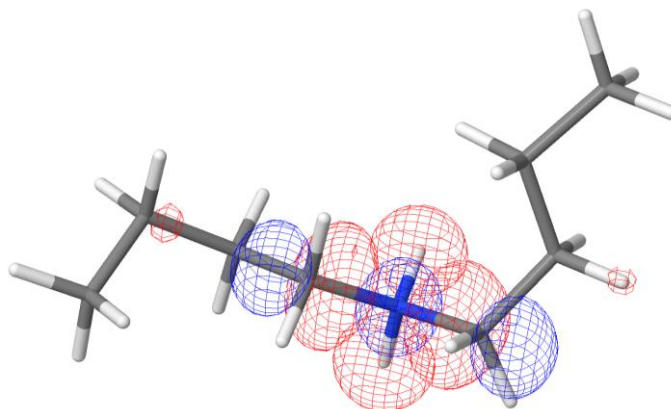


Figure 30: LUMO of dibutylamine (-3.754 eV).

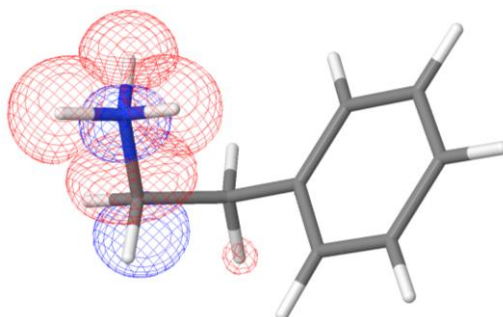


Figure 31: HOMO of phenethylamine (-3.887 eV).

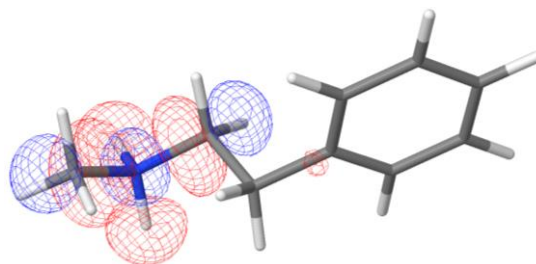


Figure 32: HOMO of N-methyl-phenethylamine (-4.020 eV).

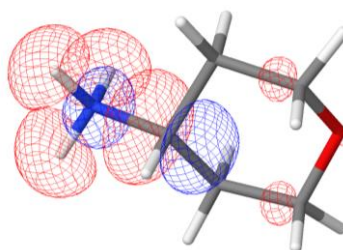


Figure 33: HOMO of 4-aminotetrahydropyran (-4.044 eV).

3D structures and molecular orbitals of intermediates:

Results from a conformational search of doxorubicin showed that doxorubicin had three possible conformations, all of which showed doxorubicin's amino group free for conjugation with the *cis*-aconityl linker.

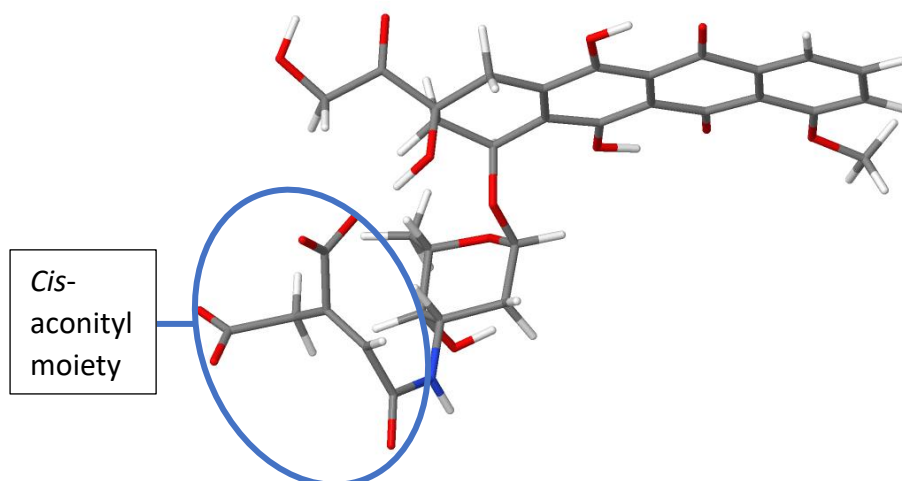


Figure 34: *N*-cis-aconityl-doxorubicin at pH 6.90. This was drawn using Jmol 14.29.55. This shows what charge the functional groups have at this pH 6.90 and which groups are available for conjugation.

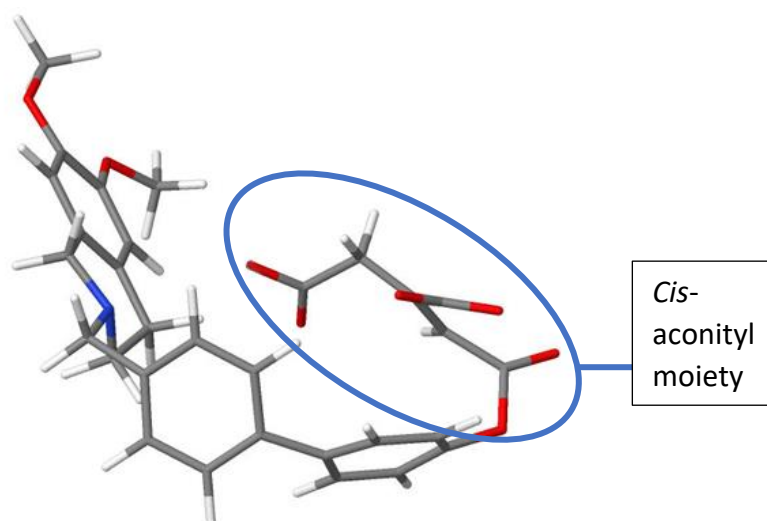


Figure 35: *N*-cis-aconityl-MC70 at pH 6.90. This was drawn using Jmol 14.29.55. This shows what charge the functional groups have at this pH 6.90 and which groups are available for conjugation. Terminal hydroxyl group on the *cis*-aconityl moiety exchanged a proton with the nitrogen atom, this is not expected to occur in pH-release studies.

Conformational searches both showed that for all conformations, the desired functional groups were available for conjugation. However, there was less steric hindrance of the linker's non-bonded terminal carboxyl functional group when conjugating doxorubicin to N-*cis*-aconityl-MC70, than conjugating MC70 to N-*cis*-aconityl-doxorubicin.

The results of modelling the simple model compounds are shown below. N-*cis*-aconityl-daunosamide showed no steric hindrance and this is shown in figure 36.

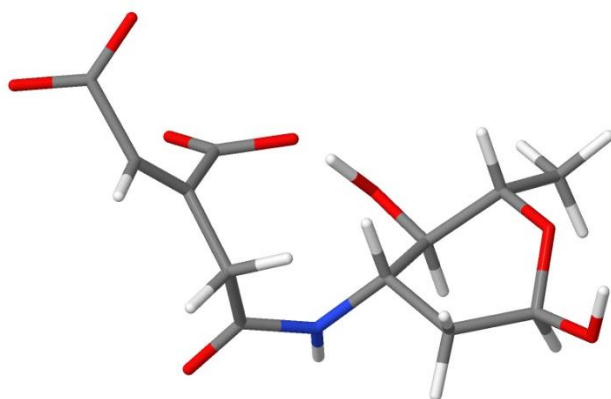


Figure 36: N-*cis*-aconityl-daunosamide at pH 6.90. This was drawn using Jmol 14.29.55.

Daunosamine was expensive to obtain and so, glucosamine was then chosen as a model amino sugar. N-*cis*-aconityl-glucosamide, upon modelling, showed no steric hindrance and this is shown in figure 37 below.

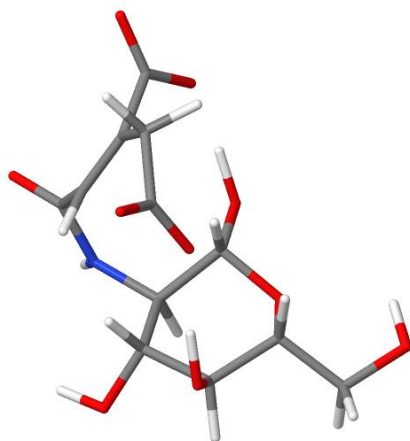


Figure 37: N-*cis*-aconityl-glucosamide at pH 6.90. This was drawn using Jmol 14.29.55.

So, the compound of dibutylamine was chosen to model norverapamil. No steric hindrance was seen when compounds were modelled.

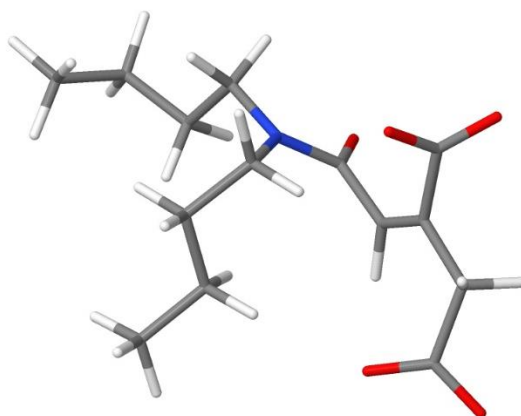


Figure 38: *N*-cis-aconityl-dibutylamide at pH 6.90. This was drawn using Jmol 14.29.55.

HOMO/LUMO orbital diagrams of intermediates preceded next.

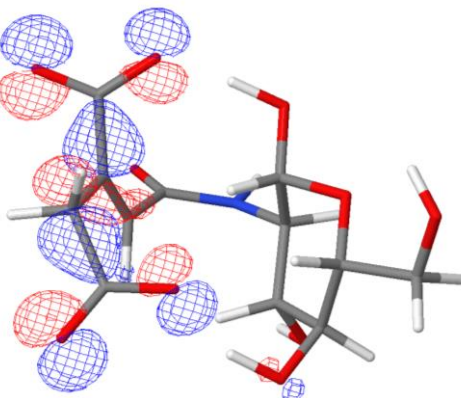


Figure 39: HOMO of *N*-cis-aconityl-glucosamide (-3.059 eV).

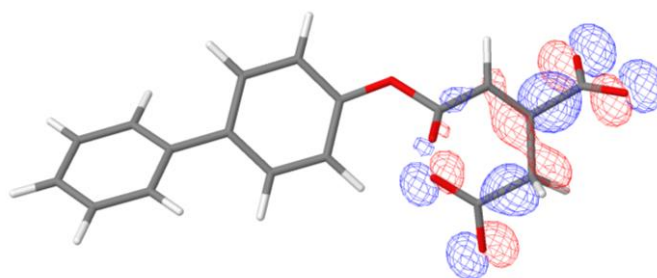


Figure 40: HOMO of *N*-cis-aconityl-phenylphenoate (-2.330 eV).

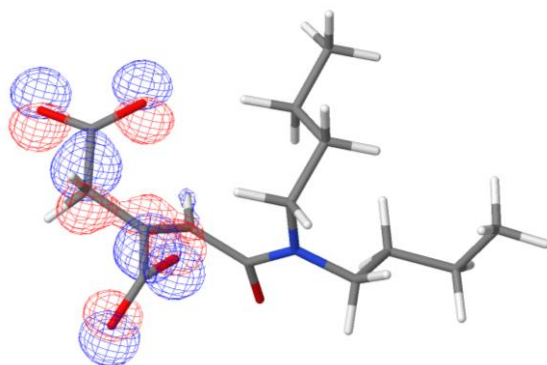


Figure 41: HOMO of N-cis-aconityl-dibutylamide (-1.827 eV).

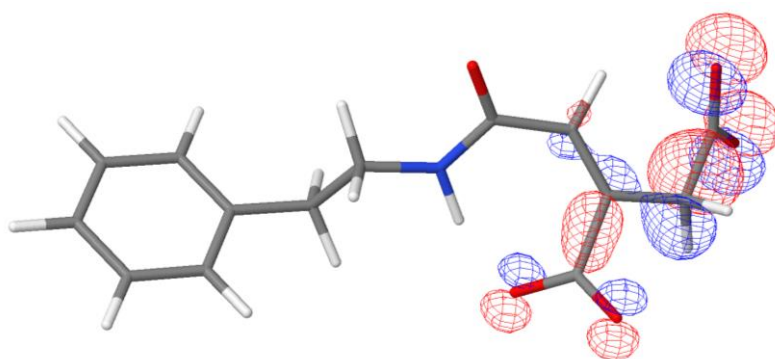


Figure 42: HOMO of N-cis-aconityl-phenethylamide (-1.956 eV).

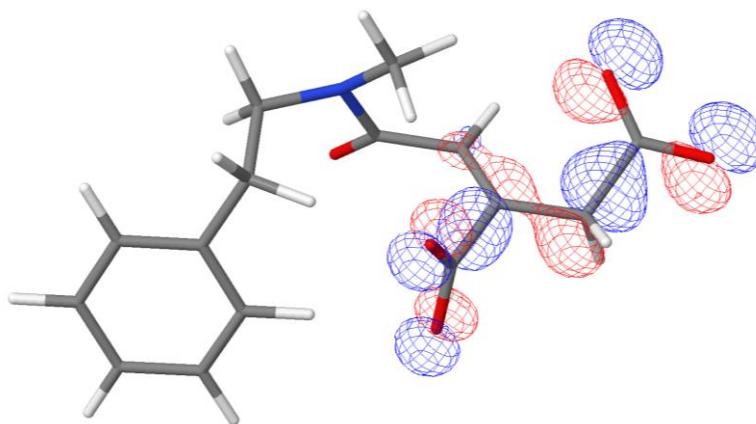


Figure 43: HOMO of N-cis-aconityl-N-methyl-phenethylamide (-2.006 eV).

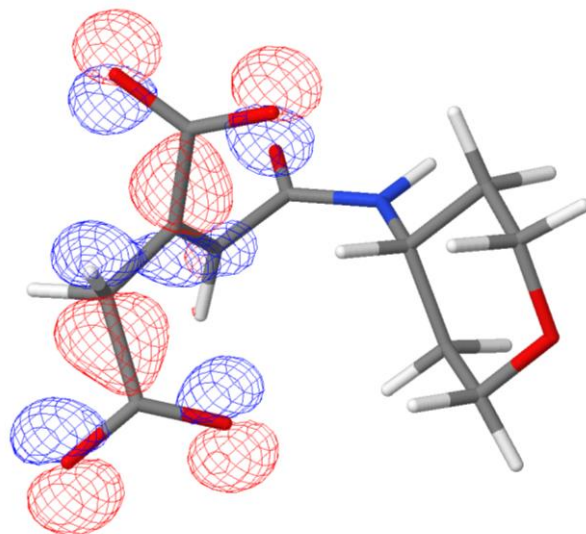


Figure 44: HOMO of N-cis-aconityl-amidotetrahydropyran (-1.971 eV).

3D structures and molecular orbitals of final conjugates:

A comparison was later done for the conjugation sequence of doxorubicin—*cis*-aconityl—MC70, and of MC70—*cis*-aconityl—doxorubicin.

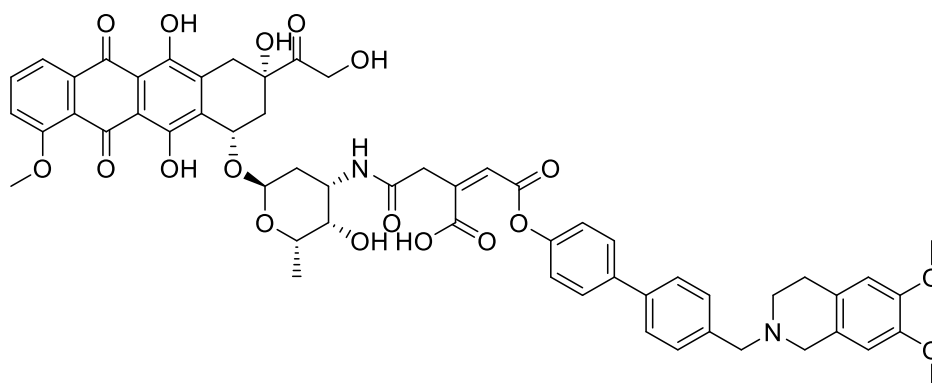


Figure 45: The complex of doxorubicin with the *cis*-aconityl linker and MC70.

An alternative model was tested using doxorubicin with one aconityl linker, a short alkyl chain, with another aconityl linker and MC70 as a possible conjugate.

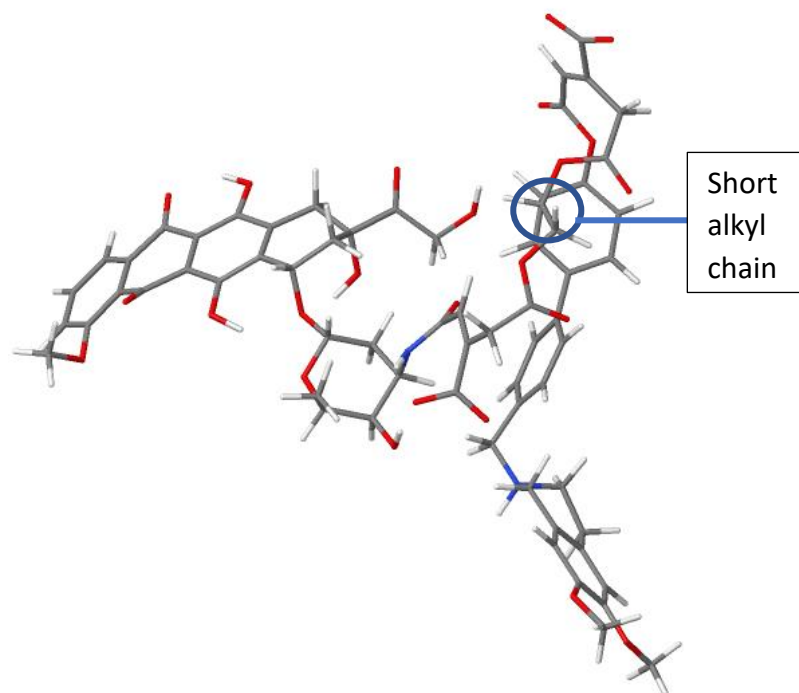


Figure 46: Doxorubicin conjugated to the *cis*-aconityl linker, MC70 also conjugated to the *cis*-aconityl linker with a short alkyl chain separating both moieties. This was drawn using Jmol 14.29.55.

The compound of norverapamil was chosen as an alternative EPI to MC70.

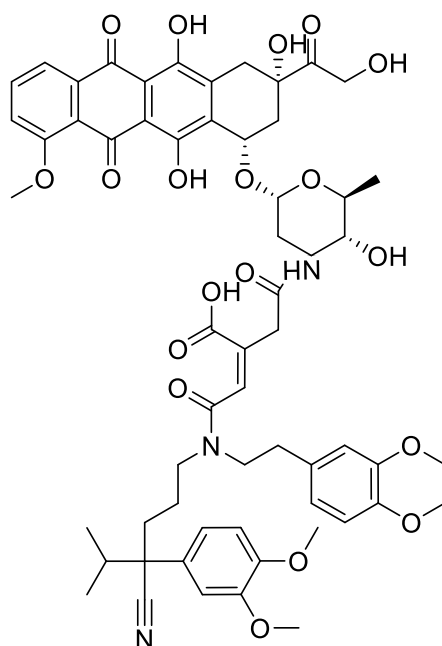


Figure 47: The complex of norverapamil with the *cis*-aconityl linker and doxorubicin.

Using the model sugar of daunosamine, a conjugate was formed with 4-phenylphenol.

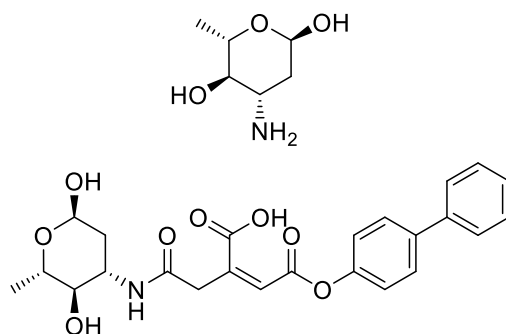


Figure 48: Top: daunosamine, bottom: daunosamide-cis-aconityl-phenylphenolate.

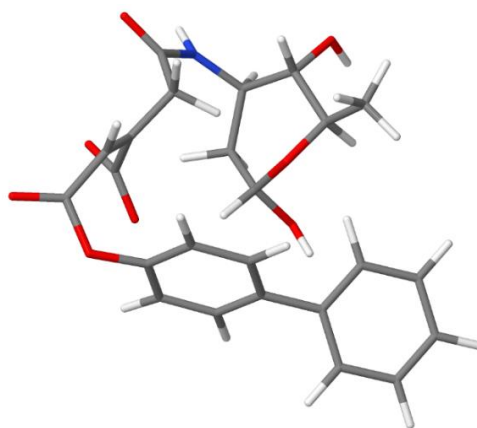


Figure 49: Daunosamide-cis-aconityl-phenylphenolate at pH 6.90. This was drawn using Jmol 14.29.55.

Glucosamine, the model compound for doxorubicin, was conjugated to N-cis-aconityl-dibutylamide. As with MC70 conjugation to form the full EPI-drug complex above, conjugating dibutylamine to the linker first, then glucosamine, resulted in a lower heat of formation value, then compared to reversing the order of conjugation. Then the dibutylamine, cis-aconityl, glucosamine conjugate was investigated to observe the effects of the norverapamil and doxorubicin respectively.

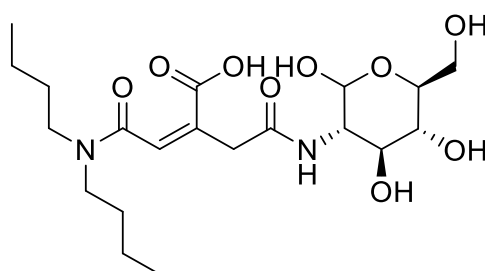


Figure 50: Dibutylamine, the cis-aconityl linker and glucosamine.

Molecular modelling was carried out to deduce if there were any obstacles in conjugate formation with for our drug-linker-epi conjugates and model compounds. A compound library which was created found that MC70 hydrochloride, out of other compounds, was the easiest to synthesize and conjugate with *cis*-aconitic linker and in turn, doxorubicin. Based on these two compounds, several simpler compounds were made to simulate the effects of MC70 and doxorubicin.

An amino sugar was selected as an alternative to the chemotherapy drug, doxorubicin. The compound that was like the amino sugar moiety of doxorubicin was daunosamine, and for the phenylphenol moiety of MC70, that was 4-phenylphenol. Daunosamine would be a good choice as it is the amino sugar moiety of doxorubicin (Pubchem, 2017d). However, glucosamine which is also an amino sugar and is similar in structure to daunosamine was chosen as an alternative as it was cheaper to obtain. 4-aminotetrahydropyran is an even simpler amino sugar model of glucosamine with this compound being less more lipophilic. Phenethylamine and N-methyl-phenethylamine are models of the secondary amine, norverapamil. Using cheaper simpler systems enabled the overall cost of chemicals to be reduced and the minimization of wastage of therapeutics until the synthetic conditions are optimized.

The compounds which modelled doxorubicin were: daunosamine, glucosamine and 4-aminotetrahydropyran. MC70 was modelled by 4-phenylphenol. Norverapamil was modelled by dibutylamine, phenethylamine and N-methyl-phenethylamine.

The reason why heat of formation values are important is that they indicate if a reaction's products are more thermodynamically stable than the reactants. The more stable, the more exothermic or negative this value is. Observing steric hindrance on possible conjugates is important to deduce if a reaction between two compounds would be possible. We aimed to achieve global energy minimum but using conformational searching. No steric hindrance of the linker's terminal non-bonded carboxyl group was observed with all model and final compounds. Whilst the heat of formation values from MOPAC, as mentioned in the results, showed that the drug should be conjugated to the linker first. It should be possible to investigate if the reverse release (EPI first followed by the release of the drug) would occur in clinical applications.

The HOMO/LUMO orbitals of all reagents and intermediate conjugates indicate which moieties will overlap in the possibility that a bond will form. The HOMO orbitals of *cis*-aconitic anhydride (figures 39-44) generally show the terminal carboxyl groups had slightly larger orbitals as compared to the adjacent double bond. This indicates that the location of the possible conjugation step will most likely be on the terminal carboxyl groups. Although further studies are needed to confirm this, the design of the rest of the final conjugates are based on these observations.

4-phenylphenol is a representative model compound for MC70, with both having the same functional group for conjugation. With the hydroxyl group being an electron activating group, the lone pairs cause resonance by shifting electrons around the two benzene rings. The electrons which are involved in the resonance are the pi (π) and HOMO orbital electrons, were disrupted from the normal distribution (which can be observed in the adjacent aromatic ring) (figure 29). The consequences for reactivity in figure 40 (and 4-phenylphenol), would be a reduction in the electron cloud around the hydroxyl group, this would lead to this moiety being less nucleophilic and in turn, less effective in attacking the electrophilic carboxyl groups on *cis*-aconitic anhydride.

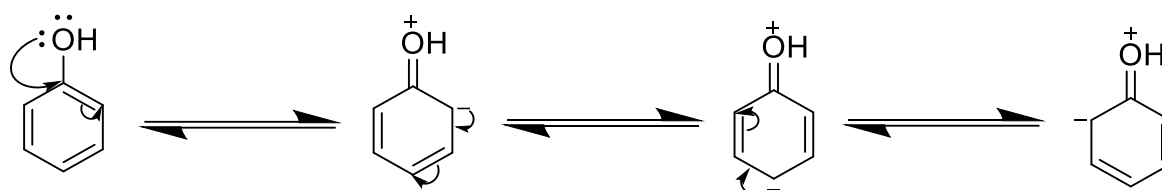


Figure 51: Resonance stabilisation of phenol showing the redistribution of electron density.

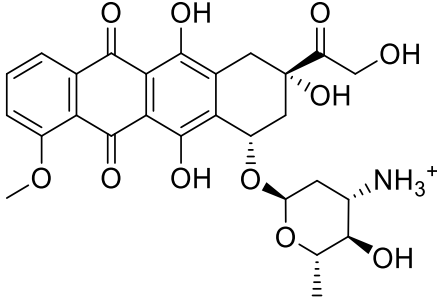
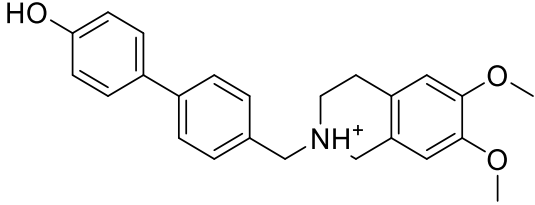
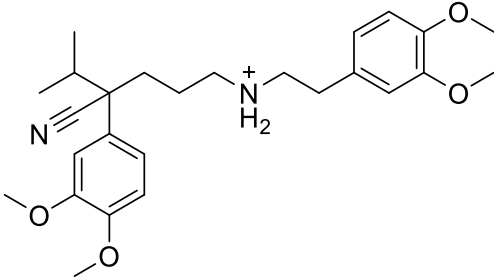
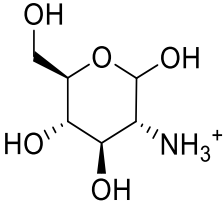
In summary, modelling showed several things which informed conjugates synthesized in synthesis. Firstly, the order of conjugation, with the heat of formation values showed that the drug should be to the linker first, however, in terms of treatment, the inhibition of P-gp before administration of a drug would be beneficial. However, there was less steric hindrance when conjugating doxorubicin to *N-cis*-aconityl-MC70, than conjugating MC70 to *N-cis*-aconityl-doxorubicin.

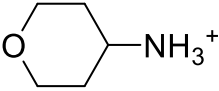
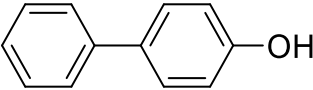
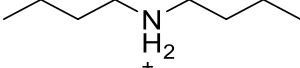
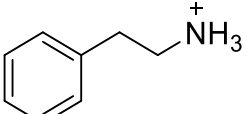
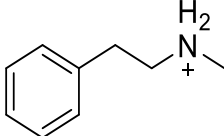
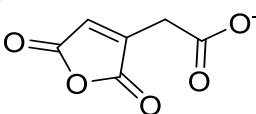
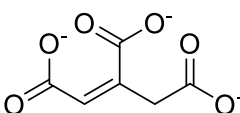
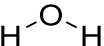
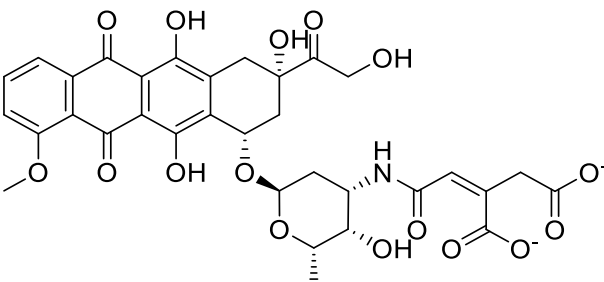
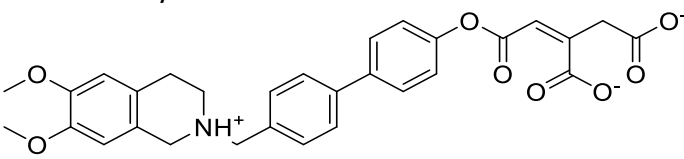
Secondly, with some figures showing LUMO orbitals on non-reacting functional groups, the heat of formation values did confirm that the desired functional groups may be formed. Differing the hydroxyl group from a terminal one to the middle group was also explored. For example, phenethylamide-*cis*-aconityl-amidotetrahydropyran had a predicted heat of formation of $-1039.25 \text{ KJ mol}^{-1}$. The conjugate where 4-aminotetrahydropyran was conjugated to the middle hydroxyl group on the linker had a value of $-1037.41 \text{ KJ mol}^{-1}$. Therefore, the more exothermic (negative) value is the more thermodynamically stable product.

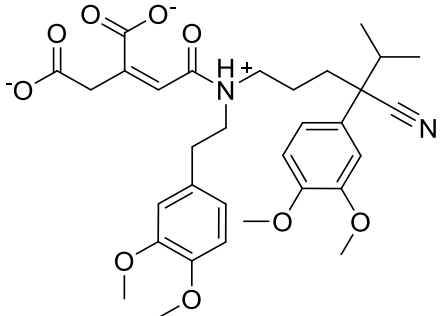
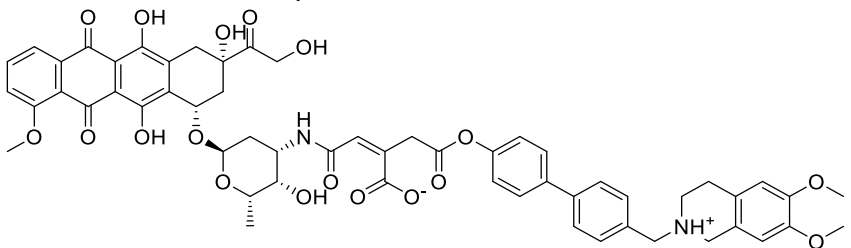
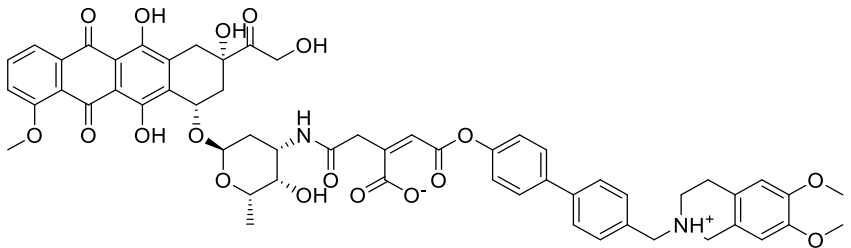
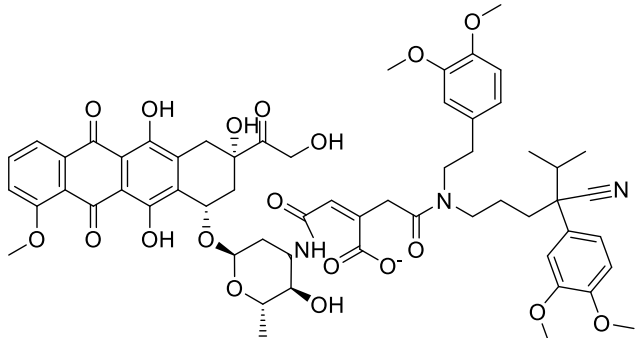
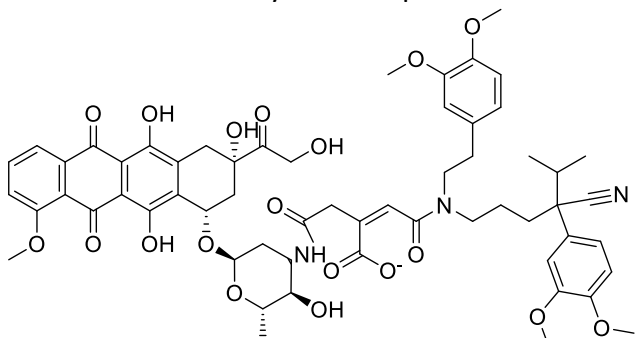
Thirdly, it was observed that that the HOMO and LUMO are on the carboxylic groups of the linker and amine groups of the model compounds respectively. That in conjunction with the absence of steric hindrance should indicate that the choice of reactants is good. The same was found for intermediates. Finally, this shows what would likely be present at pH 6.90 with possible conjugates. It showed which representative compounds would be more thermodynamically stable and more viable for conjugate synthesis.

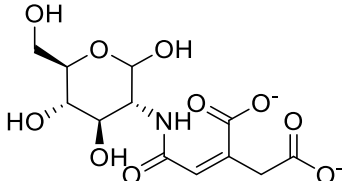
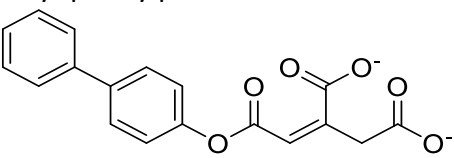
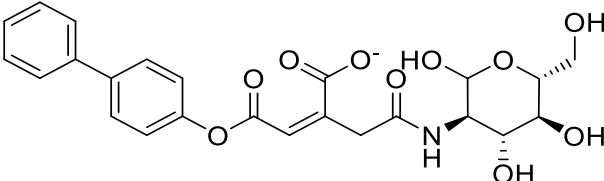
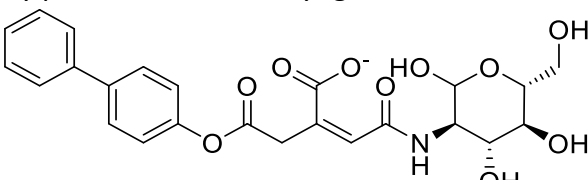
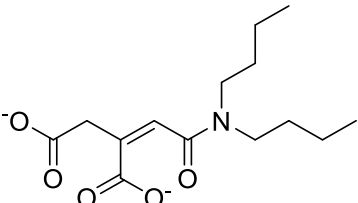
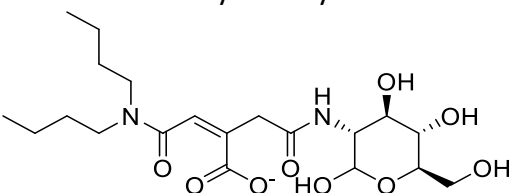
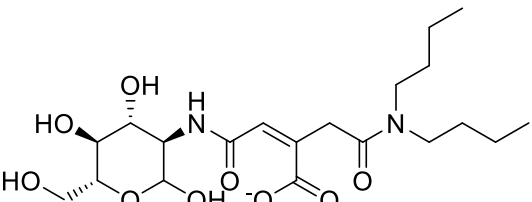
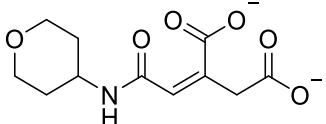
As a result, from the data obtained so far, doxorubicin was the cytotoxic drug and MC70 with norverapamil were the EPIs. For model compounds, glucosamine and 4-aminotetrahydropyran were selected for doxorubicin, 4-phenylphenol for MC70, and dibutylamine, phenethylamine and N-methyl-phenethylamine for norverapamil. The 2D and 3D structures of all selected molecules for conjugation, potential intermediates and final drug-EPI conjugates were generated and their heat of formations were predicted (Table 2).

Table 2: The charges, protonation states, and heat of formations of doxorubicin, MC70, norverapamil and their model compounds, possible model conjugates and drug conjugates is shown in figures i-xxxiii. The heat of formation values was obtained from MOPAC using the PM7 semiempirical method at a pH of 6.90.

Complex name and structure	Charge	Heat of formation (KJ mol ⁻¹)
i. Doxorubicin 	+1	-1199.60
ii. MC70 	+1	-342.90
iii. Norverapamil 	+1	-130.32
iv. Glucosamine 	+1	-343.17

v.	4-aminotetrahydropyran 	+1	-414.47
vi.	4-phenylphenol 	0	-2.22
vii.	Dibutylamine 	+1	-437.86
viii.	Phenethylamine 	+1	-678.86
ix.	N-Methyl-phenethylamine 	+1	-677.06
x.	<i>Cis</i> -aconitic anhydride 	-1	-932.28
xi.	<i>Cis</i> -aconitic acid 	-3	-647.04
xii.	Water 	0	-241.83
xiii.	<i>N-cis</i> -aconityl-doxorubicin 	-2	-2836.67
xiv.	<i>N-cis</i> -aconityl-MC70 	-1	-1212.89

<p>xv. N-<i>cis</i>-aconityl-norverapamil</p> 	-1	-1511.19
<p>xvi. MC70-<i>cis</i>-aconityl-doxorubicin</p> 	0	-2613.50
<p>xvii. Doxorubicin-<i>cis</i>-aconityl-MC70</p> 	0	-2556.88
<p>xviii. Norverapamil-<i>cis</i>-aconityl-doxorubicin</p> 	-1	-3237.05
<p>xix. Doxorubicin-<i>cis</i>-aconityl-norverapamil</p> 	-1	-3172.60

xx.	N- <i>cis</i> -aconityl-glucosamide 	-2	-2005.37
xxi.	N- <i>cis</i> -aconityl-phenylphenoate 	-2	-919.15
xxii.	Glucosamide- <i>cis</i> -aconityl-phenylphenoate 	-1	-1789.50
xxiii.	Phenylphenoate- <i>cis</i> -aconityl-glucosamide 	-1	-1851.05
xxiv.	N- <i>cis</i> -aconityl-dibutylamide 	-2	-1083.98
xxv.	Glucosamide- <i>cis</i> -aconityl-dibutylamide 	-1	-1964.16
xxvi.	Dibutylamide- <i>cis</i> -aconityl-glucosamide 	-1	-2000.65
xxvii.	N- <i>cis</i> -aconityl-amidotetrahydropyran 	-2	-1161.76

xxviii.	N- <i>cis</i> -aconityl-phenethylamide 	-2	-898.56
xxix.	N- <i>cis</i> -aconityl-N-methyl-phenethylamide 	-2	-882.86
xxx.	Amidotetrahydropyran- <i>cis</i> -aconityl-phenethylamide 	-1	-1039.25
xxxi.	Phenethylamide- <i>cis</i> -aconityl-amidotetrahydropyran 	-1	-975.37
xxxii.	Amidotetrahydropyran- <i>cis</i> -aconityl-N-methyl-phenethylamide 	-1	-1037.42
xxxiii.	N-methyl-phenethylamide- <i>cis</i> -aconityl-amidotetrahydropyran 	-1	-1033.20

Table 2 showed doxorubicin, EPIs, and the simple model compounds conjugated to the *cis*-aconityl linker, as well as full drug-EPI conjugates.

3.0. Synthesis

3.1. General

All solvents were purchased from Acros chemicals, Fisher chemicals and Sigma-Aldrich; the rest of the reagents were purchased from Sigma-Aldrich and used as received.

4-aminobiphenyl was purchased from Alfa Aesar and was used as received. 4-aminotetrahydropyran was purchased from Fluorochem and was used as received. *Cis*-aconitic anhydride was purchased from Sigma-Aldrich, then Alfa Aesar, and was used as received. Silica gel 60 was purchased from Merck chemicals and Sigma-Aldrich and used as received. N,N,N',N'-Tetramethyl-O-(1H-benzotriazol-1-yl)uronium hexafluorophosphate (HBTU) was purchased from Protein Technologies, Inc., and used as received. Hydrochloric acid (concentrated), sodium hydroxide (NaOH), sodium hydrogen carbonate (NaHCO₃), sodium carbonate (Na₂CO₃) were purchased from Fisher chemicals and used as received. Monosodium phosphate (NaH₂PO₄) and disodium phosphate (Na₂HPO₄) were purchased from Acros chemicals and used as received. Deionized water was used as received. Ninhydrin was purchased from BOD chemicals and was used as received.

NMR analysis was performed on a JEOL-JNM-EX400 FT-NMR System (400 MHz), and a JEOL-JNM-EX600 FT-NMR System (600 MHz) with JOEL Delta software version 5.3.1. IR analysis was carried out on a PerkinElmer Frontier (FT-IR) spectrophotometer with PerkinElmer Varian IR software, version 10.6.2. LCMS was performed on a Waters Acquity H Class UPLC® Plus QDa Mass Detector with a Phenomex Luna 3u C18(2) 100A, 100 mm X 2.00 mm 3 micron column. Melting point measurements were carried on out a Griffin melting point apparatus.

3.2. Methods

Reaction 1:

Attempted synthesis of *N*-cis-aconityl-dibutylamide (**3**)

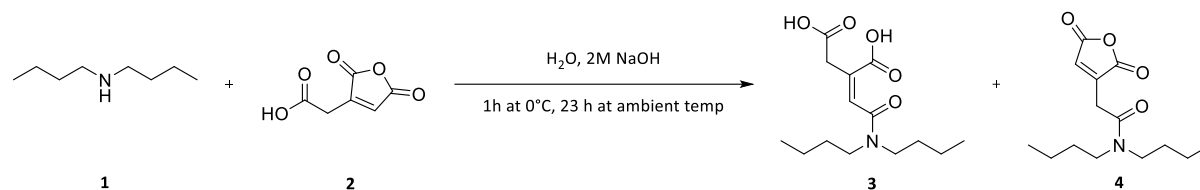


Figure 52: The reaction scheme for synthesizing compounds **3** and **4**.

This method was altered from the original study by Kang, Kim, Song, *et al.* in 2014. Dibutylamine (0.23 mL, 1.391 mmol) was added to 50 mL of deionized water in a pre-weighed round-bottomed flask. *Cis*-aconitic anhydride (108.58 mg, 0.696 mmol, 2 eq) was then added slowly, whilst stirring. Subsequently, NaOH (2M) was added dropwise to maintain the pH of the reaction mixture to 9-10. Dibutylamine was not soluble but floated on the surface, which then interfaced with *cis*-aconitic anhydride. After 1 h on ice, the reaction mixture was stirred further for 23 h at ambient temperature. The reaction mixture was freeze-dried to obtain a product as a pale-yellow solid.

TLC - Dichloromethane & methanol (1:1 – v/v), visualized with UV lamp, Rf: *Cis*-aconitic anhydride: 0.47, Reaction mixture 1: 0.63, Reaction mixture 2: 0.74

IR - ν max (film)/cm⁻¹: 3320.91 cm⁻¹ (2' amide stretch), 2957.57 cm⁻¹, 2930.73 cm⁻¹ and 2872.66 cm⁻¹ (alkane stretch), 1682.74 cm⁻¹ (carbonyl stretch acid or amide C=O), 1559.94 cm⁻¹ (alkene stretch), 1398.41 cm⁻¹ (alkane bend, rock), 1333.35 cm⁻¹ & 1314.14 cm⁻¹ (alkane bend, rock), 1228.40 cm⁻¹, 1254.96 cm⁻¹, 1193.03 cm⁻¹ & 1151.77 cm⁻¹ (carboxylic acids stretch C-O), 1085.73 cm⁻¹ (aliphatic amines stretch C-N), 953.21 cm⁻¹ & 931.30 cm⁻¹ (carboxylic acid O-H bend), 800.65 cm⁻¹, 779.51 cm⁻¹ & 678.65 cm⁻¹ (alkene bend C-H), 621.51 cm⁻¹ & 606.02 cm⁻¹ (1' amine wag N-H)

NMR - δ ¹H (600MHz; DMSO-d₆): 5.60 (d, J = 1.4 Hz, 1H), 5.39 (dd, J = 8.6, 1.7 Hz, 1H), 3.10-3.04 (m, 4H), 2.50 (t, 5H, DMSO-d₆), 1.71-1.64 (m, 4H), 1.37-1.04 (m, 4H), 0.78-0.70 (m, 6H),
 δ ¹³C (151MHz; DMSO-d₆): 99.9, 47.5, 39.9-39.1 (DMSO-d₆), 33.1, 30.4, 29.4, 19.7, 13.7

MS (Phosphate buffer pH 7.40; m/z) ESI+: 286 (100%[Compound 3 + H]⁺), 268 (45%[Compound 4+ H]⁺), 308 (22%[Compound 3 + Na]⁺), 130 (12%[Dibutylamine + H]⁺), **ESI-:** 240.3 (100%[Unknown adduct]⁻)

Melting point of product: Not obtained due to sodium salt being present.

Summary: By NMR, there were no signals for linker's CH₂ protons and CH proton. No carbonyl peaks were visible by ¹³C-NMR. But a compound same in mass as our product was detected by LCMS. A crude yield of 90.88% was obtained.

Reaction 2:

Synthesis of *N*-cis-aconityl-dibutylamide (3)

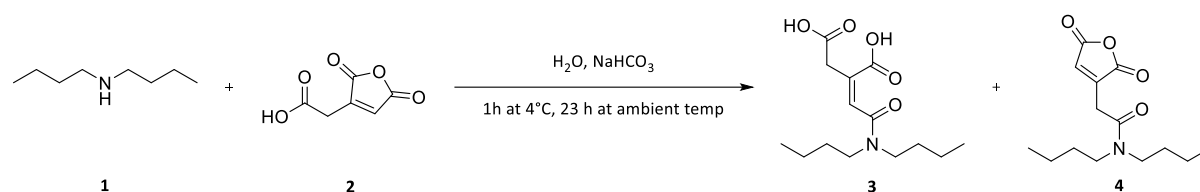


Figure 53: The reaction scheme for synthesizing compounds 3 and 4.

This method was altered from methods by Zhang, *et al.* in 2018 and Kang, Kim, Song, *et al.* in 2014. This method was amended from literature procedures. Dibutylamine (0.16 mL, 0.929 mmol), was dissolved in 30 mL of deionized water, NaHCO₃ (130.05 mg, 1.548 mmol) was added to a pre-weighed round bottomed flask. *Cis*-aconitic anhydride (120.81 mg, 0.774 mmol) in dioxane (5 mL) was added dropwise to the above dibutylamine solution under magnetic stirring at 4°C. After an overnight reaction, the mixture was extracted by 15 mL of ethyl acetate and 15 mL of 5% aqueous sodium bicarbonate solution (2-3 times). The aqueous layer was then freeze-dried.

TLC - Dichloromethane & methanol (1:1 – v/v), visualized with UV lamp, Rf.: *Cis*-aconitic anhydride: 0.26, Reaction mixture: 0.67

IR - ν max (film)/cm⁻¹: 3317.32 cm⁻¹ (2' amide stretch), 2956.40 cm⁻¹, 2929.11 cm⁻¹ and 2872.78 cm⁻¹ (alkane stretch), 1682.74 cm⁻¹ (carbonyl stretch acid or amide C=O), 1606.72 cm⁻¹ and 1558.77 cm⁻¹ (alkene stretch), 1466.92 cm⁻¹ and 1400.24 cm⁻¹ (alkane bend, rock), 1382.27 cm⁻¹ (alkane bend, rock), 1309.24 cm⁻¹, 1282.00 cm⁻¹, 1251.67 cm⁻¹, 1228.74 cm⁻¹ and 1151.30 cm⁻¹ (carboxylic acids stretch C-O), 1109.24 cm⁻¹ (aliphatic amines C-N stretch), 861.35 cm⁻¹ and 818.00 cm⁻¹ (alkene bend), 844.95 cm⁻¹ and 774.30 cm⁻¹ (2' amine wag), 654.44 cm⁻¹ (alkene bend – C-H)

NMR - δ ¹H (400MHz; D₂O): 8.37 (s, 1H), 6.50 (s, 1H, compound 3 linker CH proton), 5.97 (s, 1H), 5.79 (s, 1H, compound 4 CH proton), 5.55 (s, 1H), 4.89-4.69 (m, 5H, CH₃OH-D₄ impurity), 4.81 (D₂O, s) 3.69 (s, 2H, compound 3 linker CH₂ protons), 3.26 (s, 1H), 3.09-2.91 (m, 4H, compound's 3 and 4 CH₂ protons adjacent to amide nitrogen), 1.84 (s, 1H), 1.56-1.47 (m, 4H, compound's 3 or 4 CH₂ protons in middle of butyl chains), 1.30 (m, J = 7.5 Hz, 4H, compound's 3 or 4 CH₂ protons adjacent to terminal CH₃ groups in butyl chains), 0.86-0.80 (m, 6H, compound's 3 or 4 terminal CH₃ protons in butyl chains)

MS (Phosphate buffer pH 7.40; m/z) ESI+: 286.2 (100%[Compound 3 + H]⁺), 308.2 (32%[Compound 3 + Na]⁺), 268.2 (15%[Compound 4 + H]⁺), **ESI-:** 240.3 (100%[Unknown adduct]⁻)

Melting point of product: Not obtained due to sodium salt being present.

Summary: By NMR, there were signals for linker's CH₂ protons and CH proton. A compound same in mass as our product was detected by was LCMS. Product was obtained but had a crude yield of 84.85%.

Reaction 3:

Attempted synthesis of *N*-cis-aconityl-glucosamide (**6**)

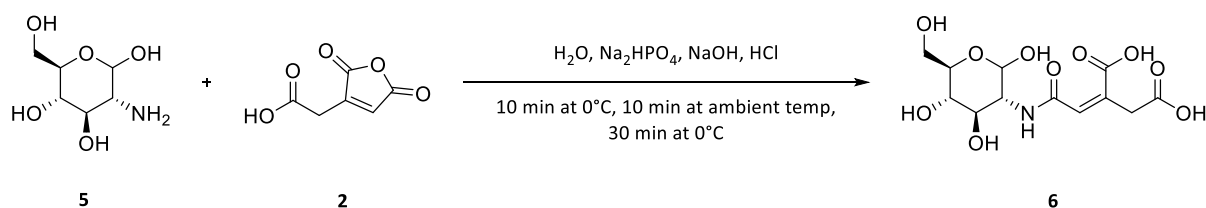


Figure 54: The reaction scheme for the attempted synthesis of compound **6**.

The method of Shen and Ryser in 1981 but with the following amendments, glucosamine (5mg, 2.319×10^{-2} mmol) was used in place of doxorubicin.

TLC - Dichloromethane, acetone & methanol (10:10:0.1 – v/v), visualized with UV lamp and ninhydrin, Rf.: Glucosamine: 0.08, *Cis*-aconitic anhydride: 0.84, Reaction mixture: 0.89

Summary: TLC indicated no reaction had taken place; therefore, the reaction was abandoned.

Reaction 4:

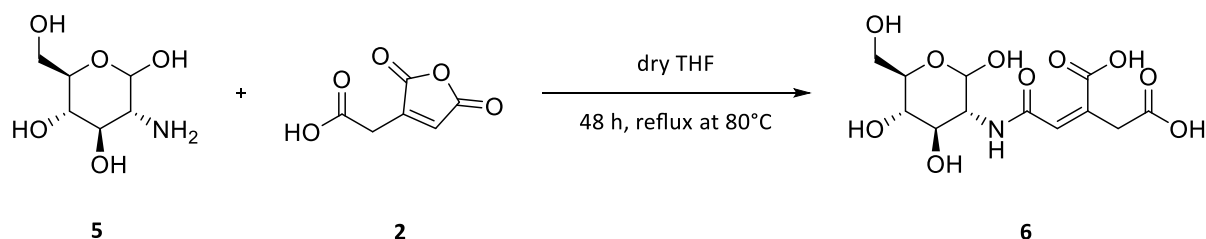


Figure 55: The reaction scheme for the attempted synthesis of compound **6**.

This method was modified from the original, as published in a patent by Hawaii Biotech Inc in 2004. Glucosamine (0.463 mmol, 100mg) was dissolved in 30 mL of THF in a pre-weighed round-bottomed flask. *Cis*-aconitic anhydride (0.695 mmol, 108.40mg), EDCI (0.463 mmol, 88.76mg), DMAP (0.463 mmol, 56.56mg) and triethylamine (0.29mL) were added slowly. The reaction was left to run for 36 hours under reflux at 80°C . After 36 hours, the solvent was evaporated off using a rotary evaporator. The reaction was then worked by evaporating off the THF. TLC analysis was then carried out to check for purity and retention factor (rf) values. Reaction ultimately did not work upon TLC analysis.

TLC - Dichloromethane & methanol (1:1 – v/v), visualized with UV lamp and ninhydrin, Rf.: Glucosamine: 0.15, *Cis*-aconitic anhydride 1: 0.13, *Cis*-aconitic anhydride 2: 0.45, Reaction mixture 1: 0.10, Reaction mixture 2: 0.48

Summary: TLC indicated no reaction had taken place; therefore, the reaction was abandoned.

Reaction 5:

Synthesis of *N*-cis-aconityl-glucosamide (6)

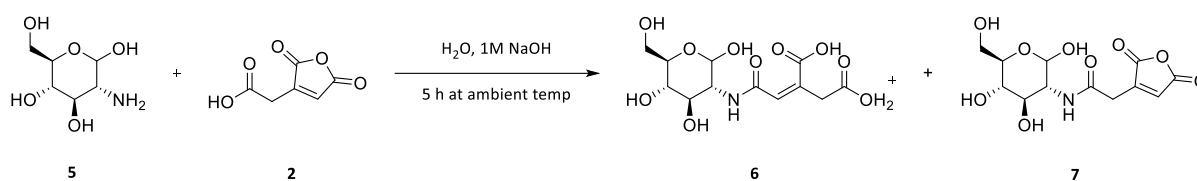


Figure 56: The reaction scheme for the synthesis of compounds 6 and 7.

This method was amended from a literature procedure by Hou, *et al.* in 2017. Glucosamine (100.00 mg, 0.464 mmol) was added to a 1M NaOH solution in a pre-weighed round-bottomed flask. Then *cis*-aconitic anhydride (108.58 mg, 0.696 mmol, 1.5 eq) was added in and the reaction was then left for 5 hours. The aqueous reaction mixture was then freeze-dried to obtain compound 3 as a pale brown solid.

TLC - Dichloromethane & methanol (1:1 – v/v), visualized with UV lamp, R_f.: Glucosamine: 0.23, *Cis*-aconitic anhydride: 0.33, Reaction mixture 1: 0.08, Reaction mixture 2: 0.85

IR - ν max (film)/cm⁻¹: 3283.01 cm⁻¹ (primary amine or secondary amide stretch – N-H), 1700.63 cm⁻¹ (carboxylic acid stretch – C=O), 1540.79 cm⁻¹ (primary amine bend – N-H), 1363.11 cm⁻¹ (alkane bend, rock – C-H), 1215.73 cm⁻¹ (aliphatic amines stretch – C-N), 1093.58 cm⁻¹ & 1031.52 cm⁻¹ (carboxylic acids stretch – C-O), 936.96 cm⁻¹ (carboxylic acid bend – O-H), 798.84 cm⁻¹ & 766.74 cm⁻¹ (alkene bend – C-H)

NMR - δ ¹H (600MHz; DMSO-D₆): 8.43 (s, 1H, compound's 6 or 7 nitrogen proton), 6.93 (s, 1H), 6.72 (s, 1H, compound 6 CH proton), 6.49 (s, 1H, compound's 6 or 7 proton adjacent to hydroxyl group and oxygen), 6.08 (s, 1H), 5.34 (s, 1H), 5.20 (s, 1H), 5.20-5.00 (m, 3H, compound's 6 or 7 hydroxyl protons directly bonded to the tetrahydropyran ring), 4.51 (d, J = 50.2 Hz, 1H), 4.27 (d, J = 8.2 Hz, 1H), 4.13 (t, J = 6.2 Hz, 1H), 3.98 (s, 1H, compound's 6 or 7 proton adjacent to hydroxyl group near amide group), 3.84 (s, 1H), 3.84-3.07 (m, 5H, compound's 6 or 7 protons in ring and glucosamine moiety CH₂), 3.35-2.94 (m, 2H, compound 6 CH₂ protons in linker), 3.06-2.94 (m, 3H), 2.61 (d, J = 2.1 Hz, 3H), 2.52-2.36 (DMSO-d₆, m), 1.89 (s, 6H), 1.36-1.23 (m, 1H), 0.95-0.85 (m, 1H), **δ ¹³C (151 MHz; DMSO-D₆):** 39.9-39.1 (DMSO-d₆)

MS - Phosphate buffer pH 7.40; m/z, ESI+: 318.2 (100%[Compound 7 + H]⁺), 358.2 (20%[Compound 6 + H]⁺), **ESI-:** 334.2 (100%[Compound 6 - H]⁻), 335.2 (18%[Compound 6]⁻)

Melting point of product: Not obtained due to sodium salt being present.

Summary: TLC plate was stained with ninhydrin to visualize glucosamine, product spot had no purple stain, indicating a reaction with glucosamine. Product was too low in concentration to provide a result on ¹³C-NMR. Product was obtained by LCMS but the crude yield was 62.13%.

Reaction 6:

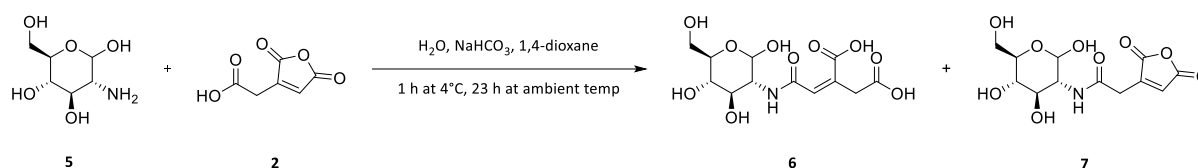


Figure 57: The reaction scheme for the synthesis of compounds 6 and 7.

This method was altered from methods by Zhang, *et al.* in 2018 and Kang, Kim, Song, *et al.* in 2014. (120.00 mg, 0.557 mmol), was dissolved in 30 mL of deionized water, sodium hydrogen-carbonate (112.15 mg, 1.335 mmol) was added to a pre-weighed round-bottomed flask. *Cis*-aconitic anhydride (69.46 mg, 0.445 mmol) in dioxane (5 mL) was added dropwise to the above solution whilst being magnetically stirred at 4°C. After an overnight reaction, the mixture was extracted by 15 mL of ethyl acetate and 15 mL of 5% aqueous sodium bicarbonate solution (2-3 times). The resulting extracted material being freeze-dried.

TLC - Dichloromethane & methanol (1:1 – v/v), visualized with UV lamp, R_f: Glucosamine: 0.32, *Cis*-aconitic anhydride: 0.22, Reaction mixture 1: 0.29, Reaction mixture 2: 0.73

IR - ν max (film)/cm⁻¹: 3291.77 cm⁻¹ (alcohols stretch – O-H), 1556.35 cm⁻¹ (primary amine bend – N-H), 1434.66 cm⁻¹ (alkane bend, rock – C-H), 1386.41 cm⁻¹ (alcohol or carboxylic acid stretch – C-O), 1259.33 cm⁻¹ & 1192.81 cm⁻¹ (amine stretching – C-N), 1081.17 cm⁻¹, 831.27 cm⁻¹, 817.97 cm⁻¹, 780.82 cm⁻¹, 766.79 cm⁻¹ & 737.73 cm⁻¹ (aliphatic amine stretch – C-N), 901.13 cm⁻¹ (carboxylic acid bend – O-H), 863.70 cm⁻¹ & 800.96 cm⁻¹ (alkene C=C bend [trisubstituted]), 680.14 cm⁻¹ (alkene bend – C-H)

NMR - δ ¹H (400 MHz; D₂O): 8.34 (d, J = 5.9 Hz, 2H, compound 6 and 7 nitrogen proton), 6.47 (d, J = 5.5 Hz, 2H, compound 6 CH proton and proton adjacent to a hydroxyl group and oxygen), 5.10-4.65 (m, 3H, compound 6 or 7 hydroxyl protons directly bonded to the tetrahydropyran ring), 4.81 (D₂O, s), 4.13 (s, 1H, compound 6 or 7 protons adjacent to hydroxyl group near amide group), 3.83 (s, 1H), 3.61-3.47 (m, 5H, compound 6 or 7 protons in-ring and glucosamine moiety CH₂), 3.32 (d, J = 5.9 Hz, 2H, compound 6 and 7 CH₂ protons in linker), 2.99 (s, 1H), 1.80 (s, 1H)

MS (Phosphate buffer pH 7.40; m/z) ESI⁺: 318.3 (100%[Compound 7 + H]⁺), 358.4 (42%[Compound 6 + Na]⁺), **ESI⁻:** 334.2 (100%[Compound 6 - H]⁻), 272.3 (73%[Unknown adduct]⁻), 290.3 (30%[Unknown adduct]⁻), 335.2 (18%[Compound 6]), 336.3 (5%[Compound 6 ion + H]⁻)

Melting point of product: Not obtained due to sodium salt being present.

Summary: TLC plate was stained with ninhydrin to visualize glucosamine, product spot had no purple stain, indicating a reaction with glucosamine, the product had a crude yield of 71.43%.

Reaction 7:

Attempted synthesis of *N*-cis-aconityl-phenylphenoate (9)

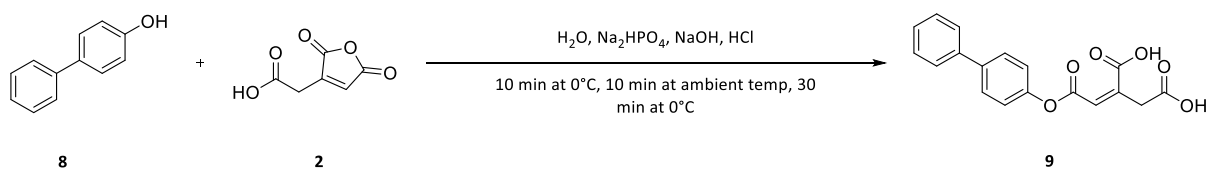


Figure 58: The reaction scheme for the attempted synthesis of compound 9.

The method of Shen and Ryser in 1981 but with the following amendments, 4-phenylphenol (5mg, 2.938×10^{-2} mmol) was used in place of doxorubicin.

TLC - Dichloromethane, acetone & methanol (30:10:0.1 – v/v), visualized with UV lamp, Rf:
4-phenylphenol: 0.15, *Cis*-aconitic anhydride: 0.03, Reaction mixture: 0.28

Summary: Product was not obtained as a triethylamine salt possibly formed. Further thought led to this aqueous method not being suitable for the lipophilic 4-phenylphenol.

Reaction 8:

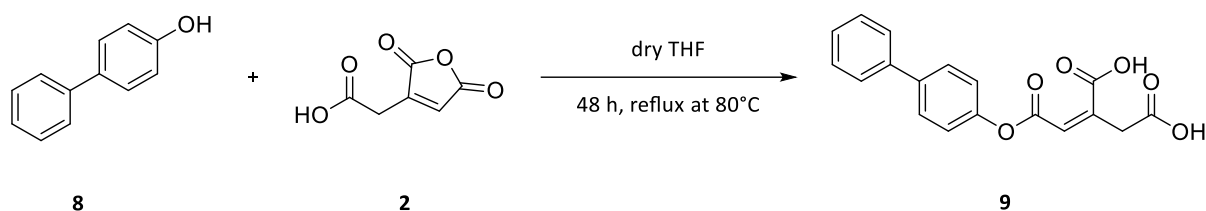


Figure 59: The reaction scheme for the attempted synthesis of compound 9.

This method was modified from the original, as published in a patent by Hawaii Biotech Inc in 2004. 4-phenylphenol (100.00 mg, 0.588 mmol) was dissolved in 30 mL of dry tetrahydrofuran in a pre-weighed round-bottomed flask. *Cis*-aconitic anhydride (137.67 mg, 0.882 mmol), DMAP (71.84 mg, 0.588 mmol) and triethylamine (0.25 mL, 1.764 mmol) were weighed out, and then added slowly, whilst stirring. The reaction was left to run for 36 hours under reflux at 80°C under nitrogen. After 48 hours, the solvent was evaporated off using a rotary evaporator. TLC analysis was carried out during the reaction and work up, to check for purity and retention factor (rf) values.

TLC - Dichloromethane & methanol (7:3 – v/v), visualized with UV lamp, Rf.: 4-phenylphenol: 0.92, *Cis*-aconitic anhydride: 0.18, Reaction mixture 1: 0.39, Reaction mixture 2: 0.61, 4-phenylphenol: 0.87

IR - ν max (film)/ cm^{-1} : 3351.72 cm^{-1} (alcohols stretch – O-H), 2979.59 cm^{-1} & 2947.03 cm^{-1} (alkane stretch - C-H), 2739.63 cm^{-1} & 2604.10 cm^{-1} (carboxylic acid stretch O-H), 2531.67 cm^{-1} , 2497.94 cm^{-1} , 1703.69 cm^{-1} (ester, acid stretch – C=O), 1647.00 cm^{-1} (carboxylic acid or amide stretch – C-H), 1563.28 cm^{-1} , 1475.06 cm^{-1} & 1444.15 cm^{-1} (aromatic stretch – C-C), 1397.26 cm^{-1} , 1383.87 cm^{-1} , 1364.82 cm^{-1} & 1331.48 cm^{-1} (alkane bend, rock – C-H), 1214.95 cm^{-1} (ester, carboxylic acid stretch – C-O), 1172.32 cm^{-1} & 1035.87 cm^{-1} (ester, carboxylic acid - stretch - C-O), 1072.31 cm^{-1} (aliphatic amines stretch [DMAP] – C-N), 851.34 cm^{-1} & 807.31 cm^{-1} (alkene C-H bend)

NMR - δ ^1H (400 MHz; $\text{CH}_3\text{OH}-\text{D}_4$): 7.53-7.21 (m, 9H, compound 9 aromatic protons), 6.86-6.82 (s, 1H, compound 9 CH proton), 4.92 (d, J = 11.8 Hz, 3H), 3.32-3.29 (m, 2H, compound 9 CH_2 protons), 2.60-2.33 (DMSO- d_6 , m), 2.17 (d, J = 7.8 Hz, 1H), 1.32-1.28 (m, 1H), 0.89 (t, J = 6.8 Hz, 1H), **δ ^{13}C (151 MHz; DMSO- D_6):** 157.1 (compound 9 aromatic carbon adjacent to ester group's oxygen), 144.6 (compound 9 carbon adjacent to middle carboxyl group), 131.6 (compound 9 CH_2 proton), 130.9-125.9 (compound 9 aromatic carbons), 115.7, 106.8, 67.0, 55.0, 45.5, 42.8 (compound 9 CH proton), 39.9-39.1 (DMSO- d_6 , m), 36.5, 34.9, 34.1, 8.7

MS: Sample had degraded.

Melting point of product: Sample had degraded.

Summary: Whilst regrettable that the sample had degraded, NMR confirmed the presence of linker's CH proton and CH_2 protons. Product was obtained but had a crude yield of 84.00%.

Attempted synthesis of (6,7-dimethoxy-3,4-dihydroisoquinolin-2(1H)-yl)(4'-hydroxy-[1,1'-biphenyl]-4-yl)methanone (**12**):

Reaction 9:

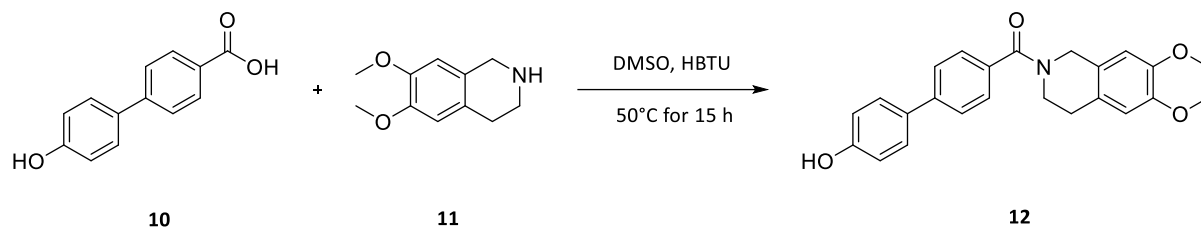


Figure 60: Reaction scheme for the attempted synthesis of compound **12**.

This method was altered from a literary procedure by Colabufo, *et al.* in 2008. 6,7-dimethoxy-1,2,3,4-tetrahydroisoquinoline (214.31 mg, 0.933 mmol) was dissolved in 83 mL of DMSO, followed by HBTU (268.38 mg, 1.400 mmol) and triethylamine (0.39 mL, 2.799 mmol). 4'-hydroxy-4-biphenylcarboxylic acid (200.00 mg, 0.933 mmol) was then added. The reaction mixture was then heated to 50°C and left for 15 hours. The organic layer was separated and washed with 0.5 M Na₂CO₃ (3x20 mL) and 3 M HCl (3x20 mL). This layer was dried over anhydrous Na₂SO₄ and the solvent was then evaporated off.

TLC – Dichloromethane & methanol (1:1 – v/v), visualized with UV lamp, Rf.: 4'-hydroxy-4-biphenylcarboxylic acid: 0.92, 6,7-dimethoxy-1,2,3,4-tetrahydroisoquinoline: 0.71, HBTU: 0.05, Reaction mixture 1: 0.79, Reaction mixture 2: 0.92

Summary: Reaction was not successful as the order of reagent addition meant HBTU could not activate the acid group.

Reaction 10:

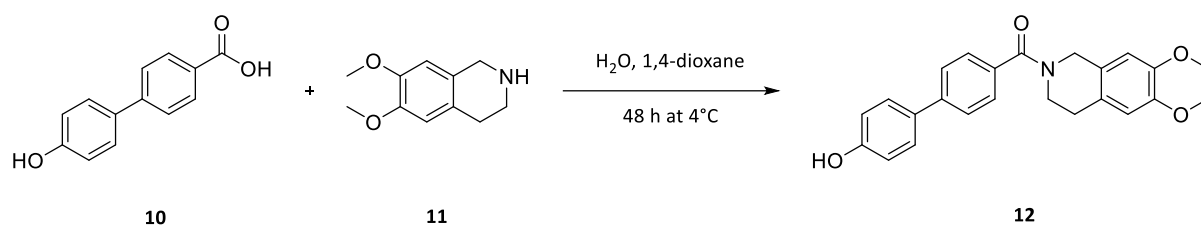


Figure 61: Reaction scheme for the attempted synthesis of compound 12.

This method was amended from two literature procedures by Kuruvilla, *et al.* in 2017 and Zhang, *et al.* in 2018. 6,7-dimethoxy-1,2,3,4-tetrahydroisoquinoline (160.84 mg, 0.700 mmol) was added pre-weighed round-bottomed flask containing 30 mL of deionized water. Then it was placed on ice. NaHCO_3 (176.42 mg, 2.100 mmol), EDCI (201.29 mg, 1.050 mmol) and HOBt (141.88 mg, 1.050 mmol) were added subsequently. 4'-hydroxy-4-biphenylcarboxylic acid (150.00 mg, 0.700 mmol) was dissolved in 5 mL of dioxane and added to the reaction mixture. The reaction was left at 4°C overnight. After 72 hours, the reaction mixture was freeze-dried. Then the mixture was extracted by 15 mL of ethyl acetate and 15 mL of 5% aqueous sodium bicarbonate solution (2-3 times). Ethyl acetate was removed by rotary evaporation.

TLC – Dichloromethane & methanol (6:4 – v/v), visualized with UV lamp, Rf.: 4'-hydroxy-4-biphenylcarboxylic acid: 0.86, 6,7-dimethoxy-1,2,3,4-tetrahydroisoquinoline: 0.80, Reaction mixture 1: 0.26, Reaction mixture 2: 0.37, Reaction mixture 3: 0.69, Reaction mixture in dichloromethane 1: 0.03, Reaction mixture in dichloromethane 2: 0.31

IR - ν max (film)/ cm^{-1} : 2935.78 cm^{-1} (carboxylic acid stretch – O-H), 1604.36 cm^{-1} (carbonyl stretch, C=O, amide), 1517.80 cm^{-1} (aromatic stretch, C-C), 1443.08 cm^{-1} (alkane bend, rock, C-H), 1259.81 cm^{-1} & 1109.04 cm^{-1} (alcohol, carboxylic acid stretch – C-O), 828.69 cm^{-1} (1,2,3,4-tetrasubstituted bend - C-H)

MS - Methanol; m/z, ESI+: 547.7 (100%[Unknown adduct, possible contaminant]), **ESI-:** 836.4 (100%[Unknown adduct, possible contaminant])

Summary: Adducts in LCMS did not correspond with the expected mass of the product, along with no new spot on TLC, this reaction did not work.

Reaction 11:

Attempted synthesis of 4'-hydroxy-4-biphenylcarbonyl chloride (**13**) and (6,7-dimethoxy-3,4-dihydroisoquinolin-2(1H)-yl)(4'-hydroxy-[1,1'-biphenyl]-4-yl)methanone (**12**)

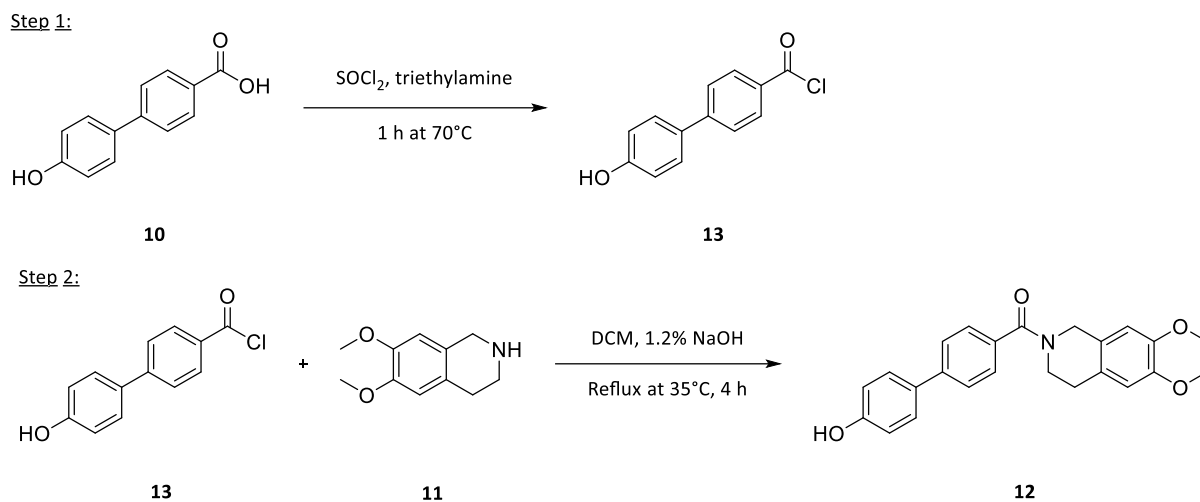


Figure 62: Reaction scheme for the attempted synthesis of compounds **13** and **12**.

This method was amended from a literature procedure by Colabufo *et al.* in 2008. 4'-hydroxy-4-biphenylcarboxylic acid (428.44 mg, 2 mmol) was dissolved in an excess of SOCl₂ (8 mL) and triethylamine (0.84 mL, 6 mmol) was stirred for an hour at 70°C. Excess SOCl₂ was removed by rotary-evaporation, crude then solubilized with DCM and evaporated till dry. Compound **13** from this reaction was then added to a solution of 6,7-dimethoxytetrahydroisoquinoline (459.40 mg, 2 mmol) in dichloromethane (30 mL) and 1.2% of NaOH (30 mL). The mixture was then left at room temperature for 4 h and the solvent was evaporated off. NMR and LCMS analysis was carried out. The organic layer was separated and washed with 0.5 M Na₂CO₃ (3x20 mL) and 3 M HCl (3x20 mL). This layer was dried over anhydrous Na₂SO₄ and the solvent was then evaporated off.

Step 1 - TLC (methanol), visualized with UV lamp, Rf.: 4'-hydroxy-4-biphenylcarboxylic acid: 0.83, 4'-hydroxy-4-biphenylcarboxylic acid and reaction mixture: 0.29, reaction mixture: 0.31,
Step 2 (methanol), visualized with UV lamp, Rf.: Step 1 product: 0.28, 4'-hydroxy-4-biphenylcarbonyl chloride and reaction mixture 2: 0.75, 6,7-dimethoxytetrahydroisoquinoline: 0.13

IR - Step 2 - ν max (film)/cm⁻¹: 2978.29 cm⁻¹ & 2933.53 cm⁻¹ (alkane stretch – C-H), 1630.84 cm⁻¹ (carboxylic acid stretch - C-O), 1549.79 cm⁻¹, 1516.71 cm⁻¹ & 1496.86 cm⁻¹ (aromatics stretch – C-C), 1430.33 cm⁻¹, 1380.03 cm⁻¹ & 1360.30 cm⁻¹ (alkane bend, rock – C-H), 1308.70 cm⁻¹, 1257.78 cm⁻¹, 1224.35 cm⁻¹, 1108.11 cm⁻¹, 1076.47 cm⁻¹ & 1012.81 cm⁻¹ (ester, alcohol, carboxylic acid stretch – C-O), 896.42 cm⁻¹ (alkyl chloride - C-Cl), 838.56 cm⁻¹, 811.75 cm⁻¹ 766.36 cm⁻¹, 733.21 cm⁻¹ & 700.50 cm⁻¹ (alkene bend - C-H), 668.13 cm⁻¹, 635.85 cm⁻¹ & 622.17 cm⁻¹ (alkyl chloride - C-Cl)

Summary: Formation of black powder (possibly due to side reaction between 4'-hydroxy-4-biphenylcarboxylic acid and triethylamine) and lack of a new TLC spot this reaction did not work.

Reaction 12:

Attempted synthesis of glucosamide-cis-aconityl-dibutylamide (14)

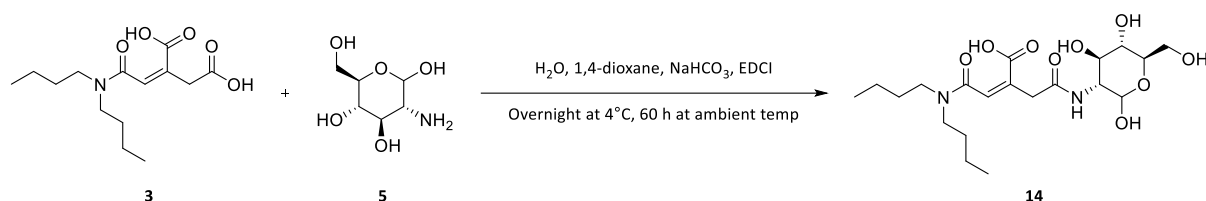


Figure 63: Reaction scheme of synthesising compound 14.

This method was amended from two literature procedures by Kuruvilla, *et al.* in 2017 and Zhang, *et al.* in 2018. Glucosamine (75.47 mg, 0.350 mmol), was dissolved in 50 mL of deionized water, NaHCO₃ (130.05 mg, 1.548 mmol), N-cis-aconityl-dibutylamide (120.00 mg, 0.421 mmol) and EDCI (80.71 mg, 0.421 mmol) were added to a pre-weighed round-bottomed flask. The reaction was left at 4°C overnight. After 72 hours, the mixture was extracted by 15 mL of ethyl acetate and 15 mL of 5% aqueous sodium bicarbonate solution (2-3 times). Ethyl acetate was removed by rotary evaporation.

TLC - Dichloromethane & methanol (1:1 – v/v), visualized with UV lamp and ninhydrin, Rf.:

Glucosamine: 0.27, N-cis-aconityl-dibutylamide: 0.80, Reaction mixture: 0.84, EDCI: 0.13

IR - ν max (film)/cm⁻¹: 3520.72 cm⁻¹ & 3436.88 cm⁻¹ (alcohols stretch – O-H), 2718.88 cm⁻¹, 2637.13 cm⁻¹ (carboxylic acids stretch – O-H), 1651.68 cm⁻¹ (carboxylic acid stretch – C=O), 1565.38 cm⁻¹ (primary amine – N-H), 1480.77 cm⁻¹ (alkane bend, rock – C-H), 1242.96 cm⁻¹, 1161.27 cm⁻¹, 1093.74 cm⁻¹ & 1036.02 cm⁻¹ (alcohol, carboxylic acids stretch – C-O), 951.55 cm⁻¹ & 902.21 cm⁻¹ (alkene bend – C-H)

MS - Phosphate buffer pH 7.40; m/z, ESI+: 447.5 (100%[Compound 14 + H]⁺), 268.3 (Compound 3 + H)⁺, 469.4 (55%[Compound 14 + Na]⁺), **ESI-:** 445.5 (100%[Compound 14 - H]⁻), 427.5 (40%[Compound 14 - H₂O - H]⁻)

Melting point of product: Not obtained due to sodium salt being present.

Summary: NMR data was not obtained as NMR spectrometers were not functional. Product was a mixture as shown by MS.

Reaction 13:

Synthesis of *N*-cis-aconityl-amidotetrahydropyran (16)

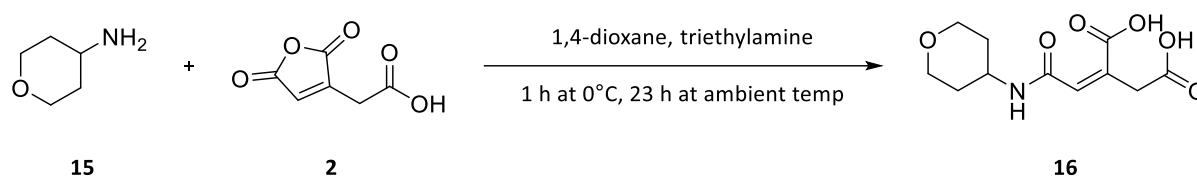


Figure 64: Reaction scheme of synthesising compound 16.

This method was amended from two literature procedures by Zhang *et al.* in 2018 and Kang *et al.* in 2014. 4-aminotetrahydropyran (0.62 mL, 5.932 mmol) and triethylamine (0.49 mL, 3.559 mmol) were added to a pre-weighed round-bottomed flask containing 10 mL of dioxane. This was then placed on ice. *Cis*-aconitic anhydride (462.96 mg, 2.966 mmol) dissolved in dioxane (5 mL) was added dropwise to the reaction mixture. After being left overnight, the mixture was extracted by 15 mL of ethyl acetate, 15 mL of acidified brine solution (2-3 times) and neutral brine solution (2-3 times). The organic layer was then evaporated to afford a product.

TLC - Dichloromethane, methanol (1:1 – v/v), visualized with UV lamp, Rf.: *Cis*-aconitic anhydride: 0.28, Reaction mixture 1: 0.39, Reaction mixture 2: 0.55

IR - ν max (film)/ cm^{-1} : 2930.79 cm^{-1} (alkane stretch – C-H), 1685.15 cm^{-1} (amide stretch – C=O), 1603.03 cm^{-1} (alkene stretch – C=C), 1492.74 cm^{-1} (unknown absorbance), 1452.34 cm^{-1} (alkane bend, rock – C-H), 1263.64 cm^{-1} , 1157.84 cm^{-1} & 1037.37 cm^{-1} (carboxylic acid stretch – C-O), 973.19 cm^{-1} (carboxylic acid bend – O-H), 770.51 cm^{-1} (1' amine wag), 698.81 cm^{-1} (alkene bend – C-H)

NMR - δ ^1H (600 MHz; $\text{CH}_3\text{OH-D}_4$): 8.53 (s, 1H, amide proton), 6.51 (s, 1H, product's CH proton), 5.33 (s, 1H), 5.01-4.82 ($\text{CH}_3\text{OH-D}_4$, d, $J = 13.1$ Hz, 1H), 3.93-3.88 (m, 4H, product's CH_2 protons adjacent to oxygen in the tetrahydropyran moiety and terminal proton in tetrahydropyran ring moiety), 3.66-3.59 (s, 1H, product's CH_2 protons as part of linker moiety), 3.50-3.29 ($\text{CH}_3\text{OH-D}_4$, m, 3H), 3.18 (t, $J = 2.4$ Hz, 0H), 2.15 (dd, $J = 31.6, 7.6$ Hz, 0H), 2.02 (d, $J = 6.2$ Hz, 4H, product's CH_2 protons adjacent to carbon conjugated to amide group), 1.88 (s, 0H), 1.59 (s, 0H), 1.28 (d, $J = 13.1$ Hz, 0H), 1.14 (s, 0H), 0.93-0.83 (m, 0H), 0.09 (s, TMS)

MS - Phosphate buffer pH 7.40; m/z, ESI+: 256.2 (100%[Compound 16 minus a hydroxyl proton]⁺), 257.4 (19%[Compound 16]⁻), **ESI-:** 308.8 (47%[Unknown contaminant]⁻), 311.2 (45%[Unknown contaminant]⁻)

Melting point of product: No melting point could be obtained.

Summary: Product was too low in concentration to provide a result on ^{13}C -NMR. The reaction was successful due to a mass corresponding with our product in LCMS and signals for the linker's CH and CH_2 protons. The reaction had a yield of 6.76%.

Reaction 14:

Reaction 13 was repeated but with 2 molar equivalents of 4-aminotetrahydropyran and without triethylamine.

TLC – Dichloromethane & methanol (1:1 – v/v), visualized with UV lamp, Rf.: *Cis*-aconitic anhydride: 0.35, Reaction mixture 1: 0.48, Reaction mixture 2: 0.65

IR - ν max (film)/ cm^{-1} : 2935.00 cm^{-1} (carboxylic acids stretch – O-H), 1602.64 cm^{-1} (alkene stretch – C=C), 1495.60 cm^{-1} (contamination, peak corresponds to aromatic stretch C-C), 1454.82 cm^{-1} (alkane bend, rock – C-H), 1266.09 cm^{-1} (carboxylic acid stretch – C-O), 762.38 cm^{-1} (primary amine wag), 699.38 cm^{-1} (alkene bend – C-H)

NMR - δ ^1H (600 MHz; $\text{CH}_3\text{OH-D}_4$): 8.53 (s, 1H, amide proton), 7.43 (d, $J = 8.9$ Hz, OH), 6.85 (s, 1H, product's CH proton), 5.01-4.85 ($\text{CH}_3\text{OH-D}_4$, d, $J = 13.1$ Hz, 1H), 4.60 (s, OH), 3.41 (m, 4H, product's CH_2 protons adjacent to oxygen in the tetrahydropyran moiety and terminal proton in tetrahydropyran ring moiety), 3.33-3.27 (m, OH), 3.18 (s, product's CH_2 protons as part of linker moiety), 1.89 (s, 4H, product's CH_2 protons adjacent to carbon conjugated to amide group), 1.28 (s, OH), 0.89 (t, $J = 6.9$ Hz, OH), 0.09 (s, TMS)

MS - Phosphate buffer pH 7.40; m/z, ESI+: 256.3 (100%[Compound 16 minus a hydroxyl proton]⁺), 257.3 (25%[Compound 16]⁺), **ESI-:** 835.8 (100%[Unknown contaminant]⁻), 836.9 (40%[Unknown contaminant]⁻)

Melting point of product: No melting point could be obtained.

Summary: Product was too low in concentration to provide a result on ^{13}C -NMR. The reaction was successful due to a mass corresponding with our product in LCMS and signals for the linker's CH and CH_2 protons. The reaction had a yield of 15.72%.

Reaction 15:

Synthesis of *N*-cis-aconityl-phenethylamide (18)

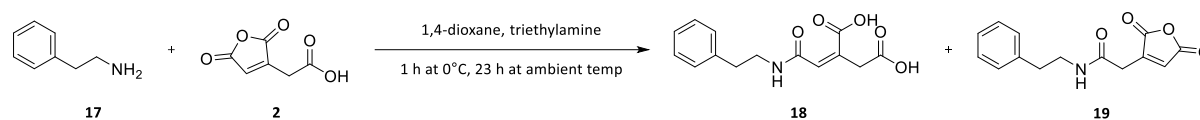


Figure 65: Reaction scheme of synthesising compounds **18** and **19**.

This method was amended from literature procedures by Zhang *et al.* in 2018 and Kang *et al.* in 2014. Phenethylamine (0.40 mL, 2.476 mmol), was added to a pre-weighed round-bottomed flask. This was then placed on ice. *Cis*-aconitic anhydride (386.48 mg, 2.476 mmol) dissolved in dioxane (5 mL) was added dropwise to the reaction mixture. After being left overnight, the mixture was extracted by 15 mL of ethyl acetate, 15 mL of acidified brine (3 times) and neutral brine (3 times). The organic layer was evaporated to afford a product.

TLC – Dichloromethane & methanol (1:1 – v/v), visualized with UV lamp, Rf.: Phenethylamine 1: 0.03, Phenethylamine 2: 0.16, Phenethylamine 3: 0.56, Phenethylamine 4: 0.66, Phenethylamine 5: 0.84, *Cis*-aconitic anhydride: 0.03, Reaction mixture 1: 0.03, Reaction mixture 2: 0.69, Reaction mixture 3: 0.84

IR - ν max (film)/ cm^{-1} : 3277.66 cm^{-1} (primary amine or 2' amide stretch – N-H), 2950.77 cm^{-1} (carboxylic acids stretch – O-H), 1691.36 cm^{-1} (amide stretch – C=O), 1625.78 cm^{-1} & 1552.54 cm^{-1} (alkene stretch – C=C), 1496.65 cm^{-1} , 1455.24 cm^{-1} & 1431.66 cm^{-1} (aromatics stretch – C-C), 1402.67 cm^{-1} & 1364.97 cm^{-1} (alkane bend, rock – C-H), 1314.50 cm^{-1} , 1265.28 cm^{-1} , 1209.13 cm^{-1} , 1167.98 cm^{-1} , 1106.27 cm^{-1} , 1057.71 cm^{-1} & 1030.92 cm^{-1} (carboxylic acid stretch – C-O), 955.28 cm^{-1} & 901.97 cm^{-1} (carboxylic acid bend – O-H), 797.42 cm^{-1} & 752.73 cm^{-1} (alkene bend – C-H), 699.34 cm^{-1} (alkene bend – C-H)

NMR - δ ^1H (600MHz; $\text{CHCl}_3\text{-D}$): 7.32-7.21 (m, 5H, compound 18 aromatic protons), 7.24 ($\text{CHCl}_3\text{-D}$, s), 6.81 (t, J = 2.4 Hz, 7H, compound's 18 and 19 CH proton), 3.88-3.85 (m, 2H, compound 18 CH_2 protons adjacent amide group), 3.71-3.63 (m, 5H, compound's 18 and 19 CH_2 protons as part of linker moiety), 2.93 (t, J = 7.6 Hz, 2H, compound 18 CH_2 protons adjacent to aromatic ring), 2.11 (s, 2H), 1.24 (s, 1H), **δ ^{13}C (600MHz; D_2O):** 128.8, 128.6, 126.8, 77.2-76.8 ($\text{CHCl}_3\text{-D}$), 67.1, 40.3

MS (Phosphate buffer pH 7.40; m/z) ESI+: 278.1 ([Compound 18 + H]⁺) 260.1 ([Compound 19 + H]⁺), **ESI-:** 232.1 ([Unknown adduct]⁻), 276.0 ([Compound 18 - H]⁻),

Melting point of product: 95-100°C.

Summary: The reaction was successful, a corresponding mass in LCMS and signals for the linker's CH and CH_2 protons. Several impurities from phenethylamine were present. The reaction had a yield of 0.14%.

Reaction 16:

Reaction 15 was repeated but 2 molar equivalents of phenethylamine.

TLC - Dichloromethane, methanol (1:1 – v/v), visualized with UV lamp, Rf.: Phenethylamine 1: 0.10, Phenethylamine 2: 0.63, Phenethylamine 3: 0.80, Phenethylamine 4: 0.90, *Cis*-aconitic anhydride: 0.03, Reaction mixture 1: 0.03, Reaction mixture 2: 0.63, Reaction mixture 3: 0.87

IR - ν max (film)/ cm^{-1} : 3274.00 cm^{-1} (1' amine or 2' amide stretch – N-H), 3028.03 cm^{-1} , 2941.60 cm^{-1} & 2625.12 cm^{-1} (carboxylic acids stretch – O-H), 1690.39 cm^{-1} (amide stretch – C=O), 1626.80 cm^{-1} & 1585.45 cm^{-1} (alkene stretch – C=C), 1524.42 cm^{-1} (primary amine bend – N-H), 1466.05 cm^{-1} , 1455.38 cm^{-1} & 1421.17 cm^{-1} (aromatics stretch – C-C), 1398.14 cm^{-1} & 1348.36 cm^{-1} (alkane bend, rock – C-H), 1298.90 cm^{-1} , 1283.63 cm^{-1} , 1243.84 cm^{-1} , 1227.97 cm^{-1} , 1213.84 cm^{-1} , 1127.31 cm^{-1} , 1086.87 cm^{-1} , 1057.71 cm^{-1} & 1036.78 cm^{-1} (alkane bend, rock – C-H), 966.85 cm^{-1} , 932.69 cm^{-1} & 908.14 cm^{-1} (carboxylic acid bend – O-H), 885.00 cm^{-1} , 836.15 cm^{-1} , 799.57 cm^{-1} & 769.48 cm^{-1} (alkene bend – C-H), 744.45 cm^{-1} (1' amine wag – N-H), 696.10 cm^{-1} (alkene bend – C-H)

NMR - δ ^1H (600 MHz; $\text{CH}_3\text{OH-D}_4$): 7.29-7.18 (m, 5H, compound 10 aromatic protons), 6.93 (s, 2H), 6.65 (s, 1H, compound 10 CH proton), 6.38 (s, 2H), 4.96 ($\text{CH}_3\text{OH-D}_4$, s), 3.88-3.76 (m, 2H, compound 10 CH_2 protons adjacent amide group), 3.65 (s, 2H, compound 10 CH_2 protons as part of linker moiety), 3.46-3.30 ($\text{CH}_3\text{OH-D}_4$, m), 2.84-2.76 (t, 2H, compound 10 CH_2 protons adjacent to aromatic ring), 2.00 (s, 1H), **δ ^{13}C (151 MHz; $\text{CH}_3\text{OH-D}_4$):** 129.9, 129.8, 129.5, 68.1, 49.4-48.6

MS - Phosphate buffer pH 7.40; m/z, ESI+: 278.0 (100%[N-*cis*-aconityl-phenethylamide + H] $^+$) 260.1 (39%[Compound 11 + H] $^+$), **ESI-:** 232.1 (100%[Unknown adduct] $^-$), 275.9 (82%[N-*cis*-aconityl-phenethylamide - H] $^-$),

Melting point of product: 105-110°C.

Summary: The reaction was successful, a corresponding mass in LCMS and signals for the linker's CH and CH_2 protons. Several impurities from phenethylamine were present. A crude yield of 88.07% was obtained as a triethylamine salt was suspected alongside the desired product.

Reaction 17:

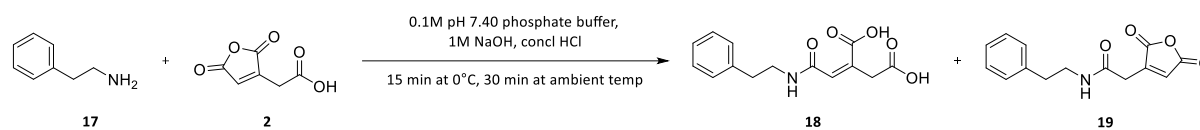


Figure 66: Reaction scheme of synthesising compounds 18 and 19.

Reaction 15 was repeated but with the following amendments. Phenethylamine (1.04 mL, 8.252 mmol) was dissolved in 10 mL of 0.1 M phosphate buffer at pH 7.40, in a pre-weighed round bottomed flask. This was then placed on ice. *Cis*-aconitic anhydride (644.00 mg, 4.126 mmol) was added in small aliquots with NaOH 1M added dropwise to maintain the pH at 9.00. Aliquots tested on universal indicator paper. After pH reached 9.00, it was left on ice for 15 min, and then at ambient temperature for 30 min. Concentrated HCl was added dropwise to obtain a pH of 3.00, following the formation of a precipitate, the reaction mixture was filtered.

TLC - Dichloromethane, methanol (2:1 – v/v), visualized with UV lamp, R_f: Phenethylamine: 0.30, *Cis*-aconitic anhydride: 0.13, Reaction mixture: 0.65

IR - ν max (film)/cm⁻¹: 3028.52 cm⁻¹ & 2934.89 cm⁻¹ (carboxylic acids stretch – O-H), 1694.63 cm⁻¹ (amide stretch – C=O), 1601.97 cm⁻¹ (alkene stretch – C=C), 1493.57 cm⁻¹ (aromatics stretch – C-C), 1452.94 cm⁻¹ & 1329.41 cm⁻¹ (alkane bend, rock – C-H), 1261.08 cm⁻¹, 1156.02 cm⁻¹, 1077.53 cm⁻¹ & 1036.43 cm⁻¹ (carboxylic acid stretch – C-O), 975.10 cm⁻¹ (carboxylic acid bend – O-H), 882.90 cm⁻¹, 746.54 cm⁻¹ (primary amine wag), 696.69 cm⁻¹ (alkene bend – C-H)

NMR - δ ¹H (600 MHz; CH₃OH-D₄): 7.34-7.16 (m, 5H, compound 18 aromatic protons), 6.92 (d, *J* = 16.5 Hz, 5H), 6.71 (s, 1H, compound 18 CH proton), 6.44 (s, 2H), 6.13 (s, 2H), 4.97 (CH₃OH-D₄, s), 3.47-3.43 (m, 2H, compound 18 CH₂ protons adjacent amide group), 3.34-3.30 (CH₃OH-D₄, m), 3.16 (dd, *J* = 8.9, 6.9 Hz, 5H, compound's 18 and 19 CH₂ protons as part of linker moiety), 2.96-2.81 (t, 2H, compound 18 CH₂ protons adjacent to aromatic ring), 0.00 (s, TMS), **δ ¹³C (151 MHz; CH₃OH-D₄):** 175.2-174.8 (compound's 18 and 19 terminal carboxyl carbons), 171.8-170.8 (compound's 18 and 19 middle carboxyl carbon), 168.0 (compound 18 amide carbon), 140.5, 140.3, 138.0 (compound 18 aromatic carbon adjacent to ethyl moiety), 130.0-127.3 (compound 18 five aromatic carbons), 49.4-48.6 (CH₃OH-D₄), 43.3-42.6 (compound's 18 and 19 CH₂ carbon adjacent to the amide group), 42.4-41.9 (compound's 18 and 19 CH₂ carbon from linker moiety), 36.3, 36.2, 34.6 (compound 18 CH₂ carbon adjacent to benzene moiety)

MS (Phosphate buffer pH 7.40; m/z) ESI⁺: 278.1 (100%[Compound 18 + H]⁺) 260.2 (49%[Compound 19 + H]⁺), 260.0 (38%[Compound 19 + H]⁺), **ESI⁻:** 232.3 (100%[Unknown adduct]⁻), 276.2 (21%[Compound 18 - H]⁻),

Melting point of product: 100-105°C.

Summary: With a new batch of phenethylamine, a cream solid was obtained with a 47.2% yield. TLC showed the formation of a new spot with a different r_f value to the reagents. Both proton and ^{13}C NMR showed signals for product's CH group. In LCMS, a compound with the same mass as our product was identified.

Reaction 18:

Attempted synthesis of *N*-cis-aconityl-*N*-methyl-phenethylamide (21)

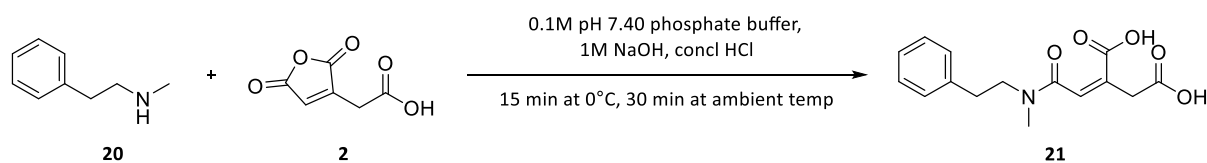


Figure 67: Reaction scheme for the attempted synthesis of compound 21.

A literature procedure was carried out with the following amendments by Zhang *et al.* in 2018 and Kang *et al.* in 2014. *N*-methyl-phenethylamine (0.61 mL, 4.438 mmol) was dissolved in 5 mL of 0.1 M phosphate buffer at pH 7.40, in a pre-weighed round bottomed flask. This was then placed on ice. *Cis*-aconitic anhydride (346.33 mg, 2.219 mmol) was added in small aliquots with NaOH 1M also added dropwise to maintain the pH at 9.00. Aliquots were tested on universal indicator paper. After pH was maintained at pH 9.00, it was left on ice for 15 min, and left at ambient temperature for 30 min. Concentrated HCl was added dropwise to obtain a pH of 3.00, following the formation of a precipitate, the reaction mixture was filtered.

TLC – Dichloromethane & methanol (2:1 v/v), visualized with UV lamp, R_f: *N*-methyl-phenethylamine: 0.31, *Cis*-aconitic anhydride: 0.09, Reaction mixture: 0.72

IR - ν max (film)/cm⁻¹: 3407.65 cm⁻¹, 3280.90 cm⁻¹ (alcohols stretch – O-H), 3164.89 cm⁻¹ (carboxylic acids stretch – O-H), 1693.64 cm⁻¹ (amide, carboxylic acid stretch – C=O) 1636.33 cm⁻¹ (carboxylic acid stretch – C=O), 1548.59 cm⁻¹ (aromatics stretch – C-C), 1403.97 cm⁻¹ (alkane bend, rock – C-H), 1051.40 cm⁻¹ & 1019.73 cm⁻¹ (carboxylic acid stretch – C-O), 928.29 cm⁻¹ (carboxylic acid bend – O-H), 800.59 cm⁻¹ (alkene bend – C-H)

NMR - δ ¹H (600 MHz; CH₃OH-D₄): 7.34-7.25 (m, 5H), 4.93 (CH₃OH-D₄, s), 3.60 (s, 1H), 3.31-3.30 (CH₃OH-D₄, m), 3.14 (t, J = 7.9 Hz, 1H), 2.95 (t, J = 7.9 Hz, 1H), 2.64 (s, 1H), 2.00 (s, 2H), 1.90-1.88 (m, 1H), 1.79 (s, 1H), 1.28 (s, 2H), 0.00 (s, TMS), **δ ¹³C (151 MHz; CH₃OH-D₄):** 180.3, 129.9, 129.8, 49.4-48.6 (CH₃OH-D₄), 24.1

MS (Phosphate buffer pH 7.40; m/z) ESI+: 228.5 (100%[unknown adduct, possible contaminant]⁺), **ESI-:** 331.2 (100%[unknown adducts, possible contaminants]⁻), 331.4 (92%[unknown adducts, possible contaminants]⁻)

Melting point of product: No melting point recorded, solid just burnt, the melting point must be above 350°C.

Summary: Reaction was not successful due to no presence of a signal around 6.7-6.8 for the CH proton of the linker. Also, no compound matched the expected mass in LCMS. A white solid was obtained with a 4.06% yield.

Reaction 19:

Synthesis of amidotetrahydropyran-cis-aconityl-phenethylamide (22)

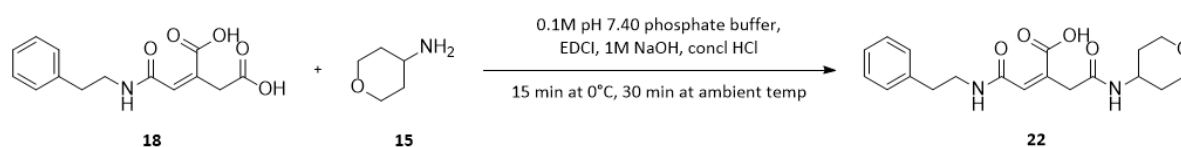


Figure 68: Reaction scheme for the attempted synthesis of compound 22.

A literature procedure was carried out with the following amendments. N-cis-aconityl-phenethylamide (200.00 mg, 0.721 mmol) and EDCI (138.27 mg, 0.721 mmol) were dissolved in 10 mL 0.1 M of pH 6.00 phosphate buffer, in a pre-weighed round bottomed flask. This was then placed on ice. 4-aminotetrahydropyran (145.92 mg, 1.443 mmol) was added in small aliquots with NaOH 1M also added dropwise to maintain the pH at 9.00. Aliquots were tested on universal indicator paper. After pH was steady, it was left on ice for 15 min, and at ambient temperature for 30 min. Concentrated HCl was added dropwise to pH of 3.00, following precipitate formation, reaction mixture was filtered (Kuruvilla et al., 2017 & Kang *et al*, 2014).

TLC – Dichloromethane & methanol (2:1 v/v), visualized with UV lamp, Rf.: N-cis-aconityl-phenethylamide: 0.42, 4-aminotetrahydropyran: 0.09, Reaction mixture: 0.58, EDCI: 0.45

IR - ν max (film)/ cm^{-1} : 2605.33 cm^{-1} (carboxylic acids stretch – O-H), 1702.06 cm^{-1} (amide stretch – C=O), 1614.98 cm^{-1} (alkene stretch – C=C), 1454.64 cm^{-1} (aromatics stretch – C-C), 1391.97 cm^{-1} & 1360.94 cm^{-1} (alkane bend, rock – C-H), 1275.43 cm^{-1} , 1227.09 cm^{-1} , 1155.59 cm^{-1} , 1104.23 cm^{-1} & 1069.33 cm^{-1} (carboxylic acid stretch – C-O), 994.35 cm^{-1} (carboxylic acid bend – O-H), 849.48 cm^{-1} & 819.62 cm^{-1} (alkene bend – C-H), 745.29 cm^{-1} , 725.44 cm^{-1} & 706.92 cm^{-1} (primary amine wag – N-H)

NMR - δ ^1H (600 MHz, DMSO-D6): 9.16 (s, 1H), 8.63 (s, 1H, amide proton of 4-aminotetrahydropyran moiety), 8.43 (d, J = 4.1 Hz, 1H), 7.93 (dd, J = 50.5, 6.5 Hz, 1H), 7.34-7.15 (m, 5H, product's aromatic protons), 6.85 (s, 1H), 6.70 (d, J = 17.2 Hz, 2H, product's CH proton), 6.46 (d, J = 11.7 Hz, 1H), 6.28 (d, J = 7.6 Hz, 1H), 6.06 (s, 1H), 3.85-3.78 (m, 4H, product's CH₂ protons adjacent to oxygen in the tetrahydropyran moiety and terminal proton in tetrahydropyran ring moiety), 3.85-3.55 (m, 1H), 3.70-3.61 (m, 2H, product's CH₂ protons adjacent amide group), 3.56-3.01 (m, 2H, one part of product's CH₂ protons as part of linker moiety), 2.86-2.66 (t, 2H, product's CH₂ protons adjacent to aromatic ring), 2.49 (DMSO-D6, m), 1.22 (4H, product's CH₂ protons adjacent to carbon conjugated to amide group), **δ ^{13}C (151 MHz; DMSO-D6):** 176.3-173.8 (compound 10-12 terminal carboxyl carbons), 171.3-169.7 (compound 10-12 middle carboxyl carbon), 167.4-166.7 (compound 10-12 amide carbon), 139.5-139.1 (compound 10-12 aromatic carbon adjacent to ethyl moiety), 138.1-137.3 (compound 10-12 linker CH carbon), 131.3-126.1 (compound 10-12 five aromatic carbons), 43.6-42.7 (compound 10-12 CH₂ carbon adjacent to the amide group),

41.5-41.3 (compound 10-12 CH₂ carbon from linker moiety), 40.8-39.2 (DMSO-D₆), 35.5-35.0 (compound 10-12 CH₂ carbon adjacent to benzene moiety)

MS (Phosphate buffer pH 7.40; m/z) ESI+: 343.3 (100%[Unknown adduct]⁻), **ESI-:** 359.2 (100%[Phenethylamide-*cis*-aconityl-amidotetrahydropyran – H]⁻), 315.1 (75%[Unknown adduct – H]⁻)

Melting point of product: 95-100°C.

Summary: Reaction was successful due signals for CH and CH₂ linker protons in ¹H and ¹³C NMR and LCMS with a dark brown solid obtained and with a 10.30% crude yield.

Reaction 20:

The procedure was carried out as in reaction 18 but with HOBt (97.46 mg, 0.721 mmol) also being added.

TLC – Dichloromethane & methanol (3:1 v/v), visualized with iodine, Rf.: *N-cis*-aconityl-phenethylamide: 0.14, 4-aminotetrahydropyran: 0.03, Reaction mixture: 0.59, EDCl: 0.78, HOBt: 0.68

IR - ν max (film)/cm⁻¹: 2940.15 cm⁻¹ (carboxylic acids stretch – O-H), 1690.85 cm⁻¹ (amide stretch – C=O), 1628.97 cm⁻¹ (alkene stretch – C=C), 1527.82 cm⁻¹, 1454.53 cm⁻¹ & 1421.26 cm⁻¹ (aromatics stretch – C-C), 1350.18 cm⁻¹ (alkane bend, rock – C-H), 1299.60 cm⁻¹, 1192.03 cm⁻¹, 1127.69 cm⁻¹, 1037.02 cm⁻¹, 967.05 cm⁻¹ & 909.63 cm⁻¹ (carboxylic acid bend – O-H), 836.37 cm⁻¹ & 800.92 cm⁻¹ (alkene bend – C-H), 744.71 cm⁻¹, 696.53 cm⁻¹ (primary amine wag – N-H)

NMR - δ ¹H (600MHz: CH₃OH-D₄): 7.88 (d, J = 8.2 Hz, 1H, amide proton of 4-aminotetrahydropyran moiety), 7.27-7.17 (m, 5H, product's aromatic protons), 6.74 (t, J = 2.7 Hz, 2H, product's CH proton), 4.92 (CH₃OH-D₄, s, 1H), 3.77 (d, J = 14.4 Hz, 4H, product's CH₂ protons adjacent to oxygen in the tetrahydropyran moiety and terminal proton in tetrahydropyran ring moiety), 3.60 (d, J = 2.7 Hz, 2H, one part of product's CH₂ protons as part of linker moiety), 3.49-3.30 (CH₃OH-D₄, m, 4H), 2.89-2.77 (t, 2H, product's CH₂ protons adjacent to aromatic ring), 1.28 (4H, product's CH₂ protons adjacent to carbon conjugated to amide group), 1.10 (s, OH), 0.00 (d, TMS), **δ ¹³C (151 MHz: CH₃OH-D₄):** 140.3, 130.0, 129.8, 129.5, 127.7, 127.4, 49.4-48.6 (CH₃OH-D₄), 42.2, 42.0, 41.1, 36.5, 36.2, 35.0, 34.6, 34.4

Melting point of product: 90-95°C.

Summary: A compound was obtained with a crude yield of 10.18%. Product was not able to be analysed by MS due to the machine being non-functional. The reaction was assumed to be successful due to expected CH and CH₂ signals being present and similar rf value for product as in reaction 19.

3.3. Discussion

Since *cis*-aconitic anhydride is quite reactive, conjugation to doxorubicin, EPIs or the simpler compounds, in theory, should be relatively easy. As stated already, the heat of formation values in table 2, showed it would be more favourable for the order of conjugation to be N-*cis*-aconityl-MC70 to doxorubicin, as opposed to, N-*cis*-aconityl-doxorubicin with MC70. This is compared to no steric hindrance in the model sugar system. The addition of an alkyl chain to both systems resulted in, no hindrance with each group (i.e. N-*cis*-aconityl-doxorubicin and N-*cis*-aconityl-MC70). With the simpler model compounds also being modelled, they showed no steric hindrance. The HOMO/LUMO studies highlighted which compounds would be used in the synthesis of conjugates. For example, the reaction mechanism for phenethylamine and *cis*-aconitic anhydride is illustrated below in figure 69.

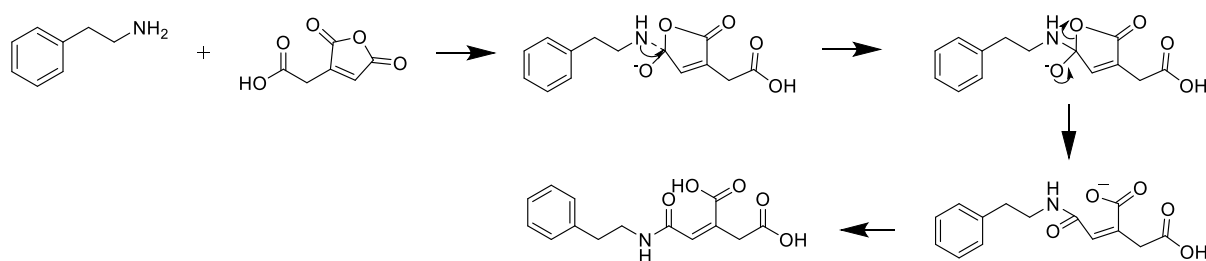


Figure 69: The mechanism of the conjugation of phenethylamine and *cis*-aconitic anhydride.

Several bases were included in these reactions for several reasons. They helped to gather hydrogen ions, in the case of triethylamine, it formed the triethylammonium cation. This ensured that the amino or hydroxyl group is present for conjugation to *cis*-aconitic acid, by removal of hydrogen ions. However, with the case of triethylamine, a triethylammonium salt formed with *cis*-aconitic acid. This caused the end products to be in a paste and not a solid, and this was characterised. The typical workup is to form a hydrochloride salt by acidification with hydrochloric acid. However, since the *cis*-aconityl linker is acid labile, we thought this would lead to product degradation. Despite this, we looked at other bases, such as NaOH, NaHCO₃ and phosphate buffer. These were ultimately successful, and this removed the issue of the triethylammonium salts. Subsequently, we also found out that it is possible to acidify a reaction mixture to precipitate the product, if this is collected and washed, and not left for an extended period. With hindsight, it should have been possible to do a quick wash with acid to remove triethylamine salts.

Despite HOMO/LUMO studies showing disruption of the delocalized electron system in the aromatic rings we still decided to use 4-phenylphenol, as a model compound for MC70. MC70 and its precursor also proved difficult to synthesize with multiple methods being unsuccessful. In method 1, step 1, thionyl chloride and triethylamine caused a very exothermic reaction. To try to prevent this, triethylamine was added dropwise after the reaction flask was cooled to ambient temperature. In step 2, the product from step 1 was reacted with 6,7-dimethoxy-1,2,3,4-tetrahydroisoquinoline to carbonyl precursor to MC70, but by TLC analysis, no new spot formed (Colabufo et al., 2008).

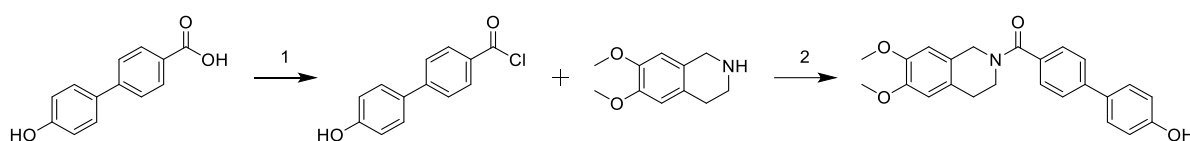


Figure 70: The reaction scheme for the formation of the carbonyl precursor to MC70.

For MC70 synthesis, a method in the paper by Colabufo et al. in 2008 was used. Step 1 involved the creation of an acyl chloride which aimed to be more reactive. Since the chlorine group is a good leaving group, in theory, it should be more reactive than the esterification of 4'-hydroxy-4-biphenylcarboxylic acid and 6,7-dimethoxy-1,2,3,4-tetrahydroisoquinoline. An amide condensation reaction was then carried out using the acyl chloride (4'-hydroxy-4-biphenylcarbonyl chloride) and 6,7-dimethoxy-1,2,3,4-tetrahydroisoquinoline. This reaction may have been unsuccessful due to published synthesis having reported a low yield due to high reactivity of the acyl chloride intermediate of the first step. This means undesired side products could have formed. Upon analysis, the MC70 precursor was not formed and so research shifted to the compound of *norverapamil*.

Dibutylamine was then used as a model compound for *norverapamil*, as well as phenethylamine. Issues with glucosamine being difficult to remove from glucosamide-*cis*-aconityl-dibutylamide meant we had to revise our model compound selection for doxorubicin. We looked at a more lipophilic compound to present the amino sugar of doxorubicin. The compound we found was 4-aminotetrahydropyran. The reduced hydrophilicity is because of having fewer hydroxyl groups as compared to glucosamine. Phenethylamine was also successful (reaction 17) with a phosphate buffer for the first step, but the second step with 4-aminotetrahydropyran was not successful upon analysis.

Due to the synthesis of second step full cytotoxic drug-linker-EPI conjugates being unsuccessful, methods were amended to use amide couplings. The first step used the very reactive *cis*-aconitic anhydride with an amine which formed an intermediate. The second step used this intermediate with a coupling agent and then an amine/phenol reagent. These were EDCI, DMAP, HOBT and HBTU. DMAP and HOBT both react with activated urea and form a more reactive product. They are then reactive enough to react with weak nucleophiles such as alcohols. They are useful nucleophilic catalysts for esterification reactions (Montalbetti & Falque, 2005). Carbodiimides such as *N,N'*-dicyclohexylcarbodiimide (DCC) or EDCI are used to activate carboxylic acid groups to make the carbonyl carbon more electrophilic, and more prone to nucleophilic attack (Sheehan, Boshart, & Cruickshank, 1961).

Amide bonds are formed from the conjugation of a carboxylic acid and amine. This occurs via a condensation reaction, but the carboxylic acid needs to be activated before conjugation can occur (Dunetz, Magano, & Weisenburger, 2016). The carboxylate ion then reacts with coupling reagents, which yields a reactive intermediate which then goes on to form the amide. Compounds like an acid halide, azide, anhydride, carbodiimides or active esters can be used for activation (Sheehan, Boshart, & Cruickshank, 1961). This is explained in figure 71. *N*-*cis*-aconityl-dibutylamide, was reacted with glucosamine, NaHCO₃, EDCI as an activating agent and DMAP as a catalyst.

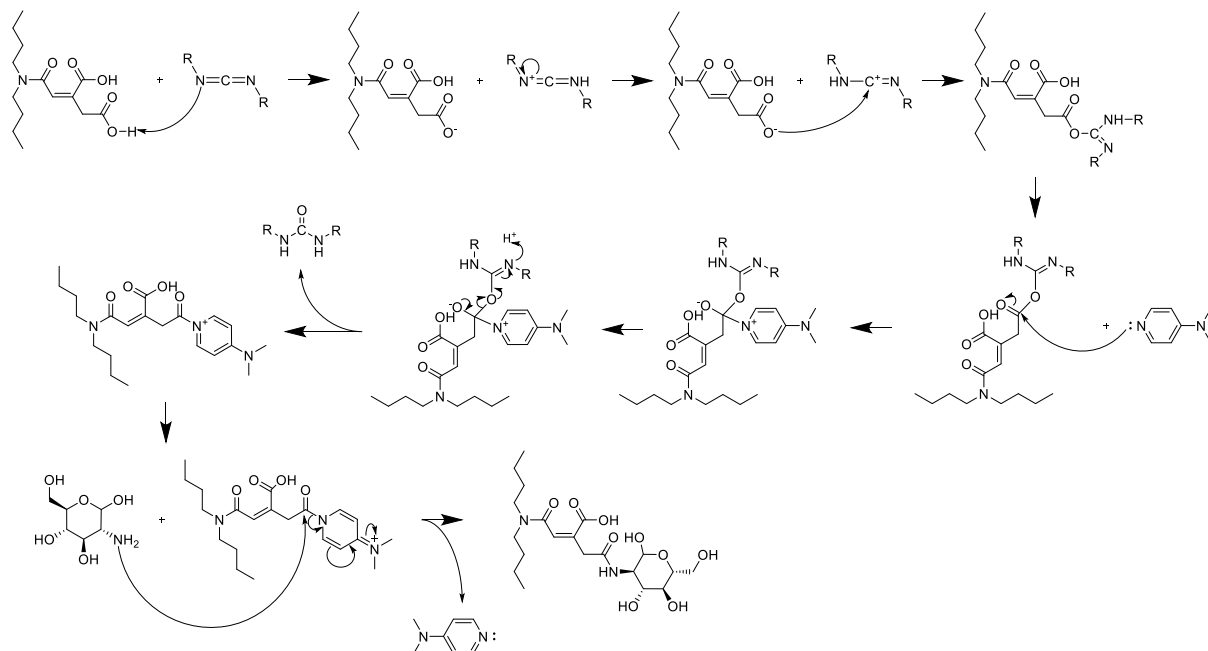


Figure 71: The mechanism for the conjugation of *N*-*cis*-aconityl-dibutylamide to glucosamine using EDCI and DMAP (Sheehan, Boshart, & Cruickshank, 1961).

3.3.1. Analysis of compounds

Some of our desired conjugates were synthesized, they were confirmed by analysis, and are discussed below. Each type of analysis is important for organic chemistry, from TLC, FT-IR, LCMS to NMR. TLC silica plates were used to check the purity of compounds, and to visualize the progress of each reaction. When a new spot was formed, and the reactants' spots had disappeared from the Rx line, this indicated that the reaction had finished. Some spots needed the use of stains to visualize compounds, e.g. iodine and ninhydrin for visualizing amine groups.

FT-IR confirmed the presence of hydroxyl, carboxyl, amino or other functional groups, with the relevant functional groups appearing when a product was analyzed. This was the case with every compound tested, for example, in reaction 6, *N-cis*-aconityl-glucosamide showed a broad peak at 3291.77 cm^{-1} , alcohol or carboxylic acid stretch at 1386.41 cm^{-1} and alkene bend at 680.14 cm^{-1} among others. In reaction 2, *N-cis*-aconityl-dibutylamide showed a second amide stretch at 3317.32 cm^{-1} , a carboxylic acid stretch at 1682.74 cm^{-1} and two peaks for carboxylic acid bend at 954.08 cm^{-1} and 935.61 cm^{-1} among others. In reaction 17, *N-cis*-aconityl-phenethylamide showed two variable carboxylic acid stretches at 3028.52 cm^{-1} and 2934.89 cm^{-1} among others.

With NMR, most spectra had many containments as product purification proved difficult. The methods tried were first, lyophilization. This was carried out to remove any water from the reaction mixture, this left impure products with the next step being purification. On page 66, with reaction 12 with glucosamide-*cis*-aconityl-dibutylamide product contained reagents and the *N-cis*-aconityl-dibutylamide conjugate, we attempted another purification method.

Secondly, column chromatography was carried out to purify products formed using silica, a solvent system and a column. However, what was extracted was not the product, leading us to surmise that the product was stuck to the silica in the column. The column was flushed with methanol to remove the reaction mixture. Finally, recrystallizations were carried out using methanol, then propanol, then dichloromethane was carried out, but the removal of starting materials still proved difficult. There was difficulty with synthesising the amidotetrahydropyran-*cis*-aconityl-phenethylamide conjugate. Crude products were analysed in some cases to check if our product was synthesized. Some of these spectra will be discussed below.

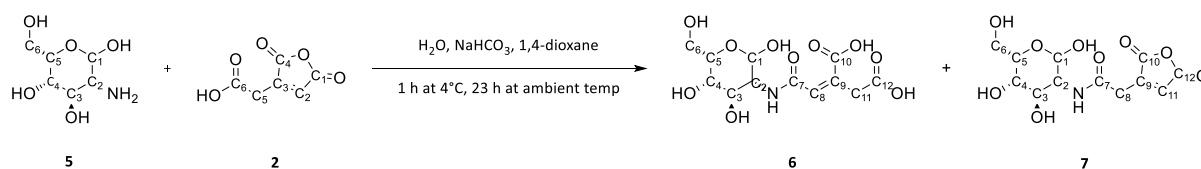


Figure 72: Reaction scheme of reaction 6 with compounds 6 and 7.

N-*cis*-aconityl-glucosamide was synthesized from reaction 6 on page 60 and was analysed in D₂O on a 400 MHz NMR spectrometer. On ¹H-NMR, 8.34 ppm is a doublet which corresponds with amide proton in the product. At 6.47 ppm is a doublet which corresponds to the compound 6, carbon 8's proton. A singlet was expected so this could mean that this signal is coupled with compound 7, carbon 8's proton. At 5.10-4.65 ppm is a multiplet which is the signal for the multiple hydroxyl groups on the tetrahydropyran ring of the glucosamine moiety. At 4.13 ppm is a singlet for the compound 6, carbon 1's proton. At 3.83 ppm is a singlet from an unknown contaminant. At 3.61-3.47 ppm is a multiplet which is the signal for protons on compound 6, carbons 2-5 protons and carbon 6's protons. At 3.32 ppm is a doublet which is the signal for compound 6, carbon 11's protons. A singlet was expected so this could mean that this signal is coupled with compound 6, carbon 11's protons. At 2.99 ppm is a singlet from an unknown contaminant. At 1.80 ppm is a singlet from an unknown contaminant. No signals were present for hydroxyl groups on the *cis*-aconityl moiety, indicating proton exchange with water present in the sample. On ¹³C-NMR did not yield any results due to an untuned probe.

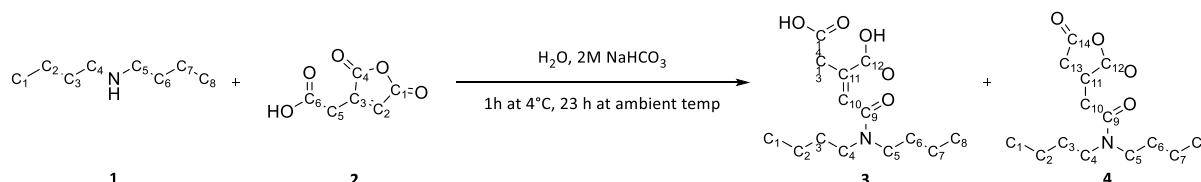


Figure 73: Reaction scheme of reaction 2 with compounds 3 and 4.

N-*cis*-aconityl-dibutylamide synthesized from reaction 2 on page 57 and was analysed in D₂O on a 400 MHz NMR spectrometer. On ¹H-NMR, at 8.37 ppm is an unknown contaminant. At 6.50 ppm is a singlet for compound 3, carbon 10's proton. At 5.97 ppm is a singlet which corresponds with a signal for compound 4, carbon 10's proton. At 5.55 ppm is a singlet of an unknown contaminant and at 4.89-4.69 ppm is a multiplet for CH₃OH-D4 impurity. At 3.69 ppm is a singlet denoting the compound 3, carbon 13's protons. At 3.26 ppm is a singlet for compound 4, carbon 13's protons.

At 3.09-2.91 ppm is a multiplet for compound 3, carbons 4 and 4 protons. At 1.84 ppm is a singlet denoting the amine hydrogen from unreacted dibutylamine. At 1.56-1.47 ppm is a multiplet for compound 3, carbons 3 and 6 protons. At 1.30 ppm is a multiplet which is for compound 3, carbons 2 and 7 protons. At 0.86-0.80 ppm is a multiplet which is for compound 3 or 4, carbons 1 and 8 protons. No signals were present for both hydroxyl groups, indicating proton exchange with water present in the sample. On ^{13}C -NMR did not yield any results due to an untuned probe.

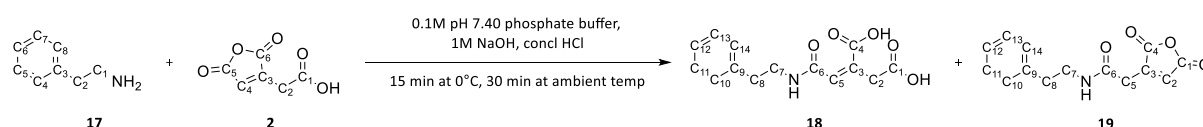


Figure 74: Reaction scheme of reaction 17 with compounds 18 and 19.

N-*cis*-aconityl-phenethylamide was synthesized from reaction 17 on page 71-72 and was analysed in methanol- d_4 on a 600 MHz NMR. On ^1H -NMR, at 7.34-7.16 ppm is the signal for a multiplet on compound 18, carbons 9-14 protons. At 6.92 ppm is a doublet for an unknown contaminant. At 6.71 ppm is a singlet which for compound 18, carbon 5 proton. At 6.44 singlet which corresponds to compound 19, carbon 5. At 6.13 ppm is a singlet which could correspond to compound 2, carbon 4 proton. At 3.47-3.43 ppm is a multiplet for compound 18, carbon 7 protons. At 3.16 ppm is a doublet of doublets which is for compounds 18 and 19, carbon 2 protons. At 2.96-2.81 ppm is a multiplet which corresponds to compound 18, carbon 8 protons. No signals were present for both hydroxyl groups, indicating proton exchange with water present in the sample.

On ^{13}C -NMR, which was also run in methanol- d_4 at 151 MHz, at 175.2 and 174.8 ppm, both correspond to compounds 18 and 19, carbon 1. At 171.8 and 170.8 ppm are the signals for compounds 18 and 19, carbon 4. At 168.0 ppm is the signal for compound compounds 18 and 19, carbon 6. At 140.5 and 140.3 ppm are signals for an unknown contaminant. At 138.0 ppm is the signal for compounds 18 and 19, carbon 9. At 130.0-127.3 ppm are the signals for compound 18, carbons 10-14. At 43.3 and 42.6 ppm are the signals for compounds 18 and 19, carbon 7. At 42.4 and 41.9 ppm are the signals for compound 17, carbon 1. At 36.3 and 36.2 ppm are the signals for compound 17, carbon 2. At 34.6 ppm is the signal for compound 19, carbon 2.

LCMS was carried out with both positive and negative electrospray ionisations being used. Chromatograms and mass spectrometry results showed. In reaction 6, N-*cis*-aconityl-glucosamide with ESI+ showed a hydrogen adduct of compound 4 at 318.3 and a sodium adduct of the parent ion at 358.4. ESI- showed the parent ion at 335.2, a hydrogen adduct of the parent ion at 334.2, and unknown adducts at 272.3 and 290.3. At 336.3 is a hydrogen adduct of compound 3 ion. In reaction 2, N-*cis*-aconityl-dibutylamide with ESI+ showed a hydrogen adduct of the parent ion at 286.2, a hydrogen adduct of compound 1 and a sodium adduct of the parent ion at 308.2. ESI- showed an unknown adduct at 240.3. In reaction 17, N-*cis*-aconityl-phenethylamide with ESI+ showed a hydrogen adduct of the parent ion at 278.1 and a hydrogen adduct of compound 19 at 260.0 and 260.2. ESI- showed an unknown ion of an unknown adduct at 232.1 and a hydrogen adduct of the parent ion at 276.2.

As noted above, some products had a closed ring, as shown in figures 72-74. The closed ring moiety is *trans*-aconitic acid, isomerisation occurred from the formation of the *cis*-aconityl product. A possible reason this occurred is could be that the *trans* closed ring form is sterically more stable. Another reason could be the breaking the carbon ring of *cis*-aconitic anhydride, upon the formation of the *cis*-aconityl product, means that this product cannot revert to its original *cis*-membered ring and results in the formation of the *trans*-membered ring. This trend was observed in a study with *cis*-aconitic acid, among other carboxylic acids, where analytes favoured internal cyclisation to 5 or 6 membered rings of their parent anhydrides in GC-MS (Hušek, Šimek, & Matucha, 2003).

4.0. Future work

As such, the logical progression of this research is outlined below.

4.1. Drug-EPI linker conjugate synthesis, pH release studies and *in vivo* testing

New compounds could be found to conjugate with the current library of compounds, methods for synthesis could be improved with current and new compounds and further modelling of compounds under more approximate theories. Methods used to synthesize the model compound conjugates would be applied to conjugate the *cis*-aconityl linker to doxorubicin, MC70, *norverapamil* and both doxorubicin and either EPI respectively. Several pH-dependant release studies would be carried out, using LCMS, at varying pH values of 6.00, 6.50, 6.80, 7.00 and 7.40. Confirmation of conjugate degradation would be observed if m/z ratios for reagents are present on the mass spectra, and not the conjugates. This is expected to occur between pH values 6.50 and 6.80, but not at 7.40.

Testing of *in vivo* drug conjugate release would then follow. A set of cancer cell lines would then be chosen based on availability or level of success based on previous studies. In 1981, a study by Shen and Ryser used WEHI-5 cells, a mouse monocytic leukaemia cell line, to test their conjugates. Azzariti *et al.* in 2011 used the colon cancer cell line Caco-2, which is resistant to doxorubicin and the breast cancer cell line (MCF7/ADR) which has overexpressed ABCB1 gene (Gottesman *et al.*, 2002).

Cell cultures would be maintained in buffer solutions of pH 5.00, 6.00, 6.50 and 7.40 respectively. Uptake of conjugates, as compared to free doxorubicin and free MC70, would be measured using flow cytometry (Kuruvilla *et al.*, 2017). Flow cytometry is a procedure which can quantify the levels of free doxorubicin and the modified doxorubicin system. This could provide a control to compare the effect of the modified system, show the cytotoxic effects of free doxorubicin and the modified system, and show the ratio of the release of MC70 and as compared to doxorubicin concentrations (Azzariti *et al.*, 2011).

4.2. Pharmacological studies

Pharmacodynamic studies would then be carried out on the final complex conjugate and model conjugates. These studies would include tests for drug toxicity, dose dependence and dose-response. Studies for linker release and possible treatment, that the levels of MC70 release will be the same as doxorubicin. Results are expected to show a decrease in cell survival, as a percentage, as the concentration of free doxorubicin and free MC70 and each of the conjugates increases (Kuruvilla *et al.*, 2017).

Doxorubicin

This is already known.

MC70:

The pharmacology activity for MC70 has not currently been fully elucidated. Previous studies show when given on its own or with an anticancer drug, such as doxorubicin, in colon cancer cells, MC70 would enhance doxorubicin's cytotoxic and cytostatic effects. On its' own, MC70 was shown to slightly inhibit cell growth (Azzariti *et al.*, 2011).

Norverapamil

A phase 1 metabolite of verapamil and has also been observed to inhibit P-gp channels, (Pauli-Magnus *et al.*, 2000). But pharmacokinetic and pharmacodynamic studies need to be carried out to observe ADME and toxicity profiles of this compound.

4.3. Alternate studies and treatments

Antimicrobial therapy

Using P-gp inhibitors can be used in antimicrobial therapy. A common mechanism of resistance in microorganisms is drug-efflux which also results in over-expression of P-gp. Multidrug resistance facilitated efflux pumps, are found in bacteria, protozoa, and fungi. As mentioned before, P-gp acts as a defence mechanism in preventing antimicrobial agents from entering cells. Also lowering drug efficacy by reducing intracellular concentration. This results in increased costs, higher morbidity, increased rates of mortality and increased hospital costs. Also, possible that the suppression of resistant strains could occur. Tariquidar, 3rd generation P-gp inhibitor, was found to have a 10-fold reduction (Amin, 2013).

A paper by Chen, Wei, Xie, Tao, Zhang, *et al.* in 2019, looked at the possibility of improving antimicrobial treatments using size/surface charge-adaptive micelles in the destruction of bacterial biofilms in *Pseudomonas aeruginosa*. At pH 5.50, degradation of the *cis*-aconityl linkers led to the decrease in size and charge reversal of micelles. This led to azithromycin being released, led to the elimination of bacterial biofilms (Chen et al., 2019).

A paper by Chen, Xie, Wei, Song, Ding, *et al.* in 2018, looked at using micelles with vancomycin-mediated targeting by using pH/lipase triggered release. The pH-labile hydrazone linker was used to release vancomycin. Then lipase triggered release was used to release ciprofloxacin at the infection site (Chen et al., 2018). With literature precedence, using EPIs and a pH-sensitive linker for treatments, the possibility of forming conjugates or antibiotic micelles should be looked at. Research into how EPI-aconityl-antibiotic conjugates would be therapeutically beneficial.

4.4. Conclusion

This study, as discussed before, took place in several parts, selection of cytotoxic drug, creation of an EPI library for selection modelling and synthesis. Doxorubicin was chosen due to the range of cancer it treats and literature precedence with this linker. MC70 and *norverapamil* were chosen as EPIs. Molecular modelling was carried out to deduced that there was no steric hindrance was observed with all model and final compounds and the linker.

While the full-scale EPIs and doxorubicin complexes were not able to be synthesized, some model complexes were. Method development towards the purification of products will be needed in future, as well as second step synthesis and in-vitro pH-release studies.

To conclude, this study has laid the groundwork for a novel way of increasing the efficacy of doxorubicin, and possibly other medicine, which will hopefully lead to more studies and eventual treatments and therapies.

5.0. References

- Abdallah, H. M., Al-Abd, A. M., El-Dine, R. S., & El-Halawany, A. M. (2015). P-glycoprotein inhibitors of natural origin as potential tumor chemo-sensitizers: A review. *Journal of Advanced Research*, 6(1), 45–62. <https://doi.org/10.1016/j.jare.2014.11.008>
- Aller, S. G., Yu, J., Ward, A., Weng, Y., Chittaboina, S., Zhuo, R., ... Chang, G. (2009). Structure of P-glycoprotein reveals a molecular basis for poly-specific drug binding. *Science*, 323(5922), 1718–1722. <https://doi.org/10.1126/science.1168750>
- Amin, M. L. (2013). P-glycoprotein inhibition for optimal drug delivery. *Drug Target Insights*, 2013(7), 27–34. <https://doi.org/10.4137/DTI.S12519>
- Axon medchem. (2018). *MC70 hydrochloride | P-gp inhibitor | MC-70 | CAS [N.A.] - [1031367-64-2] | Axon 2591 | Axon Ligand™ with >98% purity available from stock from supplier*. Retrieved 22 June, 2018, from <https://www.axonmedchem.com/product/2591>
- Azzariti, A., Quatrone, A. E., Porcelli, L., Colabufo, N. A., Cantore, M., Cassano, G., ... Paradiso, A. (2011). MC70 potentiates doxorubicin efficacy in colon and breast cancer in vitro treatment. *European Journal of Pharmacology*, 670(1), 74–84. <https://doi.org/10.1016/j.ejphar.2011.08.025>
- Blackadar, C. B. (2016). Historical review of the causes of cancer. *World J Clin Oncol*, 7(1), 54–86. <https://doi.org/10.5306/wjco.v7.i1.54>
- Bonfante, V., Bonadonna, G., Villani, F., & Martini, A. (1980). Preliminary clinical experience with 4'-epidoxorubicin in advanced human neoplasia. In *Cancer Chemo-and Immunopharmacology* (pp. 192-199). Springer, Berlin, Heidelberg.
- Borst, P., Evers, R., Kool, M., & Wijnholds, J. (2000). A family of drug transporters: The multidrug resistance-associated proteins. *Journal of the National Cancer Institute*, 92(16), 1295–1302. <https://doi.org/10.1093/jnci/92.16.1295>
- Bredas, J. L. (2014). Mind the gap! *Materials Horizons*, 1(1), 17–19. <https://doi.org/10.1039/c3mh00098b>
- Breedveld, P., Beijnen, J. H., & Schellens, J. H. M. (2006). Use of P-glycoprotein and BCRP inhibitors to improve oral bioavailability and CNS penetration of anticancer drugs. *Trends in Pharmacological Sciences*, 27(1), 17–24. <https://doi.org/10.1016/j.tips.2005.11.009>
- Cancer research UK. (2020a). *Cancer Statistics for the UK*. Retrieved 19 August, 2020, from <http://www.cancerresearchuk.org/health-professional/cancer-statistics-for-the-uk>
- Cancer research UK. (2020b). *Pancreatic cancer statistics*. Retrieved 19 August, 2020, from <https://www.cancerresearchuk.org/health-professional/cancer-statistics/statistics-by-cancer-type/pancreatic-cancer>

Cancer research UK. (2020c). *Lung cancer statistics*. Retrieved 19 August, 2020, from <http://www.cancerresearchuk.org/health-professional/cancer-statistics/statistics-by-cancer-type/lung-cancer>

Cancer research UK. (2020d). *Bowel cancer statistics*. Retrieved 19 August, 2020, from <http://www.cancerresearchuk.org/health-professional/cancer-statistics/statistics-by-cancer-type/bowel-cancer>

Chen, M., Wei, J., Xie, S., Tao, X., Zhang, Z., Ran, P., & Li, X. (2019). Bacterial biofilm destruction by size/surface charge-adaptive micelles. *Nanoscale*, *11*(3), 1410–1422. <https://doi.org/10.1039/c8nr05575k>

Chen, M., Xie, S., Wei, J., Song, X., Ding, Z., & Li, X. (2018). Antibacterial Micelles with Vancomycin-Mediated Targeting and pH/Lipase-Triggered Release of Antibiotics. *ACS Applied Materials and Interfaces*, *10*(43), 36814–36823. <https://doi.org/10.1021/acsami.8b16092>

Chen, M., Zhang, Y., Chen, Z., Xie, S., Luo, X., & Li, X. (2017). Synergistic antitumor efficacy of redox and pH dually responsive micelleplexes for co-delivery of camptothecin and genes. *Acta Biomaterialia*, *49*, 444–455. <https://doi.org/10.1016/j.actbio.2016.12.005>

Chial, H. (2008) Proto-oncogenes to oncogenes to cancer. *Nature Education* *1*(1):33

Chiarugi, P., & Cirri, P. (2016). Metabolic exchanges within tumor microenvironment. *Cancer Letters*, *380*(1), 272–280. <https://doi.org/10.1016/j.canlet.2015.10.027>

Chiche, J., Ilc, K., Laferrière, J., Trottier, E., Dayan, F., Mazure, N. M., ... Pouysségur, J. (2009). Hypoxia-inducible carbonic anhydrase IX and XII promote tumor cell growth by counteracting acidosis through the regulation of the intracellular pH. *Cancer Research*, *69*(1), 358–368. <https://doi.org/10.1158/0008-5472.CAN-08-2470>

Choi, S. Y. C., Xue, H., Wu, R., Fazli, L., Lin, D., Collins, C. C., ... Wang, Y. (2016). The MCT4 gene: A novel, potential target for therapy of advanced prostate cancer. *Clinical Cancer Research*, *22*(11), 2721–2733. <https://doi.org/10.1158/1078-0432.CCR-15-1624>

Colabufo, N. A., Berardi, F., Cantore, M., Perrone, M. G., Contino, M., Inglese, C., ... Paradiso, A. (2008). 4-Biphenyl and 2-naphthyl substituted 6,7-dimethoxytetrahydroisoquinoline derivatives as potent P-gp modulators. *Bioorganic and Medicinal Chemistry*, *16*(7), 3732–3743. <https://doi.org/10.1016/j.bmc.2008.01.055>

DeVita, V. T., & Chu, E. (2008). A history of cancer chemotherapy. *Cancer Research*, *68*(21), 8643–8653. <https://doi.org/10.1158/0008-5472.CAN-07-6611>

Dinand, E., Zloh, M., & Brocchini, S. (2002). Competitive Reactions During Amine Addition to cis-Aconityl Anhydride. *Australian Journal of Chemistry*, *55*, 467–474.

Du, C., Deng, D., Shan, L., Wan, S., Cao, J., Tian, J., ... Gu, Y. (2013). A pH-sensitive doxorubicin prodrug based on folate-conjugated BSA for tumor-targeted drug delivery. *Biomaterials*, 34(12), 3087–3097. <https://doi.org/10.1016/j.biomaterials.2013.01.041>

Dunetz, J. R., Magano, J., & Weisenburger, G. A. (2016). Large-Scale Applications of Amide Coupling Reagents for the Synthesis of Pharmaceuticals. *Organic Process Research and Development*, 20(2), 140–177. <https://doi.org/10.1021/op500305s>

Dykstra, C., Frenking, G., Kim, K., & Scuseria, G. (2011). *Theory and Applications of Computational Chemistry: The First Forty Years*. Amsterdam: Elsevier.

EBI. (2020a). *Crystal structure of the DENR-MCT-1 complex*. Retrieved 20 May 2020, from <https://www.ebi.ac.uk/pdbe/entry/pdb/6ms4>

EBI. (2020b). *Structure of the human Multidrug Resistance Protein 1 Nucleotide Binding Domain 1*. Retrieved 20 May 2020, from <https://www.ebi.ac.uk/pdbe/entry/pdb/2cbz>

EBI. (2020c). *Structure of an inhibitor-bound ABC transporter*. Retrieved 20 May 2020, from <https://www.ebi.ac.uk/pdbe/entry/pdb/6ffc>

Gottesman, M. M., Fojo, T., & Bates, S. E. (2002). Multidrug Resistance in Cancer: Role of Atp-Dependent Transporters. *Nature Reviews Cancer*, 2(1), 48–58. <https://doi.org/10.1038/nrc706>

Gu, J., Su, S., Zhu, M., Li, Y., Zhao, W., Duan, Y., & Shi, J. (2012). Targeted doxorubicin delivery to liver cancer cells by PEGylated mesoporous silica nanoparticles with a pH-dependent release profile. *Microporous and Mesoporous Materials*, 161, 160–167. <https://doi.org/10.1016/j.micromeso.2012.05.035>

Guglielmo, S., Contino, M., Lazzarato, L., Perrone, M. G., Blangetti, M., Fruttero, R., & Colabufo, N. A. (2016). A Potent and Selective P-gp Modulator for Altering Multidrug Resistance Due to Pump Overexpression. *ChemMedChem*, 11(4), 374–376. <https://doi.org/10.1002/cmdc.201500538>

Gupta, S. C., Sung, B., Prasad, S., Webb, L. J., & Aggarwal, B. B. (1976). Cancer drug discovery by repurposing: Teaching new tricks to old dogs. *Trends Pharmacol Sci*, 34(9), 508–517. <https://doi.org/10.1016/j.tips.2013.06.005>

Halestrap, A. P., & Meredith, D. (2004). The SLC16 gene family - From monocarboxylate transporters (MCTs) to aromatic amino acid transporters and beyond. *Pflugers Archiv European Journal of Physiology*, 447(5), 619–628. <https://doi.org/10.1007/s00424-003-1067-2>

Halgren, T. a. (1996). Merck Molecular Force Field. *J. Comput. Chem.*, 17(5–6), 490–519. [https://doi.org/10.1002/\(SICI\)1096-987X\(199604\)17:5/6<520::AID-JCC2>3.0.CO;2-W](https://doi.org/10.1002/(SICI)1096-987X(199604)17:5/6<520::AID-JCC2>3.0.CO;2-W)

Hanahan, D. (2014). Rethinking the war on cancer. *The Lancet*, 383(9916), 558–563. [https://doi.org/10.1016/S0140-6736\(13\)62226-6](https://doi.org/10.1016/S0140-6736(13)62226-6)

Hassanzadeh, P., Atyabi, F., & Dinarvand, R. (2018). Linkers: The key elements for the creation of efficient nanotherapeutics. *Journal of Controlled Release*, 270(October 2017), 260–267. <https://doi.org/10.1016/j.jconrel.2017.12.007>

Hawaii Biotech Inc (2004). *Structural carotenoid analogs for the inhibition and amelioration of disease*. WO2004011423.

Homma, A., Sato, H., Okamachi, A., Emura, T., Ishizawa, T., Kato, T., ... Suzuki, R. (2009). Novel hyaluronic acid-methotrexate conjugates for osteoarthritis treatment. *Bioorganic and Medicinal Chemistry*, 17(13), 4647–4656. <https://doi.org/10.1016/j.bmc.2009.04.063>

Hostaš, J., Řezáč, J., & Hobza, P. (2013). On the performance of the semiempirical quantum mechanical PM6 and PM7 methods for noncovalent interactions. *Chemical Physics Letters*, 568–569, 161–166. <https://doi.org/10.1016/j.cplett.2013.02.069>

Hou, Z., Lin, B., Bao, Y., Yan, H. ning, Zhang, M., Chang, X. wei, ... Guo, C. (2017). Dual-tail approach to discovery of novel carbonic anhydrase IX inhibitors by simultaneously matching the hydrophobic and hydrophilic halves of the active site. *European Journal of Medicinal Chemistry*, 132, 1–10. <https://doi.org/10.1016/j.ejmech.2017.03.023>

Hušek, P., Šimek, P., & Matucha, P. (2003). Smooth Esterification of Di- and Tricarboxylic Acids with Methyl and Ethyl Chloroformates in Gas Chromatographic Profiling of Urinary Acidic Metabolites. *Chromatographia*, 58(9–10), 623–630. <https://doi.org/10.1365/s10337-003-0078-7>

Irani, K., Xia, Y., Zweier, J. L., Sollott, S. J., Der, C. J., Fearon, E. R., ... Goldschmidt-Clermont, P. J. (1997). Mitogenic Signaling Mediated by Oxidants in Ras-Transformed Fibroblasts. *Science*, 275(5306), 1649–1652. <https://doi.org/10.1126/science.275.5306.1649>

Jackson, S. M., Manolaridis, I., Kowal, J., Zechner, M., Taylor, N. M. I., Bause, M., ... Locher, K. P. (2018). Structural basis of small-molecule inhibition of human multidrug transporter ABCG2. *Nature Structural and Molecular Biology*, 25(4), 333–340. <https://doi.org/10.1038/s41594-018-0049-1>

Jensen, F. (2017). *Introduction to computational chemistry* (3rd ed.). Chichester, UK: John Wiley & Sons.

Jmol. (2020). *Jmol: an open-source Java viewer for chemical structures in 3D*. Retrieved 25 September, 2020, from <http://www.jmol.org/>

Kakinoki, A., Kaneo, Y., Ikeda, Y., Tanaka, T., & Fujita, K. (2008). Synthesis of poly(vinyl alcohol)-doxorubicin conjugates containing *cis*-aconityl acid-cleavable bond and its isomer dependent doxorubicin release. *Biological & Pharmaceutical Bulletin*, 31(1), 103–10. <https://doi.org/10.1248/bpb.31.103>

Kang, S., Kim, Y., Song, Y., Choi, J. U., Park, E., Choi, W., ... Lee, Y. (2014). Comparison of pH-sensitive degradability of maleic acid amide derivatives. *Bioorganic and Medicinal Chemistry Letters*, 24(10), 2364–2367. <https://doi.org/10.1016/j.bmcl.2014.03.057>

Kim, K., Roh, J., Wee, H., & Kim, C. (2016). *Cancer drug discovery: science and history* (1st ed.). Dordrecht: Springer.

Kuhlmann, O., Carlile, D., Noe, J., & Bentley, D. (2014). Interaction potential of Carmegliptin with P-glycoprotein (Pgp) transporter in healthy volunteers. *Journal of Drug Assessment*, 3(1), 28–37. <https://doi.org/10.3109/21556660.2014.900065>

Kuruvilla, S. P., Tiruchinapally, G., ElAzzouny, M., & ElSayed, M. E. H. (2017). N-Acetylgalactosamine-Targeted Delivery of Dendrimer-Doxorubicin Conjugates Influences Doxorubicin Cytotoxicity and Metabolic Profile in Hepatic Cancer Cells. *Advanced Healthcare Materials*, 6(5), 1–15. <https://doi.org/10.1002/adhm.201601046>

Lan, A., Lagadic-Gossmann, D., Lemaire, C., Brenner, C., & Jan, G. (2007). Acidic extracellular pH shifts colorectal cancer cell death from apoptosis to necrosis upon exposure to propionate and acetate, major end-products of the human probiotic propionibacteria. *Apoptosis*, 12(3), 573–591. <https://doi.org/10.1007/s10495-006-0010-3>

Lewars, E. (2016). *Computational Chemistry* (3rd ed.). Cham: Springer.

Lin, J. H., & Yamazaki, M. (2003). Role of P-glycoprotein in pharmacokinetics: Clinical implications. *Clinical Pharmacokinetics*, 42(1), 59–98. <https://doi.org/10.2165/00003088-200342010-00003>

Liu, J., Huang, Y., Kumar, A., Tan, A., Jin, S., Mozhi, A., & Liang, X. J. (2014). PH-Sensitive nano-systems for drug delivery in cancer therapy. *Biotechnology Advances*, 32(4), 693–710. <https://doi.org/10.1016/j.biotechadv.2013.11.009>

Lomakin, I. B., Dmitriev, S. E., & Steitz, T. A. (2019). Crystal structure of the DENR-MCT-1 complex revealed zinc-binding site essential for heterodimer formation. *Proceedings of the National Academy of Sciences of the United States of America*, 116(2), 528–533. <https://doi.org/10.1073/pnas.1809688116>

Longley, D. B., Harkin, D. P., & Johnston, P. G. (2003). 5-Fluorouracil: Mechanisms of action and clinical strategies. *Nature Reviews Cancer*, 3(5), 330–338. <https://doi.org/10.1038/nrc1074>

Luqmani, Y. A. (2005). Mechanisms of drug resistance in cancer chemotherapy. *Medical Principles and Practice*, 14(SUPPL. 1), 35–48. <https://doi.org/10.1159/000086183>

Manchun, S., Dass, C. R., & Sriamornsak, P. (2012). Targeted therapy for cancer using pH-responsive nanocarrier systems. *Life Sciences*, 90(11–12), 381–387. <https://doi.org/10.1016/j.lfs.2012.01.008>

Matsui, A., Ihara, T., Suda, H., Mikami, H., & Semba, K. (2013). Gene amplification: Mechanisms and involvement in cancer. *Biomolecular Concepts*, 4(6), 567–582. <https://doi.org/10.1515/bmc-2013-0026>

Montalbetti, C. A. G. N., & Falque, V. (2005). Amide bond formation and peptide coupling. *Tetrahedron*, 61(46), 10827–10852. <https://doi.org/10.1016/j.tet.2005.08.031>

Mu, L.-M., Ju, R.-J., Liu, R., Bu, Y.-Z., Zhang, J.-Y., Li, X.-Q., ... Lu, W.-L. (2017). Dual-functional drug liposomes in treatment of resistant cancers. *Advanced Drug Delivery Reviews*. <https://doi.org/10.1016/j.addr.2017.04.006>

NHS. (2016). *The top 5 causes of premature death*. Retrieved 8 February, 2019, from <https://www.nhs.uk/live-well/healthy-body/top-5-causes-of-premature-death/>

NICE (2019a). *Doxorubicin hydrochloride | Drug | bnf content published by nice*. Retrieved 10 January, 2019, from <https://bnf.nice.org.uk/drug/doxorubicin-hydrochloride.html>

NICE (2019b). *Epirubicin hydrochloride | Drug | bnf content published by nice*. Retrieved 10 January, 2019, from <https://bnf.nice.org.uk/drug/epirubicin-hydrochloride.html>

NICE (2019c). *Paclitaxel | drug | bnf content published by nice*. Retrieved 6 May, 2019, from <https://bnf.nice.org.uk/drug/paclitaxel.html>

NICE (2019d). *Methotrexate | drug | bnf content published by nice*. Retrieved 6 May, 2019, from <https://bnf.nice.org.uk/drug/methotrexate.html>

NICE (2019e). *Fluorouracil | drug | bnf content published by nice*. Retrieved 6 May, 2019, from <https://bnf.nice.org.uk/drug/fluorouracil.html>

NICE (2019f). *Cytotoxic drugs | Treatment summary | BNF content published by NICE*. Retrieved 6 May, 2019, from <https://bnf.nice.org.uk/treatment-summary/cytotoxic-drugs.html>

Nigam, S. K. (2014). What do drug transporters really do? *Nature Reviews Drug Discovery*, 14(1), 29–44. <https://doi.org/10.1038/nrd4461>

NIH: NLM (2012). *Tariquidar and Docetaxel to Treat Patients With Lung, Ovarian, Renal and Cervical Cancer - Full Text View - ClinicalTrials.gov*. Retrieved 21 November, 2017, from <https://clinicaltrials.gov/ct2/show/NCT00069160>

Ohno, K., Esfarjani, K., & Kawazoe, Y. (2018). *Computational Materials Science: From Ab Initio to Monte Carlo Methods* (2nd ed.). Berlin: Springer.

Patil, Y., Sadhukha, T., Ma, L., & Panyam, J. (2009). Nanoparticle-mediated simultaneous and targeted delivery of paclitaxel and tariquidar overcomes tumor drug resistance. *Journal of Controlled Release*, 136(1), 21–29. <https://doi.org/10.1016/j.jconrel.2009.01.021>

Pauli-Magnus, C., Von Richter, O., Burk, O., Ziegler, A., Mettang, T., Eichelbaum, M., & Fromm, M. F. (2000). Characterization of the major metabolites of verapamil as substrates and inhibitors of P-glycoprotein. *Journal of Pharmacology and Experimental Therapeutics*, 293(2), 376–382.

Polanski, R., Hodgkinson, C. L., Fusi, A., Nonaka, D., Priest, L., Kelly, P., ... Morrow, C. J. (2014). Activity of the monocarboxylate transporter 1 inhibitor azd3965 in small cell lung cancer. *Clinical Cancer Research*, 20(4), 926–937. <https://doi.org/10.1158/1078-0432.CCR-13-2270>

Pubchem. (2017d). *Daunorubicin | C27H29NO10 - PubChem*. Retrieved 21 November, 2017, from <https://pubchem.ncbi.nlm.nih.gov/compound/daunorubicin>

Pubchem. (2019). *Norverapamil | C26H36N2O4 – PubChem*. Retrieved 22 February, 2019, from <https://pubchem.ncbi.nlm.nih.gov/compound/104972>

Ramaen, O., Leulliot, N., Sizun, C., Ulryck, N., Pamard, O., Lallemand, J. Y., ... Jacquet, E. (2006). Structure of the Human Multidrug Resistance Protein 1 Nucleotide Binding Domain 1 bound to Mg²⁺/ATP Reveals a Non-productive Catalytic Site. *Journal of Molecular Biology*, 359(4), 940–949. <https://doi.org/10.1016/j.jmb.2006.04.005>

Rangel, L. (Ed.) (2013). *Cancer treatment - conventional and innovative approaches*. Croatia: InTech.

Roast, A. (2015). *Computational chemistry – designing drugs by evolution*. *icr.ac.uk*. Retrieved 6 June 2017, from <http://www.icr.ac.uk/blogs/science-talk-the-icr-blog/page-details/computational-chemistry-designing-drugs-by-evolution>

Shen, W. C., & Ryser, H. J. P. (1981). *Cis*-aconityl spacer between daunomycin and macromolecular carriers: A model of pH-sensitive linkage releasing drug from a lysosomotropic conjugate. *Biochemical and Biophysical Research Communications*, 102(3), 1048–1054. [https://doi.org/10.1016/0006-291X\(81\)91644-2](https://doi.org/10.1016/0006-291X(81)91644-2)

Shirmanova, M. V., Druzhkova, I. N., Lukina, M. M., Matlashov, M. E., Belousov, V. V., Snopova, L. B., ... Zagaynova, E. V. (2015). Intracellular pH imaging in cancer cells in vitro and tumors in vivo using the new genetically encoded sensor SypHer2. *Biochimica et Biophysica Acta (BBA) - General Subjects*, 1850(9), 1905–1911. <https://doi.org/10.1016/j.bbagen.2015.05.001>

Sigma-Aldrich. (2018). *Sigma-Aldrich*. Retrieved 22 June 2018, from <https://www.sigmaaldrich.com/united-kingdom.html>

Sigma-Aldrich. (2019). Retrieved 3 January 2019, from <https://www.sigmaaldrich.com/catalog/search?term=Daunorubicin+hydrochloride&interface=Product%20Name&N=0+&mode=mode%20matchpartialmax&lang=en®ion=GB&focus=productN=0%20220003048%20219853286%20219853121>

Stephens, P. J., Devlin, F. J., Chabalowski, C. F., & Frisch, M. J. (1994). Ab Initio calculation of vibrational absorption and circular dichroism spectra using density functional force fields. *Journal of Physical Chemistry*[®], 98(45), 11623–11627. <https://doi.org/10.1021/j100096a001>

Stewart, J. J. P. (1990). Mopac:a Semiempirical Molecular Orbital Program. *J. Comp. Aid. Mol. Res*, 4(02), 1. <https://doi.org/02>

Stewart, J. J. P. (2009). Application of the PM6 method to modeling proteins. *Journal of Molecular Modeling*, 15(7), 765–805. <https://doi.org/10.1007/s00894-008-0420-y>

Takahashi, A., Ohtani, N., Yamakoshi, K., Iida, S., Tahara, H., Nakayama, K., ... Hara, E. (2006). Mitogenic signalling and the p16INK4a–Rb pathway cooperate to enforce irreversible cellular senescence. *Nature Cell Biology*, 8(11), 1291–1297. <https://doi.org/10.1038/ncb1491>

Thambi, T., Deepagan, V. G., Yoo, C. K., & Park, J. H. (2011). Synthesis and physicochemical characterization of amphiphilic block copolymers bearing acid-sensitive orthoester linkage as the drug carrier. *Polymer*, 52(21), 4753–4759. <https://doi.org/10.1016/j.polymer.2011.08.024>

Thorn, C. F. ., Oshiro, C., Marsh, S., Hernandez-Boussard, T., McLeod, H., Klein, T. E. ., & Altman, R. B. . (2011). Doxorubicin pathways: pharmacodynamics and adverse effects. *Pharmacogenet Genomics*, 21(7), 440–446. <https://doi.org/10.1097/FPC.0b013e32833ffb56.Doxorubicin>

Ulbrich, K., Etrych, T., Chytil, P., Jelínková, M., & Říhová, B. (2003). HPMA copolymers with pH-controlled release of doxorubicin: In vitro cytotoxicity and in vivo antitumor activity. *Journal of Controlled Release*, 87(1–3), 33–47. [https://doi.org/10.1016/S0168-3659\(02\)00348-6](https://doi.org/10.1016/S0168-3659(02)00348-6)

Waterhouse, D. N., Madden, T. D., Cullis, P. R., Bally, M. B., Mayer, L. D., & Webb, M. S. (2005). Preparation, characterization, and biological analysis of liposomal formulations of vincristine. *Methods in Enzymology*, 391(SPEC. ISS.), 40–57. [https://doi.org/10.1016/S0076-6879\(05\)91002-1](https://doi.org/10.1016/S0076-6879(05)91002-1)

WHO. (2020). *WHO | Cancer*. Retrieved 19 August, 2020, from <https://www.who.int/cancer/en/>

Wu, H.-C., Chang, D.-K., & Huang, C.-T. (2006). Targeted Therapy for Cancer. *Institute of Cellular and Organismic Biology, Academia Sinica, Taipei, Taiwan*, 2(2), 57–66. Retrieved from [https://www.researchgate.net/publication/26576352 Targeted Therapy for Cancer?enrichId=rgreq-7be1cd7f162847d03bcdd56f7c16a32b-XXX&enrichSource=Y292ZXJQYWdlOzI2NTc2MzUyO0FTOjEwNDc5OTYzODkxNzEyNEAxNDAXOTk3NTg5NDI4&el=1_x_2&_esc=publicationCoverPdf](https://www.researchgate.net/publication/26576352_Targeted_Therapy_for_Cancer?enrichId=rgreq-7be1cd7f162847d03bcdd56f7c16a32b-XXX&enrichSource=Y292ZXJQYWdlOzI2NTc2MzUyO0FTOjEwNDc5OTYzODkxNzEyNEAxNDAXOTk3NTg5NDI4&el=1_x_2&_esc=publicationCoverPdf)

Yuan, Z., Huang, J., Liu, J., Cheng, S., Zhuo, R., & Li, F. (2011). PEG-detachable and acid-labile cross-linked micelles based on orthoester linked graft copolymer for paclitaxel release. *Nanotechnology*, 22(33). <https://doi.org/10.1088/0957-4484/22/33/335601>

Zhang, L., & Ma, S. (2010). Efflux pump inhibitors: A strategy to combat P-glycoprotein and the NorA multidrug resistance pump. *ChemMedChem*, 5(6), 811–822. <https://doi.org/10.1002/cmdc.201000006>

Zhang, M., Zhu, J., Zheng, Y., Guo, R., Wang, S., Mignani, S., ... Shi, X. (2018). Doxorubicin-Conjugated PAMAM Dendrimers for pH-Responsive Drug Release and Folic Acid-Targeted Cancer Therapy. *Pharmaceutics*, 10(3), 162. <https://doi.org/10.3390/pharmaceutics10030162>

Zhao, Y., Ren, W., Zhong, T., Zhang, S., Huang, D., Guo, Y., ... Zhang, Q. (2016). Tumor-specific pH-responsive peptide-modified pH-sensitive liposomes containing doxorubicin for enhancing glioma targeting and anti-tumor activity. *Journal of Controlled Release*, 222, 56–66. <https://doi.org/10.1016/j.jconrel.2015.12.006>